A STUDY OF THE LA MACAZA SOLAR HOUSE

ANDREW J. YAGER

A Thesis

in

The Centre

for

Building Studies

Faculty

of

Engineering

Presented in Partial Fulfillment of the Requirements
for the degree of Master of Engineering (Building)
at
Concordia University
Montreal, Quebec, Canada

April, 1980

ABSTRACT

A STUDY OF THE LA MACAZA SOLAR HOUSE

Andrew J. Yager

The results of studies performed on the solar house at La Macaza during the winter of 1978-79 are presented. The augmentation of incident solar radiation on the vertical air collector due to reflection from the snow covered ground was measured to be in the order of 35% above the theoretical "sky only" radiation for clear days. More incident solar radiation was measured on the vertical collector than on a surface tilted at 60° during a sixty day period after winter solstice.

Modifications were made to the solar system: the air flow direction in the collector was reversed, the temperature of the rock storage was horizontally stratified, and the dampers were automated. The instantaneous collector efficiency near noon is calculated to be between 40 and 50% over a wide range of operating conditions between January and May. The daily collector efficiencies and a seasonal solar fraction are calculated. The results are compared to those reported in the studies of two previous winters, before the modifications. There is little quantitative difference in the results, partly because of a different monitoring system and partly because of a change in occupancy, but the effects of the changes are discussed.

Monitoring of the solar radiation, temperatures, and the electric baseboard heaters was done. An energy balance is performed on the entire system (i.e. the house, the collector, and the storage) using the

measured data. The performance of the system is analyzed on 17 days to determine the effects of infiltration, storage losses and passive solar gains. The daily heat balances agree to within 9% with the seasonal heat balance. The results of the energy balance are compared to those of a simulation model presented in a previous study. This analysis indicates that wind speed and direction, and cold ambient temperatures have a considerably greater effect on the overall heat loss of the house than was predicted by the model. The heat loss due to wind infiltration can be reduced economically, increasing the solar fraction.

ACKNOWLEDGEMENTS

I wish to express my sincerest thanks to Dr. Marvin Shapiro, my thesis supervisor, for his perceptive guidance throughout this work, and for many hours of insightful and meaningful discussion.

I want to thank Dr. Paul Fazio, Director of the Centre for Building Studies, for providing financial support and for obtaining the site; and also Mr. R. Beaupré, directeur de l'Institution La Macaza, for allowing access to the site.

The efforts of Hans Obermeir and Joseph Zilkha are greatly appreciated. Hans designed and implemented some of the system controls and was invaluable at the site for troubleshooting and assisting in the experiments. Joseph provided technical assistance and kept the data acquisition system operating.

A special thanks to Oksana Szulhan for maintaining her good humour through many long days of typing and proofreading this thesis.

I appreciate the support and encouragement of many friends, teachers and colleagues who made valuable contributions throughout the duration of the writing.

And finally, the love and continued support of my family is most gratefully acknowledged.

TABLE OF CONTENTS

LIST OF FIGURES

LIST OF TABLES

CHAPTER 1

INTRODUCTION AND BACKGROUND

1.1 INTRODUCTION

Construction of the La Macaza solar house was begun in 1975 under the direction of the Shelter Systems Group of the McGill University School of Architecture. It was one of four prototype houses conceived within a project to develop "Appropriate Building and Energy Systems for Québec Indian Communities" [1]. The La Macaza house was the only one of the four to be completed. It was designed for construction with indigenous labour and materials, and at low cost. The reader can refer to the theses of Hamilton [2] and Kerr [3] for details of the construction materials and methods used.

Monitoring of the house's thermal performance was begun by Hamilton and further studied by Kerr. The present report documents the results of the system's performance during the winter of 1978-79. This is the third and final thesis to be presented.

Instrumentation of the house and its components and analysis of the results were undertaken in order to contribute to a data base for solar heating design in Québec. Initial contributions to the effort and continued interest by Hydro-Québec's Institut de Recherche d'Énergie (I.R.E.Q.) attest to this fact. It is hoped that the present work will further contribute to this effort.

An experimental study was performed to determine the enhancement of incident solar radiation on the vertical collector due to

reflections from the snow covered foreground. Actual total radiation measurements were recorded continuously for four months. One solarimeter was mounted on the vertical face of the collector, and another, tilted at 60° was placed at roof level, to avoid reflection from the glazing. The vertical solarimeter was at mid-collector height, and the location of the 60° solarimeter is approximately where the center of a collector installed on a sloped roof would be. The total daily radiation incident on each surface was compared on clear days and cloudy days.

The advantages of a site-built vertical collector, integral with a south facing wall, are discussed.

The house was unoccupied during the study. Because of the remoteness of the site, visits were made only every two or three weeks. Therefore, the data acquisition system and controls were selected for reliable operation when unattended. Continuous readings were taken of the two solarimeters, nine temperatures, and the on/off status of six baseboard heaters, the collector fan, and power failures. Details of the instrumentation and system controls are presented in Chapter 3.

Modifications were made to the system before the present study. These were designed to improve the overall system performance. The collector air circulation was reversed, the storage was stratified, the dampers were automated, leaks in the air handling system were sealed, and the floor above the storage was insulated. The details of these changes are described in Section 1.3 and the results are discussed in Chapter 4.

The efficiency of the solar collector was calculated according to accepted standards [21], and the results are compared to the two previous studies by Hamilton and Kerr.

An energy balance was performed on the entire system (i.e. the house, the collector, and the storage) based on the measured data. The results of the heat balance are compared to the computer model simulation presented by Kerr. The heat balance analysis indicates certain areas where a degree of refinement in predictive models is desirable. The largest discrepancies appear in the treatment of infiltration and thermal bridges.

1.2 THE HOUSE

The house was constructed with both standard and unconventional building materials. For instance, the north, east, and west walls were made of stacked 13cm x 13cm rough cut spruce timbers; treated peat moss insulation panels were used in the north wall, and polystyrene insulation in the east and west walls . Frame construction was used on the south wall, and the solar collector was built integrally with it. The house is oriented with its long axis in the east-west direction. The location of the site is at 46° 24' north latitude, 250 meters above sea level.

1.2.1 The Building Envelope and Surroundings

The house was built in an open land area with no natural protection from the elements. However, several energy conserving features

were incorporated in the building envelope design to reduce the winter heating load. Earth berms were built up on the east, west and north walls to reduce the exposed wall surface to 6 feet in height. The doors on the east and west walls were enclosed with vestibules. However, the outer door on the west vestibule had been removed before this study. The north wall glazing was limited to one window of less than 0.5 square meters. A south facing skylight in the bathroom had five glazings. The living room and kitchen had large glazing areas (on the east and west walls respectively) to allow passive solar heat gains, and natural lighting.

The 42 square meter, vertical solar collector covered the entire south wall. A considerable saving in capital cost was achieved because the collector acted as part of the insulation and the cladding for the south wall. An additional advantage of integrating the collector with the south wall is that heat is transferred to the inside of the house by conduction when the collector is heated above room temperature on sunny days. Thus, collector back losses are recovered directly in the house. A reduction of the heat loss through the south wall of the house can occur on partly cloudy days when there is insufficient light to operate the collector, because the temperature of the air behind the glazing can increase well above the ambient.

The conductive thermal resistance of the walls is approximately 3.5°C m^2/w (20°F hr ft^2/BTU), and the resistance to heat flow through the roof is about 4.3°C m^2/w (24°F hr ft^2/BTU). While these values are on the low end of recommendations for new standards, they do

provide results on the performance of the La Macaza house which are comparable to many homes being built today. Because of the log construction, infiltration through the east, north and west walls was higher than normal.

There was a large amount of open space around the house. As this ground is covered with snow during most of a usual six month winter, significant augmentation of the energy incident on the collector is achieved due to light reflected and scattered from the snow. Enhancement of the passive solar heat gain also occurs at the east and west windows due to the snow reflection.

1.2.2 The Building Interior

The living quarters are on one level and cover approximately 90 m^2 of floor area. The kitchen and living room are in the south half of the main floor and the three bedrooms and bathroom are in the north half (see Fig. 1). The interior is of standard stud construction with wooden wall panelling. The only energy conserving feature is that the electric baseboard heaters in each room are controlled by individual thermostats. This can help prevent overheating at the time of passive solar gains. One negative feature is the sloped ceiling (conforming to the roof line) which rises to 3.5 m above the floor at the south wall. This area acts as a heat trap, resulting in an increased heat loss through this portion of the roof. No provision was made to recirculate this warmer air to the living space.

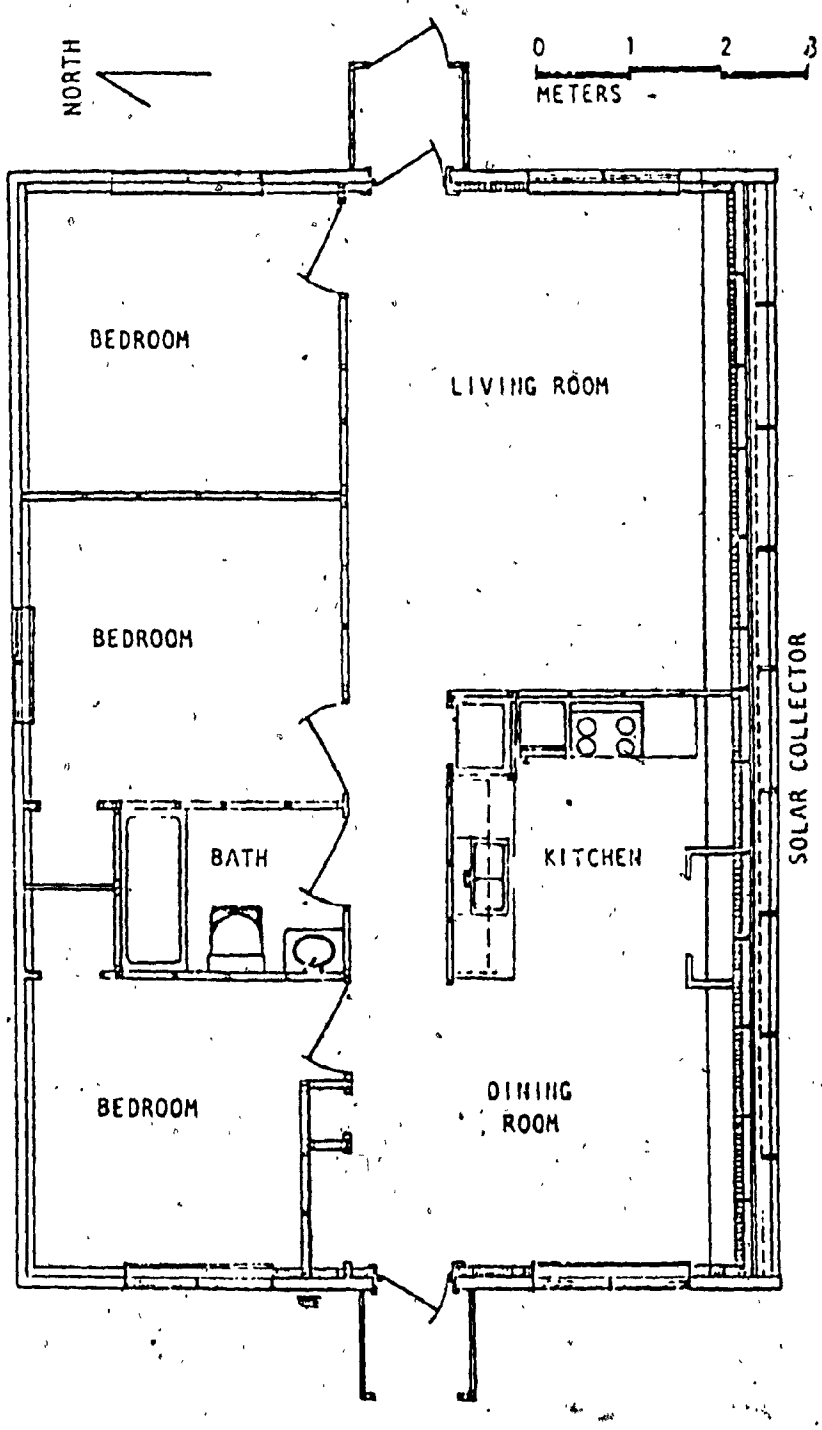

FIG. 1 - PLAN OF SOLAR HEATED HOUSE AT LA MACAZA, QUEBEC [ADAPTED FROM REF. 2]

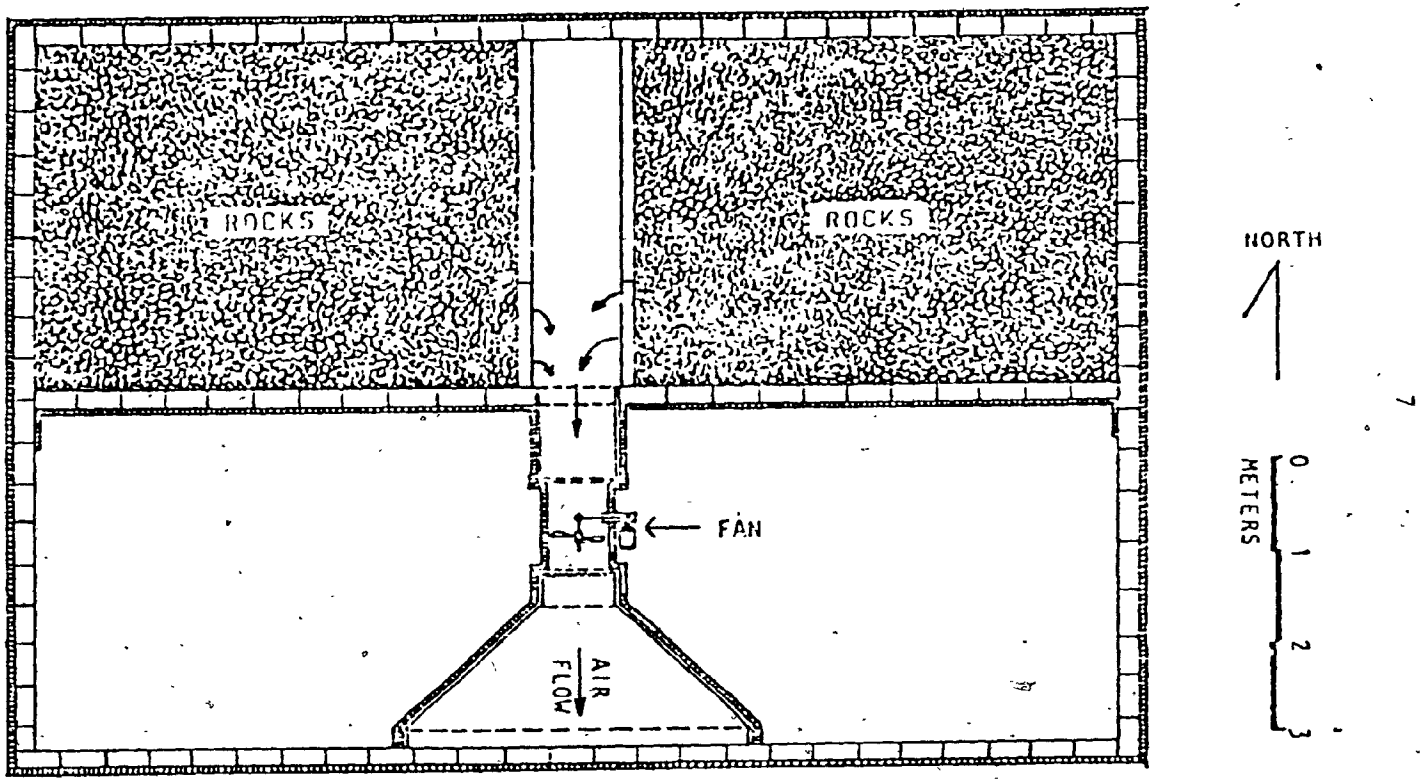

FIG. 2 - PLAN OF HOUSE AT LA MACAZA - STORAGE LEVEL [ADAPTED FROM REF. 2]

The rock bed thermal storage is located below the bedrooms and covers the north half of the 1½ meter high basement area (see Fig.2). The storage covers the entire 45 m^2 floor area to a depth of 3/4 meters. This storage configuration provides the house with a well distributed thermal mass of large surface area. The south half of the basement is unheated and unfinished. The collector fan and storage to collector duct are in the center of this space. The return ducts were made by covering some of the floor joists above the unheated basement. These joist areas are open to the top of the south wall of the storage. This further distributes the potential of the storage mass by directly heating the floor below the south half of the living space.

1.3 THE SOLAR HEATING SYSTEM AND MODIFICATIONS

The solar heat collection system consists of a south facing vertical air collector, a rock thermal storage, and a fan to circulate air between the storage and collector. The fan and the storage were oversized, resulting in lower than usual collector operating temperatures, and a large volume low temperature thermal energy storage. Figure 3 is a section through the midline of the house showing the three main components of the solar heater. The arrows indicate the flow direction when the fan is on.

The 42 square meter collector consists of a galvanized sheet metal absorber, painted black, an expanded metal mesh with 50% openings, also black, a sealed double glazing and a 2 cm sheet of chipboard behind the absorber to provide some thermal inertia in the

collector. It is built in a wooden frame integral with the south wall of the house. There are nine vertical flow channels and 27 standard aluminum frame double glazing units.

There are 24,000 kg of rocks in the storage having a heat capacity of 9.4 kwh/°C. The rocks are 5 to 10 cm in diameter and covered the 45 squake meter storage floor area to a depth of about 75 cm (i.e. approximately one half the height of the storage compartment). A thermal blanket consisting of three layers of aluminized building paper, with the reflecting surface downwards, covers the rocks of the south two-thirds of the storage. Air is removed from storage through the openings in building blocks below the south 1/3 of the storage.

The 1 h.p. axial fan is located in an insulated duct in the unheated basement, midway between the storage and the base of the collector. The fan motor is attached to the outside of the duct for easy access. The fan is controlled by a differential thermostat. It is automatically turned on when the collector temperature exceeds that of the storage by 10°C, and it is turned off when the collector temperature drops to within 2°C of the storage temperature.

When the fan is on, air is drawn from the cold end of storage, through the fan, and blown into the v-duct to enter the central third of the collector at the base. The air is then distributed horizontally to the nine vertical flow channels in the collector and rises between the metal absorber and the mesh, as shown in Fig. 4. The heated air returns behind the absorber to the insulated flow channels between the floor joists in the two outer thirds of the house. This air

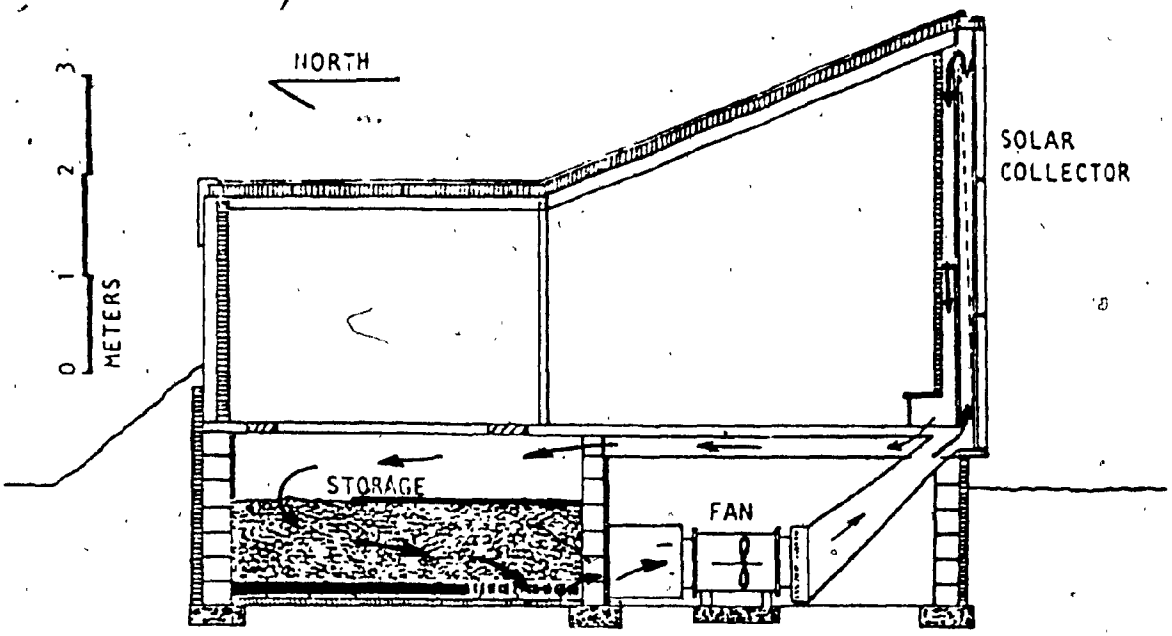

FIG. 3 - SECTION OF HOUSE AT LA MACAZA [ADAPTED FROM REF. 2]

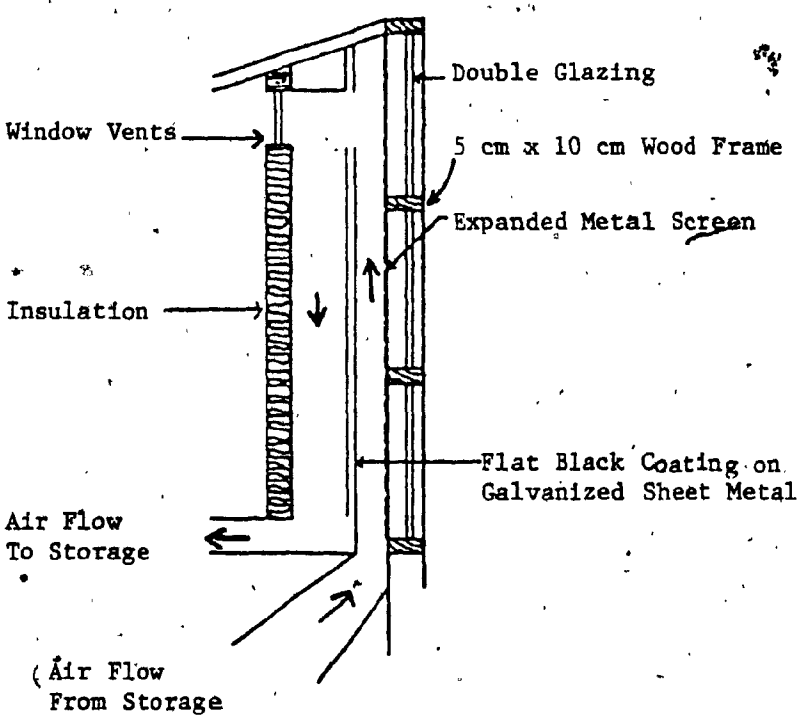

FIG. 4 - SECTION OF COLLECTOR [ADAPTED FROM REF. 3]

enters the storage at the top (Fig.3), and moves across the top of the aluminized reflecting paper, entering the rocks in the north third, where it is then drawn down through the rocks to the south end of the storage. Heat is removed from the air as it moves downward and across the rocks, and the coldest storage air is then returned to the fan along a horizontal flow channel on the floor of the storage in the south third.

Figure 5 shows typical sections at the base of the collector in the heat collection mode. When the fan is turned on, the dampers are automatically raised to allow the cold storage air to enter the base of the collector through the v-duct in the central third, and to allow the warm collector air to return to storage between the floor joists in the two outer thirds. The dampers are attached to the base of the collector with spring loaded hinges and are connected in parallel to a motorized winch at the west end of the collector by flexible steel cables, as shown in Fig. 6. When the fan is turned off, the winch releases the tension on the cables and the dampers close to the position shown in Fig. 7. In this mode, heat from storage is distributed to the house by natural convection. Warm air from storage moves between the joists, warming the floor, and enters the south zone of the living space through air vents in a 30 cm square bench over the dampers which runs the full length of the south wall. Cold air is returned to storage through vents in the central third of the bench. Storage heat is also distributed directly to the bedrooms through the baseboard heat registers by natural convection, and by conduction through the floor.

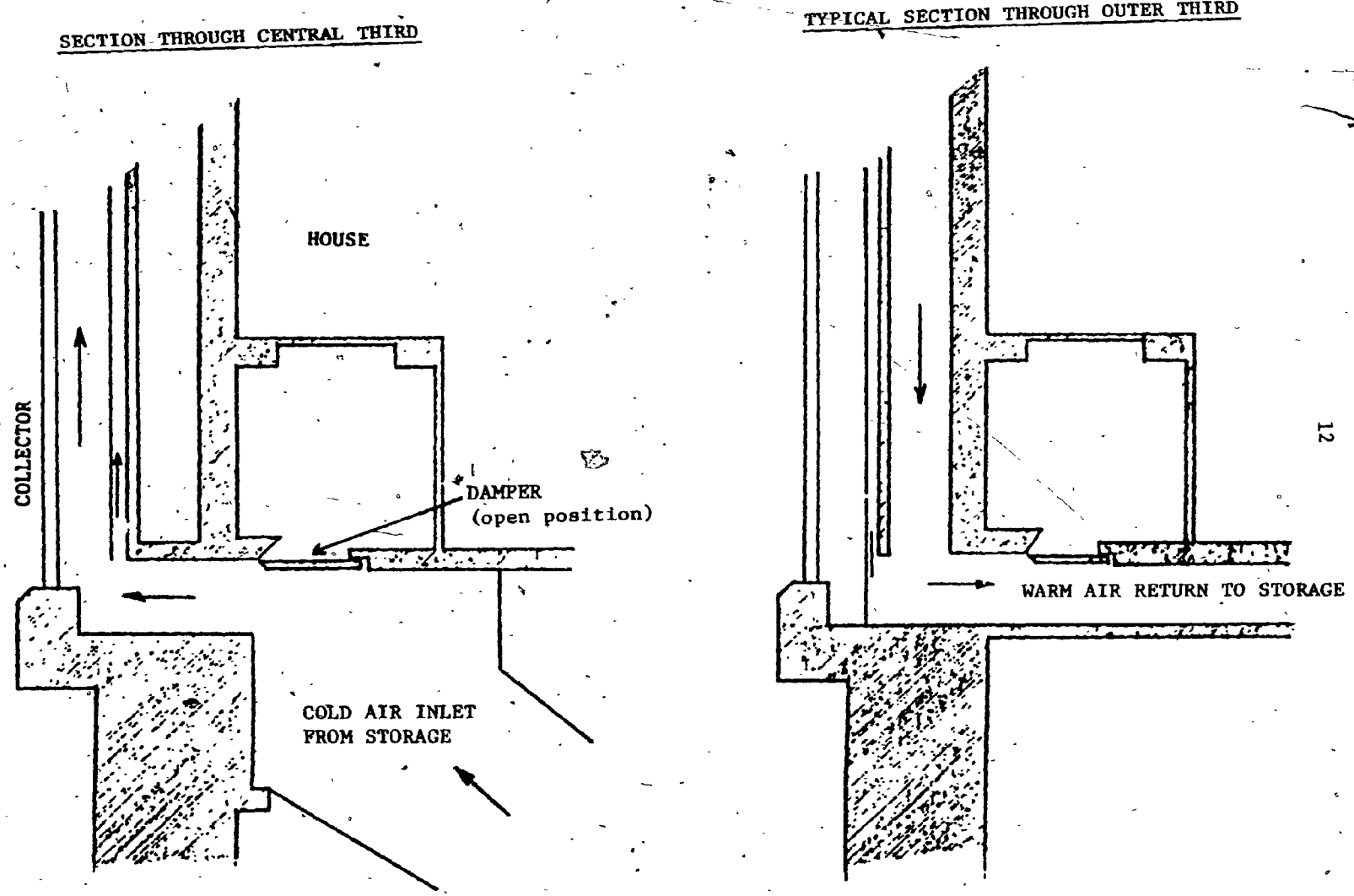

FIG. 5 - DAYTIME HEAT COLLECTION CIRCUIT [ADAPTED FROM REF. 3]

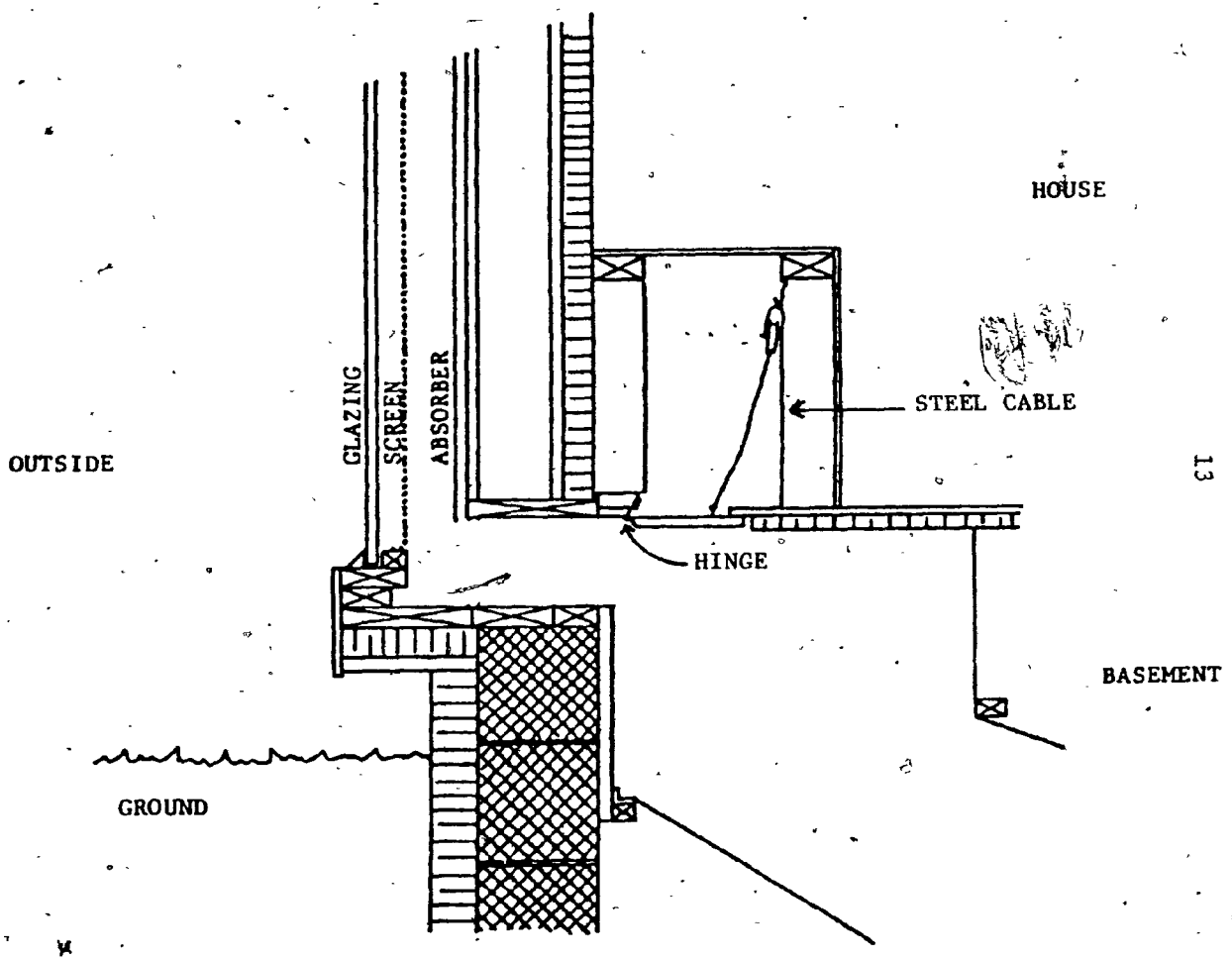

FIG. 6 - SECTION AT BASE OF COLLECTOR AT V-DUCT [ADAPTED FROM REF. 3]

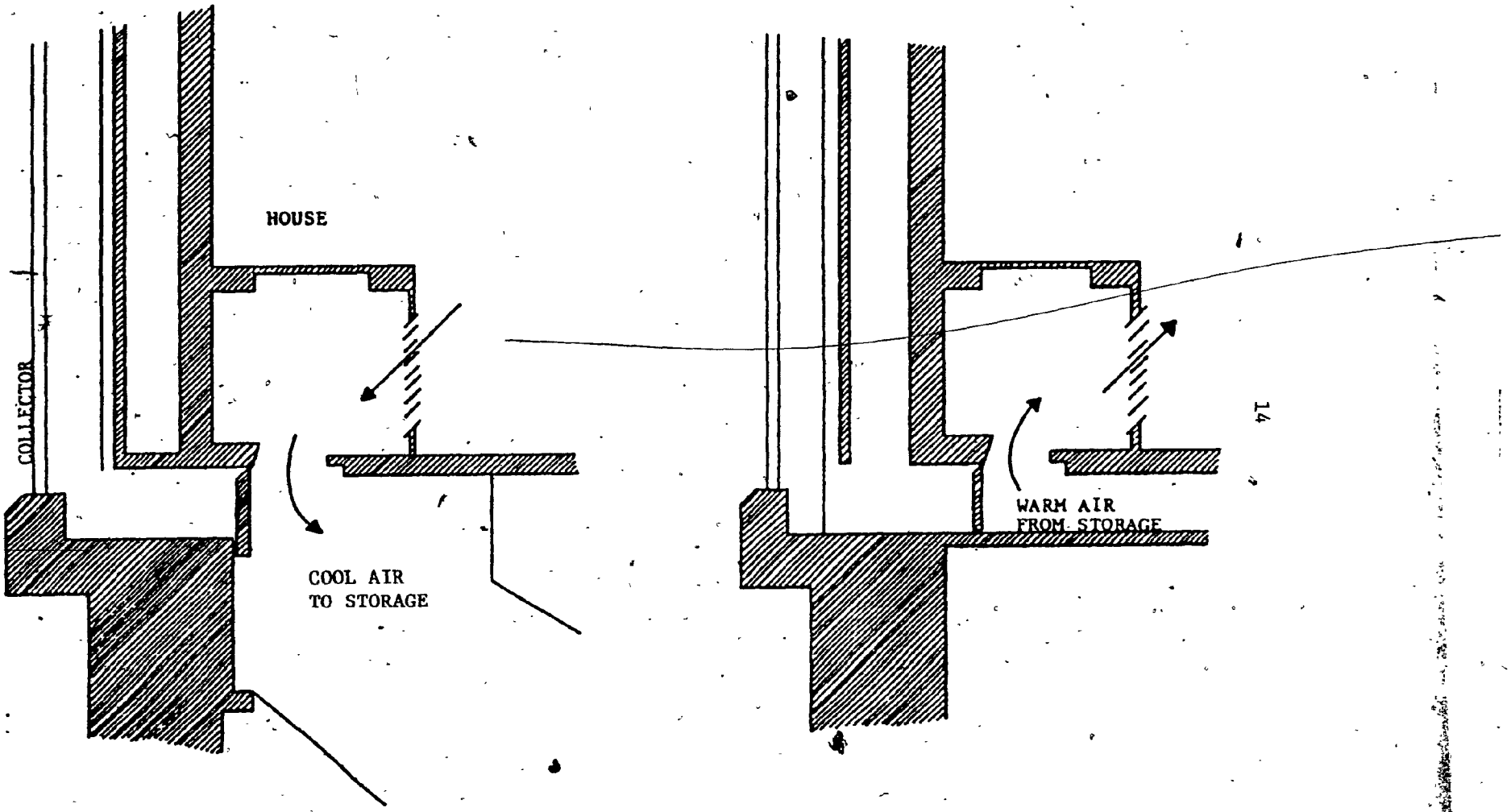

FIG. 7 - NIGHTTIME HEAT DISTRIBUTION CIRCUIT [ADAPTED FROM REF. 3]

Three major modifications were made to the system since the work of Hamilton [2] and Kerr [3] :

1) the fan direction was reversed;

2) the south two-thirds of the storage rocks was covered with a thermal blanket;

3) the dampers at the base of the collector were automated to operate in conjunction with the fan.

The reasons for these changes and their possible effects are described as follows. In the original installation, the collector inlet air was taken from the top of an isothermal storage, blown through the floor joists, up behind the absorber and drawn down between the absorber and the mesh. The hottest solar heated air was close to the glazing before returning to the bottom of the storage through the duct in the unheated basement. By reversing the direction of the fan, colder air is now drawn from the bottom of the storage, and rises near the glazing. This reduces the duct losses in the unheated basement and supplies colder inlet air to the collector, reducing the collector losses by reducing its average operating temperature and the temperature of the air next to the glazing. The use of the thermal blanket over the south two-thirds of the rocks further lowered the collector inlet air temperature by producing a stratification of the storage temperature. Most of the heat is removed from the collector outlet air at the north end of the storage; therefore, the collector inlet air is held more constant as heat is added to the north end. This increased storage temperature under the bedrooms makes more heat available to them by

conduction through the floor and by the natural convection flow through the registers. Additional insulation was added to the south 3/4 of the bedroom floor area above the storage. The insulation added below the bedrooms was left off the north quarter of the floor to increase convective flow up the north walls of the bedrooms.

Before the dampers were automated, they were operated by a hand winch. The gates were opened when the fan came on and closed when the sun went down. They were usually left open during intermittent cloudy days, when collector losses during cloudy periods can exceed collector gains during sunny periods. For optimum operation of a manual system, the occupants should be present in the house daily. This was not always possible, and so losses of collected heat occurred. Because the house was unoccupied during the winter of this investigation, it was necessary to automate the dampers.

CHAPTER 2

SNOW REFLECTOR EFFECTS

2.1 INTRODUCTION

The use of the natural snow foreground of the solar collector at the house at La Macaza has proven to have a favourable effect for energy collection. During the winter of 1978-79, the augmentation on the vertical collector, due to the reflections, was found to be in the order of 35% greater than the theoretical maximum clear day "sky only" radiation. The vertical surface received more incident radiation than the one tilted at 60° above the horizontal during a 60-day period after winter solstice, when snow was present. The augmentation by reflection would be the same for 60 days before solstice.

A major advantage of a snow reflector is that it is free. The snow reflector can be undependable, as in the unusual winter of 1979-80, where significant snow cover was not obtained until January 22nd. One minor disadvantage is that light reflected by the collector glazing tends to melt the snow in front of the collector; however, in an average Québec winter, this will rarely cause complete melting of the snow. On several occasions at La Macaza, it was noted that this effect, plus wind scouring, caused a snowdrift about a meter from the collector. If the collector extends too close to the ground (lower than a meter from the ground), the shadow from this drift can cause large differential expansions during cold weather, leading to damage to the collector frame or glazing.

2.2 PREVIOUS REFLECTOR STUDIES AND RELATED WORKS

Two previous studies have been conducted which report the performance of the solar collector on the house at La Macaza [2,3]. While both studies refer to the positive effect of the snow covered collector foreground, a detailed analysis was not made [4]. Hamilton and McConnell [5] report an estimated annual total radiation curve for the vertical collector at La Macaza (Fig. 8). Though they do not state the basis of their calculations, their estimate shows an incident energy increase of approximately 60% during the winter months with snow covered collector foreground.

Kerr et al. [6] determined that for six sunny days in late February and early March, 1977, 23% of the total radiation incident on the collector was caused by light reflected and scattered from the snow foreground. The results of snow reflector experiments conducted at La Macaza during the 1978-79 winter are analyzed in the present study.

Many studies by others report the results of analytical and experimental work on various reflector/collector configurations. McDaniels et al. [7] conducted a crude experiment to determine the optimum collector/reflector orientation for a site in Oregon ($45° \pm 1°$ north latitude) in December 1965. They measured the time required to evaporate a drop of water on the absorber of a flat plate collector. The collector was tilted at 45°, 60°, 90° and 110° above the horizontal. The shortest evaporation time was recorded for the collector vertical and the reflector horizontal. In addition, they developed an analytical model which verified that the optimum collector tilt is

approximately vertical for a horizontal reflector of infinite size (i.e. the length and width of the reflector are greater than three times those of the collector). A collector was subsequently installed on the Mathew house, tilted at 82° above the horizontal, with a reflector at 8° below the horizontal, for architectural reasons.

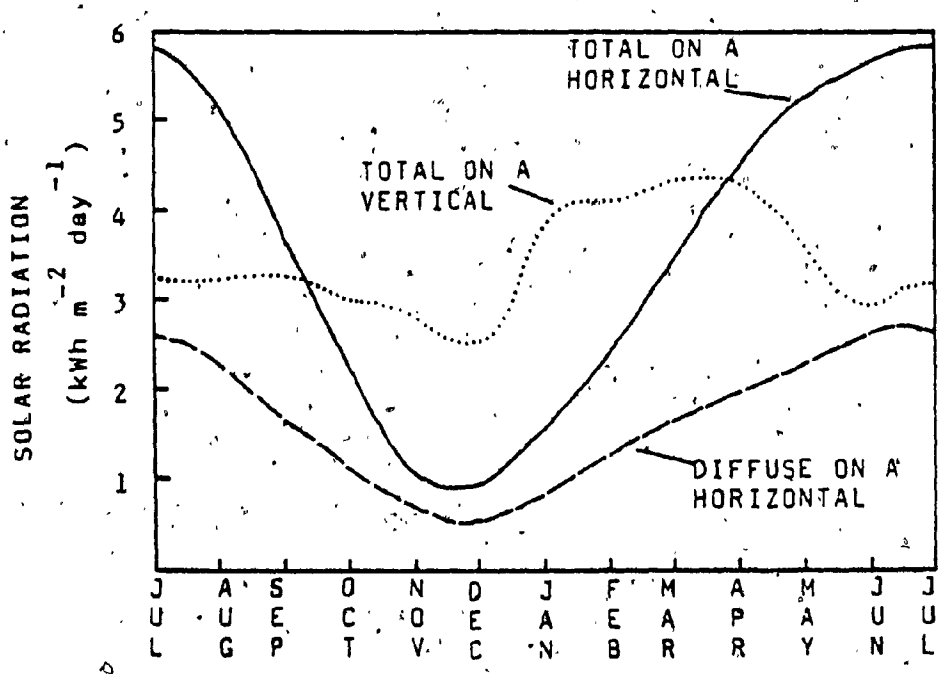

FIG. 8 - ESTIMATED SOLAR RADIATION RECEIVED ON HORIZONTAL AND VERTICAL SURFACES AT LA MACAZA, QUEBEC

(From Hamilton & McConnell [4])
The vertical surface includes snow reflection effects

Grassie and Sheridan [8] have developed a mathematical model to simulate flat plate collector/reflector performance. The contributions of both diffuse and specular reflectors were considered. The diffuse reflection is handled as a radiative exchange between two plates in space - reflector and collector; i.e. they used an isotropic intensity distribution from the reflector. The specular reflection component is the product of the direct solar beam, the cosine of the angle of incidence, and the reflectivity of the reflector surface. Two water heating collectors were built to verify the model. In each experiment, the collectors were mounted in the same plane, one with a reflector and one without. Two reflectors were used. The diffuse reflector was a matt white reflective paint (reflectivity = 0.75) and the specular reflector was an aluminum foil (reflectivity = 0.85). The latitude of the tests was 27.5° south, that of Brisbane, Australia. Collector inclinations ranged from 25° to 35° above the horizontal. The reflectors were mounted above the collector at angles of 70°, 80° and 90° above the horizontal; or below the collector at angles of 10°, 20° and 30° above the horizontal. The reflector height was equal to the collector height, and the reflector width was equal to the collector width plus the reflector height. In all instances, the diffuse reflector/collector system showed an insignificant increase in heat collection over the simple collector. A computer calculation was used to determine annual theoretical performance. The collector experiments were performed at low sun angles (i.e. June,

July). Figure 9 is their plot of collector-specular reflector performance for a clear day. The integrated daily increase in energy production with the reflector is 14%.

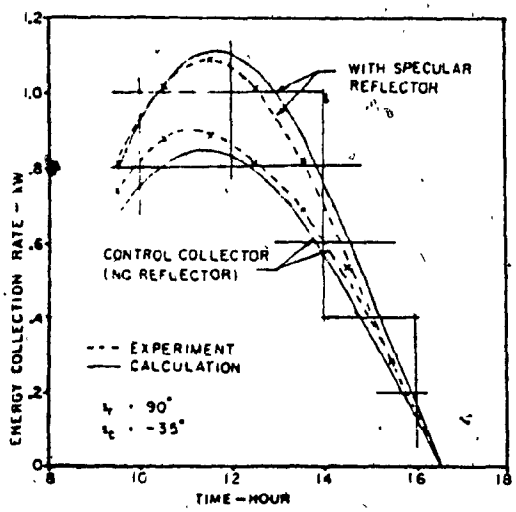

Fig. 9 Collector-specular reflector performance for clear day.

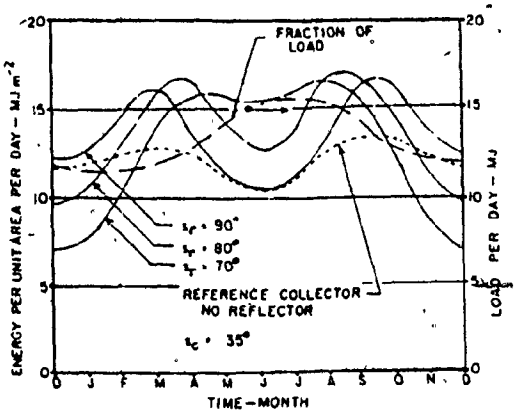

Fig. 10. Performance of collector-reflector system with reflector above collector.

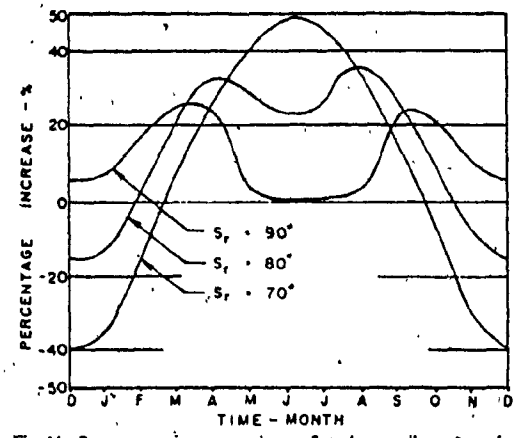

Fig. 11. Percentage increase above flat-plate collector performance due to a reflector above the collector.

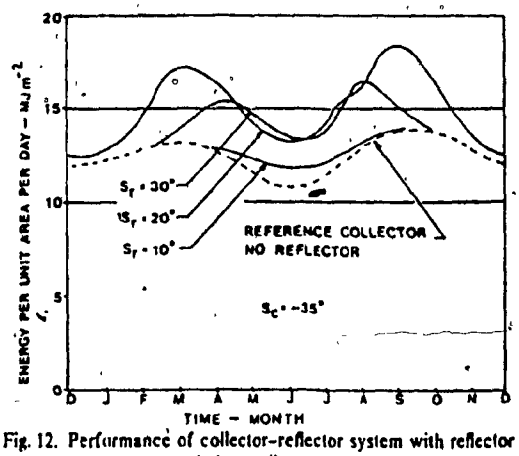

Fig. 12. Performance of collector-reflector system with reflector below collector.

FIGS. 9 - 12 : FROM GRASSIE AND SHERIDAN [8]

In Fig. 11, the curve for the reflector vertical (90°) shows a positive effect throughout the year and has the least annual variation. This would be best for domestic hot water heating. However, for space heating, Fig. 10 shows that the reflector at 70° gives a better match to the higher load during the cold months (i.e. June, July, August). The 20° reflector below the 35° tilted collector yields a large enhancement during the spring and fall, but is deficient during the winter months when the load is greatest (Fig. 12).

Grimmer et al. [9] considered three reflector types : specular, diffuse, and specular/diffuse, the latter having an asymmetrical distribution of intensity about the specular reflection angle. The effects of the reflectors were modeled analytically and tested experimentally. The tests were meant to simulate winter conditions at 36° north latitude by tilting both the reflector and collector in August. This type of simulation can be subject to errors because the air mass and diffuse light distribution in winter are different from those in August. (Böer [10] uses an average winter air mass which is about 50% greater than in the fall, near noon, at 40°N latitude). A theoretical comparison, with summer sun angles through a shorter air path, of the sky only direct solar component for 36°N latitude on a collector in December to one tilted to have the same solar incident angles, but shorter path length in the atmosphere in August, is shown in Table 1. A maximum reduction of about 6% in available beam radiation for the summer experiment is calculated.

TABLE 1

SKY ONLY DIRECT RADIATION FOR SIMULATION EXAMPLE

Month	THEORETICAL SKY ONLY DIRECT SOLAR COMPONENT ON A VERTICAL SURFACE* (Latitude 36°N) (W/m^2)	THEORETICAL SKY ONLY DIRECT SOLAR COMPONENT ON A SURFACE TILTED IN AUGUST TO SIMULATE A VERTICAL SURFACE (Latitude 36°N) (W/m^2)	Percent Difference
August	359**	359	---
September	542	520	4.1
October	687	646	6.0
November	775	737	5.1
December	803	772	3.9

* Clear sky; no ground reflectance

** Direct solar radiation values determined at noon on a south facing surface

The beam component determination is based on the ASHRAE [11] equation for direct normal radiation :

$$I_{DN} = \frac{A}{EXP\left(\frac{B}{\sin(\beta)}\right)} \qquad (2.1)$$

where :

I_{DN} = direct normal solar radiation (clear sky; no ground reflection)

A = apparent solar radiation at air mass = 0

B = atmospheric extinction coefficient (function of air mass)

β = solar altitude angle

The solar altitude angle, β, at noon, can be expressed as :

$$\beta = \frac{\pi}{2} - \text{latitude} + \text{solar declination}$$

The beam radiation incident on a vertical surface can be expressed as:

$$I_{vert} = I_{DN} \cdot \cos(i) \qquad (2.2)$$

where :

i is the angle of incidence.

Substituting equation (2.1) into equation (2.2) yields :

$$I_{vert} = \frac{A \cdot \cos(i)}{EXP\left(\frac{B}{\sin(\beta)}\right)} \qquad (2.3)$$

The values of A, B, and β in equation (2.3) vary with the month for the actual vertical calculations, but remain constant for all simulations and are the values which apply at the time of the simulations (i.e. August). The values of the angle of incidence, i, are the actual angles that the solar beam makes with the normal to the collector surface at the time of the simulations.

The ASHRAE [11] method assumes a uniform diffuse radiation distribution. Dave [12] has shown that the Mie and the Rayleigh diffuse light distributions increase by a factor of about 10 near the horizon. In the simulation by Grimmer et al.[9], the collector/reflector system was tilted in a way that obscured the collector's view of the horizon. However, this loss of scattered light from the horizon is somewhat compensated by a gain in forward scattered light. In the

diffuse Mie model, the scattered light is ten times greater than the horizon scattering within the region of about 10° of the direct beam.

The results of the simulation by Grimmer et al. [9] agree reasonably well with the experimental results at La Macaza. They determined that for the winter season a vertical collector with horizontal reflector gave the best heat collection. They also point out that a considerable reduction in capital expense can be achieved by integrating the collector with the construction of a south-facing wall; this was a major consideration in the La Macaza house design.

The effect of reflector length to collector height was also reported. It was found that reducing the reflector length from three to two times the collector height decreased the energy collection by only one percent. As the snow foreground at La Macaza was much larger than the collector, the reflector was considered to be of infinite dimensions (i.e. the reflected light incident on the collector was the maximum available).

Seitel [13] has reported a computer analysis of flat plate solar collector performance enhancement with flat reflectors. He considers the effects of redirecting solar radiation onto a horizontal surface; for example, a rooftop water pond or a swimming pool. Although the results of the investigation do not relate quantitatively to the studies at the La Macaza house, several useful conclusions are noted. The enhancement with reflectors is described in two ways : 1) the reflector can redirect the solar radiation to more nearly normal

incidence on the collector, and 2) the reflector increases the effective collector area. Seitel also points out that reflectors are inherently cheaper to construct than collectors per unit area. Hence, savings in capital investment can be realized when reflectors are used to replace some collector area.

It should be noted that when reflectors are used, the increased incident radiation per unit collector area can increase the collector operating temperature. Unless the mass flow rate of the collector heat exchange fluid is increased to compensate for the increased solar input, collector losses will increase, reducing the utility of the radiation enhancement due to the reflector.

2.3 SNOW REFLECTANCE VALUES

Liu and Jordan [14] have presented a formulation for determining the monthly average reflectivity (ρ) of snow covered ground :

$$\rho = (.2)(1-c) + (.7)(c)$$

where :

c is the fractional time during the month when snow of more than one inch thickness is present.

Hence, when snow of greater than one inch thickness covers the ground for the entire month (i.e. c=1), the reflectivity of the snow is 0.7 (or 70%).

Hunn and Calafell [15] performed a photographic study of foregrounds with partial snow cover in various winter landscapes. They used average reflectivities reported by others for 15 characteristic ground surfaces, and then determined an integrated reflectivity for each representative winter landscape. They report the overall reflectance of mostly snow covered fields to be in the order of 60 to 70%. They conclude that this "average ground reflectivity...is accurate for most rural landscapes in winter where snow cover is predominant".

Kalitin [16] made almost daily careful measurements of the albedo of an undisturbed snow cover over a three month period, near Leningrad, in 1929. He defines the term albedo as "...the amount of radiant energy reflected and expressed in per cents in respect of the direct energy". During a period of nine days at the beginning of April, the albedo decreased almost linearly from 79 to 59%, in the absence of a fresh snowfall. Although the diurnal mean air temperature during this period was below freezing, the maximum air temperature exceeded the freezing point on certain days, so changes in the crystal structure of the snow particles could have occurred.

Hague and Werren [17] have reported the results of an experimental study of incident radiation increase on a south facing wall due to reflection from a snow covered foreground. They measured the solar radiation on various surfaces for a clear day in February near Montréal. They calculated the augmentation of radiation on the south wall to be between 22 and 39% with an albedo ranging from 84 to 92% for

different hours of the day. This agrees well with the augmentations observed at La Macaza (c.f. Table 2).

2.4 EXPERIMENTAL PROCEDURES AND RESULTS

2.4.1 Clear Days

Two flat glazed solarimeters were mounted on the south facing vertical air collector on the house at La Macaza. A Dodge Products model SS100 silicon cell solarimeter was fixed to the vertical surface at mid collector height and a Hollis Observatory model MR-5 silicon cell was placed at a 60° tilt from the horizontal at roof level (Fig. 13). The two solarimeters were placed side by side in the vertical position at mid collector height before and after the data gathering period for intercalibration. The relative agreement between the two solarimeters at the end of the test period was within 2% at all intensities.

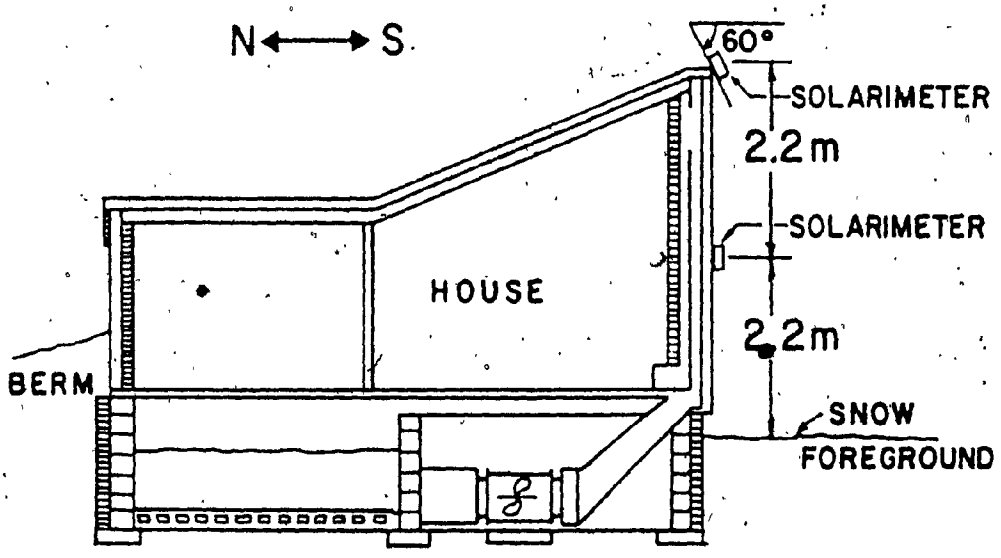

FIG. 13 - LOCATION OF SOLARIMETERS

Continuous total radiation measurements were recorded for both solarimeters on 6 cm. wide carbon loaded paper moving at the rate of 2.54 cm. per hour. The area under each curve was computed by summing simple trapezoids at hourly intervals for 13 clear days between November 1st and March 9th. The actual data curves are given in Appendix A (Figs. A.1 - A.13). In each case, the data curves were redrawn as shown in Figs. A.14 and A.15. The measured radiation values reported in Table 2 assume the day was completely clear; hence, corrections were made for intermittent cloudiness. (Note: For this reason, there will be a discrepancy with the values in Table 7, where actual recorded intensities are summed). The radiation curve for a clear day is typically a smooth parabola with its vertex at noon. Due to various effects at the horizon, the first and last fifteen minutes of each day do not fall on the parabolic curve but are slightly to the outside. The main reason for this phenomenon is the extra forward scattering of diffuse light in the region of the direct solar beam. Hence, a collector exposed to light from the horizon will receive a small amount of "directed diffuse" light for about 15 minutes before sunrise and after sunset in a cloudless atmosphere. On a clear day, this light is less than 1% of the total daily raddation and is neglected here for simplicity. A smooth radiation curve was assumed from sunrise to sunset.

The integrated values of total daily radiation for each clear day are given in Table 2 and plotted in Fig. 14. Figure 14 shows the total daily radiation on both the vertical and the 60° tilted surfaces

giving the experimental and the computed "sky only" values. The experimental data on the 60° tilted surface in Table 2 is incomplete due to the malfunction of a potentiometer in the recorder.

The "sky only" values were determined according to the method described by Farber and Morrison [18]. The total radiation is the sum of the direct and the diffuse components. The direct component is the product of the direct normal radiation and the cosine of the angle of incidence. The direct normal intensity is given by equation (2.1):

$$I_{DN} = \frac{A}{EXP\left(\frac{B}{\sin(\beta)}\right)}$$

TABLE 2

CLEAR DAY SOLAR RADIATION VALUES

DAYS FROM SOLSTICE	DATE	CLEAR DAY MEASURED TOTAL RADIATION (MJOULES/m^2.DAY)			THEORETICAL SKY ONLY (MJOULES/m^2.DAY)			AUGMENTATION OF VERTICAL BY REFLECTION
		VERTICAL	60° TILT	% DIFF	VERTICAL	60° TILT	% DIFF	%
0	Dec 21	-	-	-	16	16	-4	-
8	Dec 29	21	18	+15	16	17	-4	31
25	Nov 26	23	-	-	16	17	-6	43
26	Jan 16	22	-	-	17	18	-6	31
30*	Nov 21	21	-	-	17	18	-6	27*
33	Jan 23	23	20	+14	18	19	-7	31
43**	Nov 8	21	-	-	18	19	-9	19**
44	Feb 3	26	24	+8	19	20	-9	38
47	Feb 6	26	24	+8	19	21	-10	35
50**	Nov 1	22	-	-	18	20	-11	19**
52	Feb 11	26	25	+5	19	22	-11	35
55	Feb 14	26	24	+7	19	22	-12	34
59	Feb 18	26	24	+7	19	22	-13	34
78*	Mar 9	23	-	-	19	24	-20	20*

* Partial Snow
** No Snow

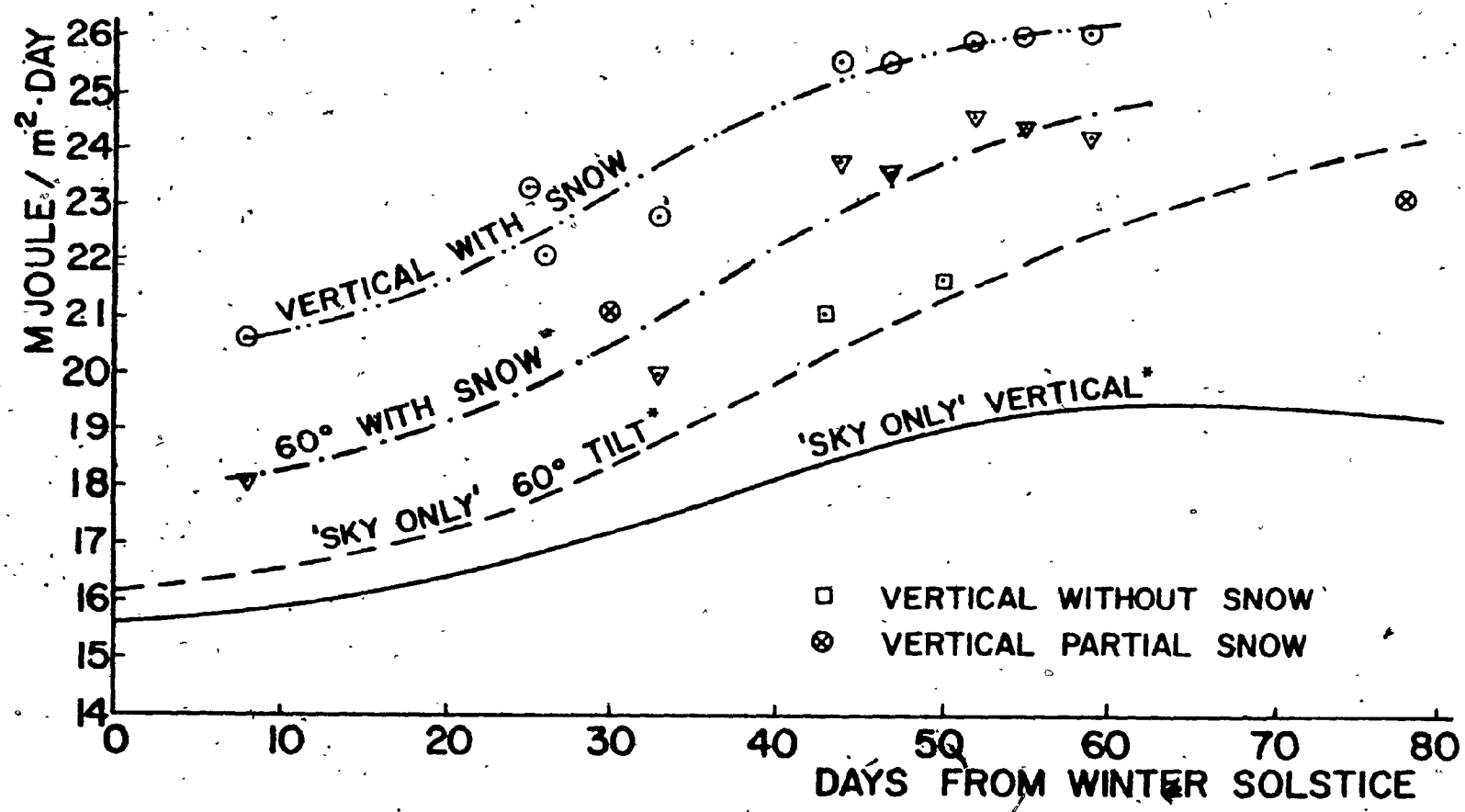

*CLEARNESS FACTOR = 1.0 ; 0 % GROUND REFLECTANCE

FIG. 14 - CLEAR DAY TOTAL DAILY RADIATION

The values of A and B are taken from reference [11], Table 1, given for the 21st day of each month. They are derived from experimental data taken at three locations in the United States in 1964 and are relative to a defined standard atmosphere [19]. Intermediate daily values are found by linear interpolation.

The diffuse component, I_{ds}, is determined by :

$$I_{ds} = C \cdot I_{DN} \cdot F_{ss}$$

where :

C is the dimensionless constant from reference [11], Table 1, (i.e. uniform blue sky luminosity is assumed).

F_{ss} is the projection factor for the portion of the sky dome exposed to the collector.

$F_{ss} = [(1 + \cos(\text{tilt angle}))/2]$

for a vertical collector, $F_{ss} = 0.5$

for a 60° tilted collector, $F_{ss} = 0.75$

The total "sky only" values were generated by adapting a computer program which had previously been developed [20].

It should be emphasized that while the vertical solarimeter recorded a greater amount of winter incident energy than the "rule of thumb" (latitude + 15°) 60° solarimeter due to enhancement by reflection (Figs. 14 & 15), the solarimeter tilted at 60° will always receive more clear day "sky only" radiation (Fig. 14). This is due to the smaller cosine factor for the direct solar rays on the 60° tilted surface over that of the vertical, at all times of the year, plus exposure to a larger portion of the diffuse sky dome for the 60° surface.

Figure 15 shows that when snow was present, the vertical surface received more radiation than the one tilted at 60°. The curve suggests that the maximum advantage for the vertical collector of approximately 16% would occur on the winter solstice. The values plotted are for the seven clear days in Table 2 for which complete data was available. For these seven days, the total energy incident on the vertical detector was 174 MJ/m^2.day, while that on the 60° detector was 159 MJ/m^2.day, giving a 10% seasonal advantage for the vertical collector.

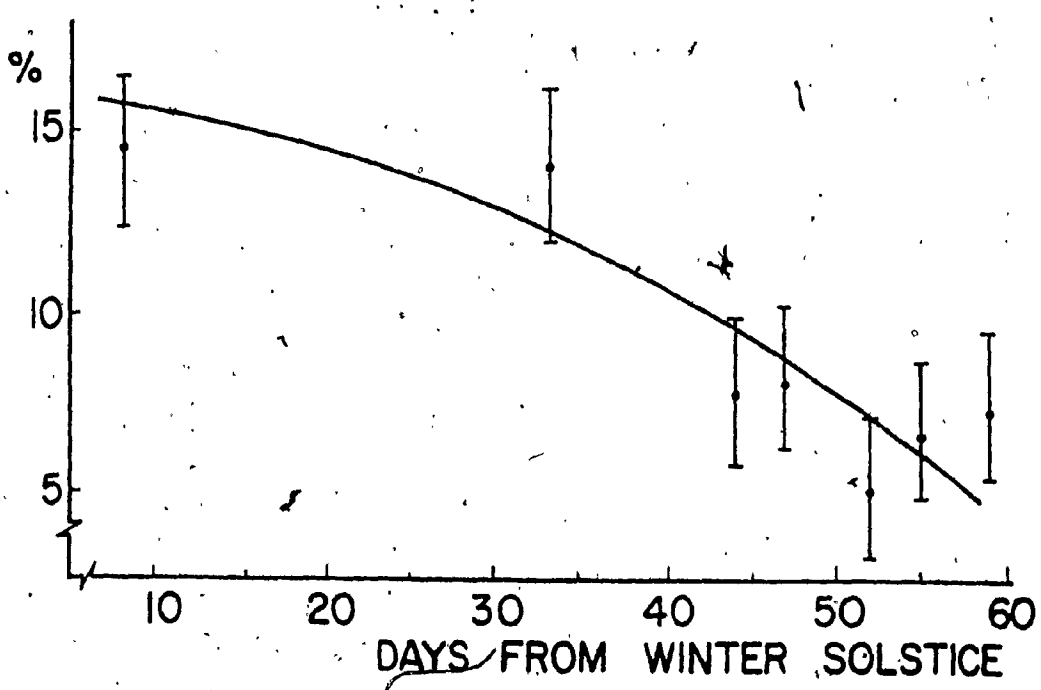

FIG. 15 - EXCESS OF MEASURED CLEAR DAY TOTAL DAILY RADIATION ON THE VERTICAL. $\left[\frac{\text{Vertical} - 60^\circ}{60^\circ}\right] \times 100$

NOTE : The vertical bars indicate the range of the percent excess for a 2% error in the vertical measurements.

2.4.2 Cloudy Days.

In addition to the clear day condition described above, there are also certain cloudy days on which useful solar heat energy may be collected. Cloudy days have been considered as either hazy or scattered cloudy. A hazy day is one in which a continuous low level of insolation is available to the collector (Fig. A.16). A scattered cloudy day is characterized by higher radiation peak values which are intermittent (Fig. A.17). A collector with low thermal mass is desirable on a hazy day. However, a collector with greater thermal mass will permit the collection of low temperature heat throughout a scattered cloudy day. The reduced losses under lower temperature operation on cloudy days will increase collector efficiency and the annual solar fraction.

The measured total daily radiation values on nine overcast days with enough radiation to cause fan operation were determined manually by tracing each data curve three times with a planimeter. The estimated maximum error is 2% with three repetitions. This was determined by comparing the maximum deviation with the average. These values for the vertical and the 60° tilted solarimeters are compared in Table 3. The percent difference varies between -8.5 and +14.2. It is evident that there is no consistent pattern in the variation within the scope of the data collected. (The only light measurements recorded were total radiation on the two solarimeters and no data is available which gives the distribution of the sky brightness for each cloudy day). Figures 14 & 15 show that the measured clear day radiation on the

vertical is consistently greater than on the 60° tilted surface for a 120 day period centered on winter solstice, when snow is present. For the nine typical cloudy days in Table 3, the total measured radiation for the two solarimeters was about equal. Thus, the seasonal advantage remains with the vertical collector, which is superior on clear days.

TABLE 3

CLOUDY DAY SOLAR RADIATION VALUES

DAYS FROM SOLSTICE	DATE	MEASURED RADIATION (MJOULES/m^2.DAY)			TYPE OF OVERCAST	THEORETICAL CLEAR DAY "SKY ONLY" (MJOULES/m^2.DAY)	
		1 VERTICAL	2 60°TILT	$\frac{1-2}{1}$x100%		VERTICAL	60°TILT
0	DEC 21					16	16
3	DEC 18	11(.4)*	11(.0)	3.7	scattered	16	16
7	DEC 28	14(.5)	14(.0)	3.4	scattered	16	16
10	DEC 11	12(.4)	12(.1)	2.2	scattered	16	16
12	DEC 9	12(.6)	12(.0)	4.6	scattered	16	16
13	JAN 3	13(.1)	13(.3)	-1.7	scattered	16	17
22	JAN 12	8(.8)	8(.9)	-1.4	scattered	16	17
45	FEB 4	8(.1)	8(.8)	-8.5	hazy	19	20
46	FEB 5	12(.4)	11(.4)	8.1	scattered	19	21
61	FEB 20	7(.6)	6(.5)	14.2	hazy	19	23

* Parentheses indicate 3-figure accuracy is questionable.

The last column of Table 2 gives the percent incident radiation augmentation due to snow reflection on the vertical solarimeter above the theoretical "sky only" value for a clear day. However, on a scattered cloudy day, the maximum instantaneous radiation on the vertical was often observed to be higher than the recorded clear day values near solar noon. This further radiation increase is believed to be due to the luminosity of white clouds added to the direct solar beam

when no clouds cover the sun. The increased instantaneous radiation due to the presence of clouds over that of a clear day with snow reflection was observed on twelve occasions to vary between 12% and 48%, and averaged 24%. An example of the actual recorded data is shown in Fig. A.18.

On February 8th, an experiment was conducted to determine the fraction of the total energy incident on the vertical solarimeter contributed by the snow foreground. Light from 23 metres of snow foreground (ten times the height of the solarimeter) was shaded from the vertical solarimeter by means of a 60 cm radius semicircular disk mounted in front of the solarimeter. The total measured insolation is then the sum of the actual direct and diffuse sky components plus a small amount reflected by the disk. The disk was of light-weight sheet metal and was coated with a flat black paint of low reflectivity.

The experiment was conducted under a uniform hazy sky with very light snow falling. Five instantaneous readings were made within three hours on either side of noon. The percent reflected light was observed to be between 22% and 37% with an average of 30%. This agrees well with the calculated augmentations in Table 2.

2.5 CONCLUSIONS

It has been shown that a vertical collector will receive more incident radiation than one tilted at 60° during the coldest winter months when light reflected from a snow covered collector foreground

is considered (c.f. Figs. 14 & 15). This enhancement was observed to be as much as 15% near winter solstice on a clear day (Fig. 15). There is no consistently significant difference on cloudy days (Table 3).

A collector built integral with a south wall is inherently easier to construct than one on a roof. As stated in Chapter 1, a cost advantage can be realized because the collector replaces the wall cladding and some insulation. Together with the incident energy augmentation due to the free snow reflector, a vertical collector appears to be the most favourable choice for northern latitudes.

CHAPTER 3

PERFORMANCE ANALYSIS AND RESULTS

3.1 INSTRUMENTATION AND CONTROLS

The data acquisition system consisted of four strip chart recorders using carbon-treated, pressure sensitive paper. The paper was 6 cm. wide and travelled at the rate of 2.54 cm. per hour. Each roll of paper lasted one month.

The choice of this system was made for several reasons. The recorders are mechanically and electronically reliable and can operate for several months without maintenance. Their purchase and operating costs are low and were within the budget allotted for equipment. They are lightweight and easily portable. (Since access to the house was at times difficult, this was an important consideration). Since no ink is used, they can neither run dry nor have information blotted out when unattended.

The four recorders were used to accumulate data as follows : two for solar radiation measurements; one for temperatures; and one for events. One solarimeter was installed at mid-collector height in the vertical position, and the other was at the top of the collector tilted upwards 60° from horizontal. The temperature recorder was modified to accommodate nine thermistor temperature sensing probes. Each temperature was recorded continuously for one minute, every twenty minutes. The thermistor locations were as follows : collector outlet air, collector inlet air, ambient air, bedroom air (2 m above floor),

kitchen air (3 m above floor) or collector air, and four storage temperatures (evenly spaced in the N-S direction at approximately the mid-depth of the rocks). Eight events were monitored: power failures, fan operation, and the six electric baseboard heaters. All the recorders, except the one monitoring the vertical solar radiation, operated during power failures as they were hooked up to an auxiliary 12-volt power supply.

A RHO SIGMA Model 12 differential thermostat was used to control the fan operation. The fan turned on automatically when the temperature in the collector was 10°C above the storage temperature, and turned off when the collector temperature dropped to within 2°C of the storage temperature. In this way, the fan did not operate unless the collector was hotter than storage. The air flow dampers at the base of the collector were controlled by the same thermostat, in parallel with the fan operation. A 12-volt battery power supply was used to drive the DC motor for the winch which moved the dampers. In the event of a power failure, the winch motor would automatically close the dampers.

There are several gaps in the data collected due to instrument and control failures. A voltage divider in the recorder which monitored the solar radiation on the 60° tilted solarimeter did not always operate satisfactorily. The cause of this malfunction was never determined; however, the erroneous data was easily identified and discarded. Frequent fan cycling occurred for about six weeks during February and March on clear days. This caused overheating of the

in the differential thermostat was discovered and repaired, which corrected this malfunction. Two types of sensors were used to monitor the baseboard heater events. Initially, a thermal switch was installed on the top panel of each heater. This was found to be unsatisfactory because of variable time lags between the heater and switch on/off times. On February 8th, 220 volt single pole relays were installed in the heater circuits to replace the thermal switches. A 24 volt D.C. power supply was connected through each relay switch to one of the event recorder inputs so that the recorder switched simultaneously with the heater current.

3.2 THEORY OF COLLECTOR EFFICIENCY

The instantaneous thermal efficiency, η_c, of a flat-plate solar collector is defined according to the first law of thermodynamics as the actual useful energy collected divided by the total solar energy incident on the collector aperture. In equation form :

$$\eta_c = \frac{Q_u}{A_c . I_c}$$

where :

η_c = collector efficiency

Q_u = total useful heat output of the collector

A_c = collector aperture area

I_c = total solar radiation incident on the collector per unit aperture area

The useful heat ouptut of the collector, Q_u, is determined by the product of the mass flow rate of the heat transfer fluid, $\dot{m}$, the specific heat of the heat transfer fluid, C_p, and the difference between the collector inlet and outlet temperatures, T_{in}, and T_{out}, respectively, such that :

$$Q_u = \dot{m}C_p(T_{out}-T_{in})$$

The instantaneous collector efficiency is often expressed in the form :

$$\eta_c = F_R\left[\tau\alpha - U_c\frac{(T_{in}-T_{amb})}{I_c}\right] \quad [21]$$

where :

F_R is the collector heat removal factor

$$F_R = \frac{\text{actual useful energy collected by a flat-plate collector}}{\text{useful energy that could be collected if the collector losses were the minimum possible}}$$

In equation form :

$$F_R = \frac{\dot{m}C_p\,(T_{out} - T_{in})}{\tau\alpha I_c - U_c(T_{in} - T_{amb})}$$

τ is the transmittance of the collector glazings

α is the absorptance of the collector surface

T_{in} is the inlet temperature of the collector fluid

T_{out} is the outlet temperature of the collector fluid

T_{amb} is the ambient air temperature

U_c is the collector heat loss coefficient

I_c is the incident solar radiation

The above equation is a convenient form for comparison with other collectors. The instantaneous efficiency, η_c, is often plotted against $(T_{in} - T_{amb})/I_c$, resulting in a straight line, where $F_R\tau\alpha$ is the y-intercept and $F_R U_C$ is the slope of the line.

The product $\tau\alpha$ is dependent on the angle of incidence between the collector and the solar beam, and is relatively constant over the range of incidence (less than 30°) specified in the ASHRAE Standard 93-77 [21] for testing collectors. The collector heat loss coefficient, U_c, is a function of the collector temperature and ambient conditions; however, it can be assumed constant for most flat plate collector efficiency plots within normal operating ranges.

3.3 CALCULATION OF COLLECTOR EFFICIENCY

The efficiency curve plotted in Fig. 16 is based on experimental data collected on nine days. The data points result from calculations made at 1100, 1130, 1200, 1230 and 1300 hours (solar time) on each of the days on which the instantaneous collector efficiency was determined. The data are selected symmetrically about solar noon in order to compensate thermal inertia effects. Table 4 contains the data used

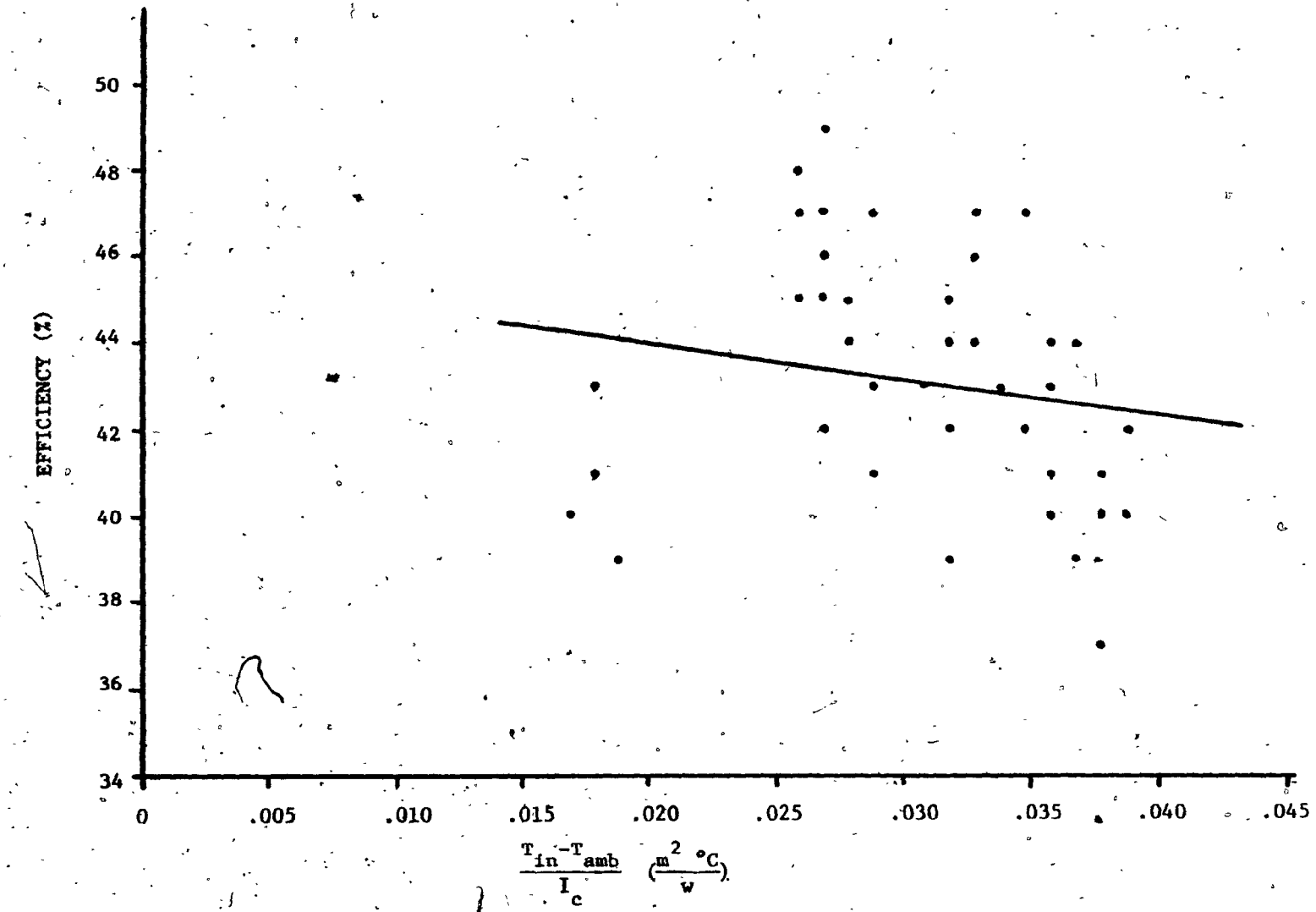

FIG. 16 - INSTANTANEOUS COLLECTOR EFFICIENCY PLOT

TABLE 4

INSTANTANEOUS COLLECTOR EFFICIENCY DATA

DATE	HOUR OF DAY	COLLECTOR TEMPERATURES		T_{amb} (°C)	I_c (w/m²)	η_c	$\frac{T_{in}-T_{amb}}{I_c}$ (m²°C/w)
		T_{in} (°C)	T_{out} (°C)				
JAN 16	11:00	22	38	-13	951	.39	.037
	11:30	23	41	-13	1002	.40	.036
	12:00	23	43	-13	1008	.43	.036
	12:30	24	43	-13	1002	.44	.037
	13:00	25	43	-13	977	.42	.039
JAN 23	11:00	19	38	-10	1011	.41	.029
	11:30	20	41	-9	1049	.44	.028
	12:00	21	42	-8	1065	.44	.028
	12:30	22	43	-8	1052	.45	.028
	13:00	22	43	-8	1017	.47	.029
FEB 3	11:00	23	41	-11	1046	.39	.032
	11:30	23	43	-11	1074	.42	.032
	12:00	24	45	-10	1090	.43	.031
	12:30	24	46	-10	1074	.44	.032
	13:00	26	46	-9	1046	.44	.033
FEB 6	11:00	24	42	-15	1033	.37	.038
	11:30	25	43	-14	1062	.39	.037
	12:00	25	44	-14	1071	.41	.036
	12:30	26	45	-14	1052	.40	.038
	13:00	27	45	-13	1017	.40	.039
MAR 9	11:00	19	34	4	882	.40	.017
	11:30	19	36	4	910	.40	.017
	12:00	20	36	3	917	.39	.019
	12:30	20	37	3	907	.43	.018
	13:00	20	36	4	882	.41	.018
APR 8	11:00	24	37	-1	709	.42	.035
	11:30	24	38	0	731	.44	.033
	12:00	24	39	1	740	.45	.032
	12:30	25	40	1	731	.46	.033
	13:00	25	40	2	709	.47	.033
APR 11	11:00	28	40	3	662	.41	.038
	11:30	28	41	4	687	.42	.035
	12:00	28	42	4	693	.43	.034
	12:30	29	42	4	687	.44	.036
	13:00	29	43	6	668	.47	.035
APR 20	11:00	29	41	12	611	.43	.029
	11:30	30	43	13	627	.46	.027
	12:00	31	43	13	636	.45	.027
	12:30	31	44	14	627	.48	.026
	13:00	31	44	15	605	.47	.027
MAY 6	11:00	25	35	11	539	.42	.027
	11:30	25	36	11	554	.45	.026
	12:00	26	37	11	561	.47	.026
	12:30	26	38	12	554	.47	.026
	13:00	26	38	12	536	.49	.027

to determine the efficiency curve plotted in Fig. 16. The equations and procedures used are described below. A sample calculation is given in section 3.3.3.

3.3.1. Mass Flow Rate

An experimental determination of the mass flow rate of air through the main duct was made on March 13th. As the sky was not sufficiently clear, a determination of the instantaneous collector efficiency was not possible on the day of the test. The volumetric flow rate of 2760 cubic metres per hour (m^3/hr) calculated from the measured data is the value used in all the efficiency calculations. Because of the complexity of the flow rate measurements, and the remoteness of the site, it was not possible to measure the actual flow rate on each of the nine sunny days. Thus, the procedure outlined in ASHRAE Standard 93-77 [21] requiring that the mass flow rate be determined concurrently with the other measurements necessary for instantaneous efficiency calculations could not be followed. The volumetric flow rate of 2760 m^3/hr is acceptable because the collector inlet temperature was within 1°K of the test temperature of 289.5°K during the entire test.

The mass flow rate was determined in a nearly square section (79 cm. high by 69 cm. wide) of duct midway between the rock storage bed and the fan at a distance of 36 cm. upstream of the fan air filter. Velocity measurements were recorded using an Alnor velometer. The pitot tube was placed in the duct facing the flow and pressure measurements were taken on a 30 point grid as shown in Fig. 17.

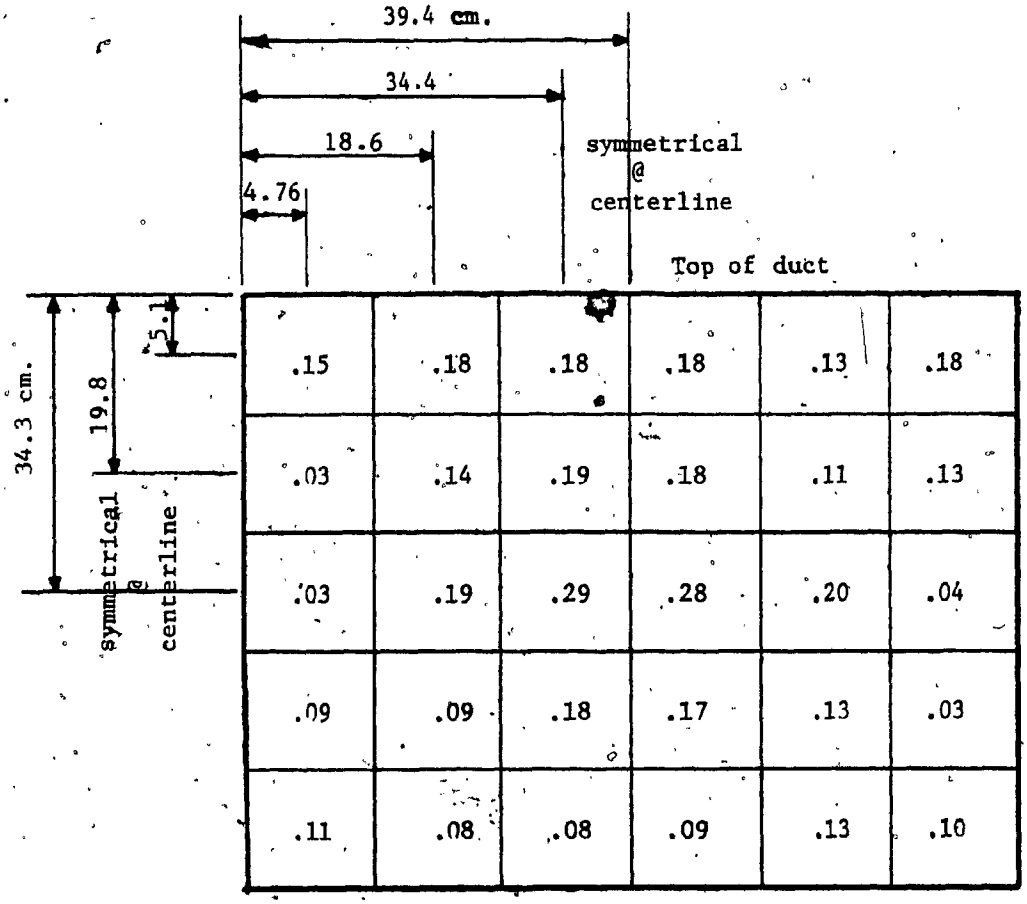

FIG. 17 - PITOT TUBE VELOCITY HEAD MEASUREMENTS

NOTES : Air flow direction is into page
Duct dimensions are in centimeters
The velocity heads, h_v, are in units of mm H_2O.

The air velocity at each point on the grid was determined from the equation :

$$V = 4.05 \frac{m}{sec} \sqrt{\frac{760}{B} \cdot \frac{T}{293} \cdot \frac{10350}{10350+h_s} \cdot h_v}$$

where :

B = barometric pressure (mm Hg)

T = absolute temperature (°K)

h_s = static head in duct (mm H_2O)

h_v = velocity head in duct (mm H_2O)

The static pressure head, h_s, was in the order of 2-3mm water gage and the correction of $10350/(10350+h_s)$ is taken as unity. The atmospheric pressure correction factor 760/B is also taken as unity. Hence, the velocity equation is reduced to :

$$V = 4.05 \frac{m}{sec} \sqrt{\frac{T}{293} \cdot h_v}$$

where :

T is the temperature of 289.5°K measured during the test. Substituting T into the above equation and simplifying yields :

$$V = 4.05 \frac{m}{sec} \sqrt{\frac{289.5}{293} \cdot h_v}$$

$$= 4.05 \frac{m}{sec} (.994) \sqrt{h_v}$$

$$V = 4.03 \frac{m}{sec} \sqrt{h_v}$$

The velocity at each point on the grid in Fig. 17 was determined using the above simplified equation. The average velocity through the .54 m^2 duct area was calculated to be 1.42 m/sec.

The mass flow rate is determined by the equation:

$$\dot{m} = \rho \cdot A \cdot V$$

The air density, ρ, was determined with a sling psychrometer as 1.2 kg/m^3. Thus, the mass flow rate, $\dot{m}$, is :

$$\dot{m} = \left(\frac{1.2 \text{ kg}}{\text{m}^3}\right)(0.54 \text{ m}^2)\left(\frac{1.42 \text{ m}}{\text{sec}}\right)\left(\frac{3600 \text{ sec}}{\text{hr}}\right) = 3340 \text{ kg/hr}$$

3.3.2 Useful Heat Collected

The specific heat of air is 0.24 kcal/kg°C.

The useful heat output of the collector can now be determined as:

$$Q_u = \dot{m}C_p(T_{out}-T_{in})$$

$$Q_u = \frac{3340 \text{ kg}}{\text{hr}} \cdot \frac{0.24 \text{ kcal}}{\text{kg°C}} \cdot \frac{4180 \text{ J}}{\text{kcal}} \cdot \frac{\text{W sec}}{\text{J}} \cdot \frac{\text{hr}}{3600 \text{ sec}} \cdot (T_{out}-T_{in})$$

$$Q_u = 933\ (T_{out}-T_{in})\frac{(W)}{(°C)}$$

3.3.3 Instantaneous Collector Efficiency

The instantaneous collector efficiency can be determined by :

$$\eta_c = \frac{Q_u}{A_c I_c} = \frac{933\ (T_{out} - T_{in})\ (W)}{41.67\ m^2\ I_c\ (°C)}$$

Expressing T_{out} and T_{in} in °C, and I_c in W/m^2, the efficiency, η_c, becomes dimensionless.

Example : From Table 4, η_c, for Jan. 16 at 11:00 a.m. is :

$$\eta_c = \frac{933(38-22)}{41.67(951)} = 0.39 \quad (39\%)$$

ASHRAE Standard 93-77 requires that wind velocity measurements be taken during the test. The wind speed measurements for Ste-Agathe-des-Monts are given in Table 5. (The Ste-Agathe wind values were used because local data was unavailable). Kerr has shown that the wind regimes are nearly identical at the two sites, whenever the wind is steady.

TABLE 5

WIND SPEED AND DIRECTION FOR THE EFFICIENCY CURVE ANALYSIS

DATE	TIME OF DAY		
	11:00 am	NOON	1:00 pm
JAN 16	17 (W)	17 (NW)	15 (WNW)
JAN 28	9 (NW)	11 (W)	11 (W)
FEB 3	11 (NW)	17 (WNW)	15 (WNW)
FEB 6	33 (WNW)	26 (NW)	19 (WNW)
MAR 9	6 (S)	4 (W)	17 (W)
APR 8	26 (WNW)	28 (WNW)	22 (NW)
APR 11	28 (WNW)	22 (NW)	22 (WNW)
APR 20	9 (NW)	4 (WNW)	calm
MAY 6	N/A	N/A	N/A

NOTE : Wind speeds are in km/h for Ste-Agathe-des-Monts, Québec.

3.3.4 Daily Collector Efficiency

The daily collector efficiency, η_D, is the "Calculated Heat Collected" divided by the "Total Daily Solar Radiation Measured on the Vertical Solarimeter". The Calculated Heat Collected, Q_u, is determined by the equation :

$$Q_u = \dot{m}C_p[\int T_{out}dt - \int T_{in}dt]$$

The value of $[\int T_{out}dt - \int T_{in}dt]$ was found by tracing the area between T_{out} and T_{in} by planimeter, when the fan was on. The maximum error with three repetitions was less than 2%.

The values of Q_u and η_D are given in Table 6. The values of "Total Daily Solar Radiation Measured on the Vertical Solarimeter", I_D, are given in Table 7. These were also determined by planimeter with a maximum error of less than 2%.

The average monthly efficiencies are the total monthly "Calculated Heat Collected" divided by the monthly total of the "Total Daily Solar Radiation Measured on the Vertical Solarimeter". These values are given in Table 8.

TABLE 6

CALCULATED HEAT COLLECTED, Q_u, (KWH)
AND DAILY EFFICIENCY, η_D, (%)

DAY	DEC		JAN		FEB		MAR	
	Q_u	η_D	Q_u	η_D	Q_u	η_D	Q_u	η_D
1	23	26						
2	84	38			82	34		
3			37	34	103	35		
4								
5					28	21		
6			20	27	88	31	20	33
7					75	31	20	38
8			15	22				
9	58	40			74	30	122	47
10	52	30	50	30	86	35		
11	51	35	70	31	132	44	58	45
12			14	14	81	39	66	29
13					135	46		
14	55	36			135	45		
15			74	34	139	47	63	31
16			82	35	66	37	36	25
17					131	44	97	40
18	40	31	58	30	108	36	93	40
19	22	22	40	23	101	36	91	37
20							89	36
21							78	33
22	43	33					84	38
23	16	22	77	35	21	20	71	33
24	37	30					55	31
25					105	40		
26								
27								
28	58	34			63	33	61	31
29	89	39						
30								
31								
TOTAL	628		537		1753		1104	

NOTE : Daily Efficiency $= \eta_D = \frac{Q_u}{I_D} = \frac{\text{Calculated Heat Collected}}{\text{Total Daily Solar Radiation Measured on Vertical Solarimeter}}$

TABLE 7

TOTAL DAILY SOLAR RADIATION MEASURED ON THE VERTICAL SOLARIMETER, I_D, (KWH)

DAY	DEC	JAN	FEB	MAR
1	87	8	37	65
2	219	9	238	33
3	29	152	291	31
4	7	50	91	29
5	5	45	135	13
6	27	73	288	61
7	N/A	40	241	53
8	7	67	61	34
9	144	47	247	262
10	173	168	243	31
11	144	224	297	130
12	13	98	207	224
13	13	22	291	68
14	154	5	299	30
15	19	217	298	204
16	39	235	178	144
17	19	15	296	244
18	128	195	302	232
19	100	173	282	245
20	39	43	85	244
21	33	15	57	239
22	129	59	N/A	223
23	73	223	107	217
24	125	53	50	175
25	12	12	264	56
26	36	18	54	68
27	50	32	32	109
28	169	25	191	195
29	226	28		10
30	29	26		39
31	12	31		16
TOTAL	2260	2408	5162	3724

TABLE 8

AVERAGE MONTHLY EFFICIENCY

	Q_u(KWH)	I(KWH)	η(%)
DECEMBER	628	2260	28
JANUARY	537	2408	22
FEBRUARY	1753	5162	34
MARCH	1104	3724	30
TOTAL	4022	13554	29%

3.3.5 Comparison with Previous Studies and Discussion of Results

Figure 18 is a plot of the instantaneous collector efficiency of the present study with the lines obtained by Hamilton and Kerr [2,3] for this collector. The efficiency results for the present study were obtained from data spanning five months. Although the data does not cover a wide range of $(T_{in}-T_{amb})/I_c$, the instantaneous efficiency is consistently within the range of 40 to 50%. This indicates that a desirable effect has been obtained from the modifications made to the system since the work of Hamilton and Kerr; that is, the collector efficiency has become less sensitive to variations in T_{amb} and I_c.

One major modification to the collector system is that the fan has been turned around to blow in the opposite direction from that of Hamilton's and Kerr's studies. There was a considerable amount of air leakage at the dampers and in the V-duct between the fan and the collector, which has been corrected. These leaks occurred before the fan in the previous studies, which meant that the air flow measured at the

fan was greater than the flow rate in the collector. Kerr used a mass flow rate of 2600 m^3/hr, which is about 6% less than the value of 2760 m^3/hr used in the present study. No measurements were made to quantify the effect of the leak plugging. However, from the amount of leak plugging that was done, it is apparent that the flow rate reported by Kerr should be reduced. Since collector efficiency is directly proportional to the mass flow rate, the instantaneous collector efficiencies reported by Kerr and Hamilton should be reduced accordingly.

The instantaneous efficiency calculations may be useful for comparing collectors but not for system analysis. The efficiency calculations for March 9th (c.f. Table 4) suggest that a misrepresentation of the instantaneous collector efficiency is possible if the data points are not selected appropriately. In a standard efficiency test, the collector inlet temperature is a closely controlled parameter. This was not the case at La Macaza because the inlet temperature was dependent on the storage temperature, and therefore on the amount of solar input in the preceding few days. Most of the days used in the instantaneous efficiency calculations (c.f. Table 4) were preceded by a day when energy was added to storage, resulting in a horizontally stratified temperature gradient in storage. However, March 9th was preceded by a period of about ten cloudy days when the storage dropped to a uniform temperature several degrees below its normal operating temperature. Hence, the response of the storage on March 9th was slower than on the other days and the collector inlet temperature remained almost constant during the efficiency test. The ambient temperature on March 9th was unseasonally high. This resulted in a

lower than usual value of $(T_{in}-T_{amb})$ for the appropriate I_c. Hence, the data points for March 9th are to the left of the main grouping in Fig. 18.

Curve A in Fig. 18 is for the data in Table 4, excluding March 9th. The slope of this line is similar to the result reported by Hamilton. Curve B includes the data of March 9th, and approximates the results of Kerr's investigation. The data of the present study did not cover as wide a range of $(T_{in}-T_{amb})/I_c$ as in the previous studies. However, the data in Table 4 covers a period of five months. The results of the present instantaneous efficiency determination indicate that the vertical collector will operate within the range of 40 to 50% efficiency near noon on clear days throughout the entire heating season. For design purposes, this type of collector characteristic is desirable, since the rest of the system can be optimized for a narrow range of operating conditions.

It has been shown that the instantaneous collector efficiency calculations produce results which are sensitive to the selection of appropriate data. The results indicate that this means of evaluating the performance of the collector at La Macaza is subject to large discrepancies, because the method does not consider the influence of system parameters explicitly. A more valuable indicator of the effectiveness of the solar collector in this real case, is through an analysis of the entire system performance. The contribution of the solar system to the total heating needs of the La Macaza house can be determined by an energy balance with the three main components of the house (i.e. the house, the collector, and the storage) considered explicitly. This analysis is treated in the following section.

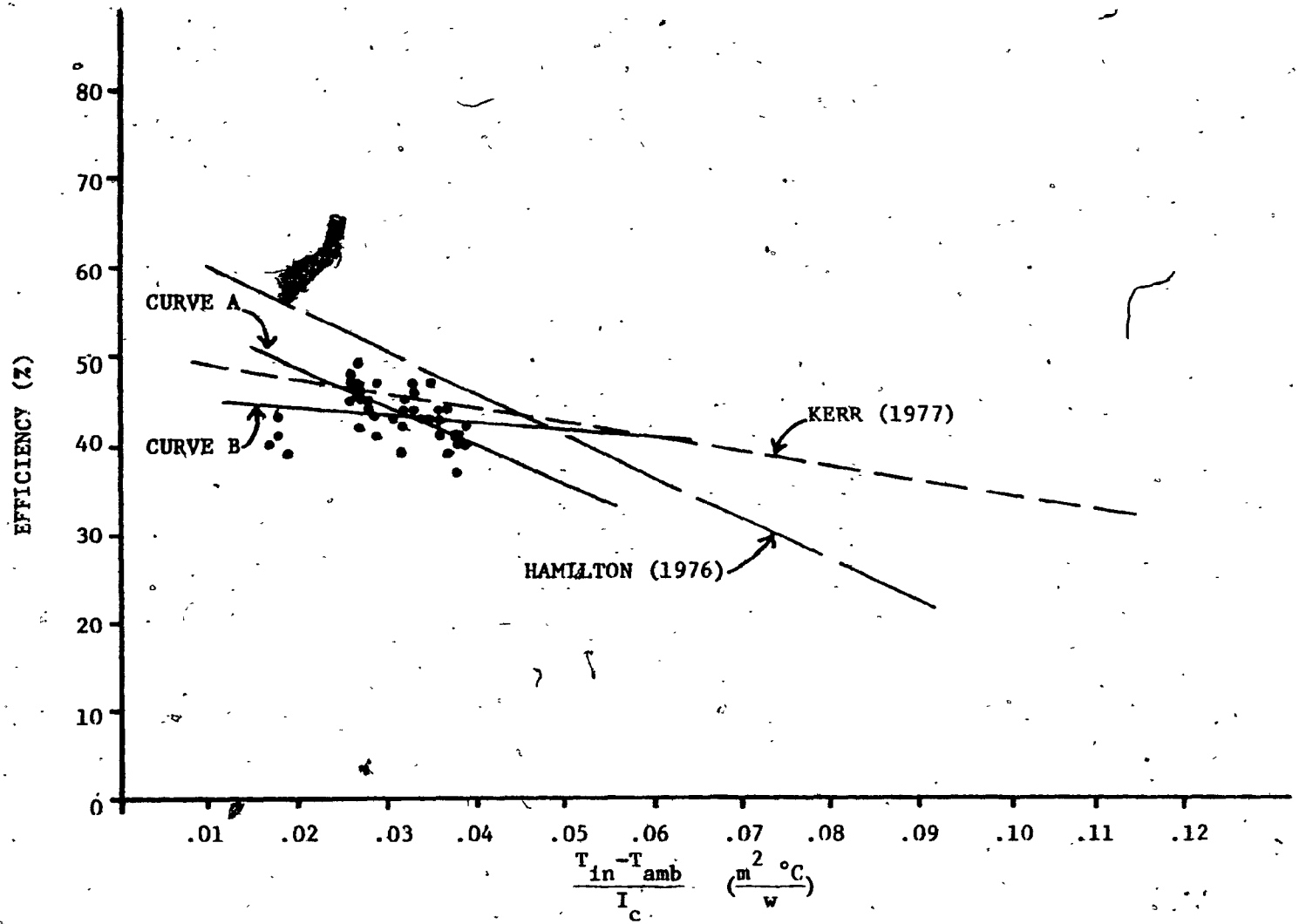

FIG. 18 - COMPARISON OF INSTANTANEOUS COLLECTOR EFFICIENCY WITH PREVIOUS STUDIES

3.4 HEAT BALANCE CALCULATIONS

The efficiency of the collector was presented in section 3.3. In some cases where solar collectors are "added on" to a building for space heating, the amount of solar heat supplied to storage or directly to the space on clear days can be estimated by the product of the incident solar radiation and the daily collector efficiency. In this case, the solar collector and storage are treated as one system and the space to be heated as another. However, at La Macaza, the collector and storage were built to interact with the house as a single system. Both the collector and the storage were oversized to provide a large amount of low temperature heat. This resulted in overheating of the house during a sunny period at the end of March, so energy was stored in the heat capacity of the walls and furniture of the house. The collector covers the entire south wall which results in heat being transferred directly to the living space by conduction. Heating the mass of this $40m^2$ wall contributes to internal comfort conditions by raising the mean radiant temperature, and also smooths out the daily fluctuations of the house temperature. Even though the south facing window area is less than $.5m^2$, a significant passive solar heat gain enters the house through the east and west windows.

For the purpose of determining the energy balance on the house, it is convenient to consider two base cases : 1) no solar input, low wind speed, minimal change in storage temperature; and 2) no electric baseboard input, large solar gain. Using the results obtained in 1) and 2), a third case with a combination of effects is considered. Two

days are examined which contribute heat to the space from the mass of the house which had previously been overheated. The daily electric baseboard heater inputs are given in Table 9.

TABLE 9

ELECTRIC BASEBOARD HEATER INPUT (KWH)

DAY	DEC	JAN	FEB	MAR
1	101	82	111	53
2	88	88	101	63
3	124	93	72	67
4	91	104*	96	66
5	88*	115	107	53
6	84*	112	90	59
7	95*	106	72	55
8	94	98	89	56
9	88	109	97	43
10	112	104	112	53
11	100	105	116	74
12	102	124	108	108
13	75	131	117	101
14	84	121	119	81
15	87	97	109	116
16	69	75	130	80
17	101	127	125	46
18	139	101	103	38
19	113	97	99	35*
20	120	99	103	30*
21	121	93	89	-
22	100	101	82*	-
23	88	73	80	-
24	79	80	67	-
25	93	81	72	-
26	88	71	89	36
27	110	64	74	91
28	105	64	49	43
29	75	85		43
30	98	100		41
31	86	108		33
TOTAL	2998	3008	2678	1564

* Data was unavailable; these values were determined by comparing to days with similar ambient weather conditions.

The monthly degree-day data for Ste-Agathe-des-Monts and for La Macaza are given in Table 10. The La Macaza data was derived from the Ste-Agathe values as follows. At Ste-Agathe, the data base is 18°C. During December, the La Macaza house temperature averaged about 22°C, therefore, 4°C are added for each day. The adjustment for January, February and March is 3°C. However, in March there was overheating in the house, particularly when the fan was operating. This accounted for an additional 64 degree days (°C).

TABLE 10

MONTHLY DEGREE DAY DATA

MONTH	STE-AGATHE-DES-MONTS (base 18°C)	LA MACAZA
December	868	992
January	927	1020
February	952	1036
March	623	780
TOTAL	3370	3828

The monthly wind speed and direction data for Ste-Agathe is given in Table 11. This is the data used for the La Macaza site.

TABLE 11

MONTHLY WIND SPEED AND DIRECTION AT STE-AGATHE-DES-MONTS

MONTH	WIND SPEED (km/hr)	DIRECTION
December	14	NW
January	13	W
February	14	NW
March	11	ESE

3.4.1 Case 1 : No Solar Input

On March 29th and March 31st, a negligible amount of solar radiation was measured on the collector. The daily wind speeds were low. The daily outside air temperatures were relatively constant, and the storage temperatures declined linearly through each 24 hour period. The only significant heat gains to the house were the electric baseboard heater input and the heat transfer from storage. The pertinent data used in the following calculations, for both days, are given in Table 12.

TABLE 12

HEAT BALANCE DATA FOR MARCH 29 & 31

DATE	MARCH 29	MARCH 31
Incident Solar Radiation on Collector (kwh)	10	16
Average Wind Speed and Direction (km/h)	12(variable)	8(west)
Daily Average Outside Temperature (°C)	1.9	5.8
Indoor Temperature (°C)	21	21
Electric Baseboard Heater Input (kwh)	43	33
Initial Mean Storage Temperature (°C)	30.0	25.6
Final Mean Storage Temperature (°C)	27.2	23.9

Kerr [3] has determined the heat transfer coefficient through the storage exterior walls and storage floor to be 14.4 w/°C (27.4 BTUH/°F). Assuming the storage to be at its average temperature throughout the day, and a ground temperature of 6°C, the heat loss from storage to ground on March 29th is :

$$Q_{s,g} = \left(\frac{14.4\ w}{°C}\right)\left(\frac{30.0 + 27.2}{2} - 6\right)\ (°C)\ (24\ hr) = 7.8\ kwh$$

Similarly, the storage to ground heat loss on March 31st is 6.5 kwh.

Kerr also determined the heat transfer coefficient through the wall between storage and the unheated basement to be 7.0 w/°C (13.2 BTUH/°F). During the days of March 29 and 31, the temperature of the storage adjacent to the interior wall was at the average storage temperature, that is, 28.6 and 24.75°C, respectively. Assuming the unheated basement temperature to remain constant at 9°C, the heat loss from storage to basement on March 29th is :

$$Q_{s,b} = \left(\frac{7.0\ w}{°C}\right)\ (28.6 - 9)\ (°C)\ (24\ hr) = 3.3\ kwh$$

Similarly, the storage to basement heat loss on March 31st is 2.6 kwh.

Kerr also gives the heat capacity of the storage as 9.4 kwh/°C (17.9 MBTU/°F). Therefore, the total heat loss from storage on March 29th is :

$$Q_{s,loss} = \left(\frac{9.4\ kwh}{°C}\right)(30.0 - 27.2)\ (°C) = 26.4\ kwh$$

Similarly, the total heat loss from storage on March 31st is 16.0 kwh.

The total heat loss from storage is the sum of the heat loss to the ground, the heat loss to the basement, and the heat transferred to the house, $Q_{s,h}$. In equation form :

$$Q_{s,loss} = Q_{s,g} + Q_{s,b} + Q_{s,h} \qquad (3.1)$$

Rearranging equation (3.1) and substituting the above values yields :

$$Q_{s,h} = 26.4 - 7.8 - 3.3 = 15.3 \text{ kwh} \qquad \text{(March 29)}$$

$$Q_{s,h} = 16.0 - 6.5 - 2.6 = 6.9 \text{ kwh} \qquad \text{(March 31)}$$

The total heat input to the house, $Q_{h,in}$, is $Q_{s,h}$ plus the electric baseboard heater input, plus the internal gain, Q_{int}. The internal gain was taken as 5 kwh per day for the data acquisition system and occasional lighting.

On March 29, $Q_{h,in} = 15.3 + 43 + 5 = 63$ kwh

On March 31, $Q_{h,in} = 6.9 + 33 + 5 = 45$ kwh

The overall heat transfer coefficient through the house envelope, $UA_{overall}$, can now be determined by dividing the total heat input to the house, $Q_{h,in}$, by the temperature difference across the envelope.

$$\text{On March 29, } UA_{overall} = \frac{63 \text{ kwh}}{(21 - 1.9)\ (°C)\ (24 \text{ hr})} = 137 \text{ w/°C}$$

$$\text{On March 31, } UA_{overall} = \frac{45 \text{ kwh}}{(21 - 5.8)\ (°C)\ (24 \text{ hr})} = 123 \text{ w/°C}$$

3.4.2 Case 2 : No Auxiliary Heat Input

The house was totally solar heated from March 21st to 25th. These five days were the only ones during which the electric baseboard heaters did not contribute any heat to the load on the house during the four months of December through March.

The total heat supplied to meet the load requirements of the house on these days was from three sources : 1) heat supplied by storage, 2) internal heat gains; and 3) passive solar heat gains through the windows.

The hourly temperatures of the ambient, the storage, and the inside of the house are given in Table 13 for March 22 and 23. The energy balance will be performed on each of these two days to determine the influence of each of the heat sources in satisfying the heating load requirements.

Figure 19 shows the daily variations of the storage, house, and ambient temperatures for the period of March 21st to 28th. On the first four days of this period, beginning on the 21st, the "Useful Heat Collected" was 78, 84, 71, and 55 KWH with daily efficiencies of 33, 38, 33 and 31%. During these days, the storage became fully charged and underwent a daily temperature cycle of a maximum of 43°C at 4:00 p.m. to a minimum of about 36° near 10:00 a.m. The ambient temperature underwent a similar cycle, peaking at about 17°C in mid-afternoon and reaching a night-time low of about -4°C near 4:00 a.m.

The mechanism by which stored heat was distributed to the house was by natural convection through standard duct grilles in the floor

above the storage. As the house was unoccupied, the manually operated grilles were not adjusted to account for temperature fluctuations in the house. Hence, overheating was observed in the bedroom during these four days on which heat was collected. The bedroom temperature cycled between about 26°C at 8:00 a.m. to 35°C at 4:00 p.m.

TABLE 13

TEMPERATURE DATA FOR MARCH 22 AND 23

HOUR OF DAY	MARCH 22			MARCH 23		
	$T_{ambient}$ (°C)	$T_{storage}$ (°C)	T_{inside} (°C)	$T_{ambient}$ (°C)	$T_{storage}$ (°C)	T_{inside} (°C)
1	-3	38	27	-3	41	29
2	-3	38	27	-3	40	28
3	-3	38	26	-3	40	27
4	-4	38	26	-4	39	27
5	-4	38	25	-4	39	26
6	-4	38	24	-4	39	26
7	1	38	24	-1	39	26
8	4	37	24	5	39	26
9	8	37	24	9	39	26
10	14	36	27	13	38	27
11	17	37	28	13	38	29
NOON	19	37	30	16	38	31
13	18	38	31	17	39	32
14	18	39	33	18	40	33
15	18	41	34	18	42	35
16	17	42	36	17	42	36
17	16	42	35	16	42	36
18	12	42	34	13	42	35
19	8	41	33	6	42	34
20	3	41	32	3	42	33
21	1	41	31	1	41	32
22	-1	41	31	0	41	31
23	-1	41	30	-1	41	31
MDNT.	-2	41	29	-1	41	29
AVG.	6	39	29	6	40	30

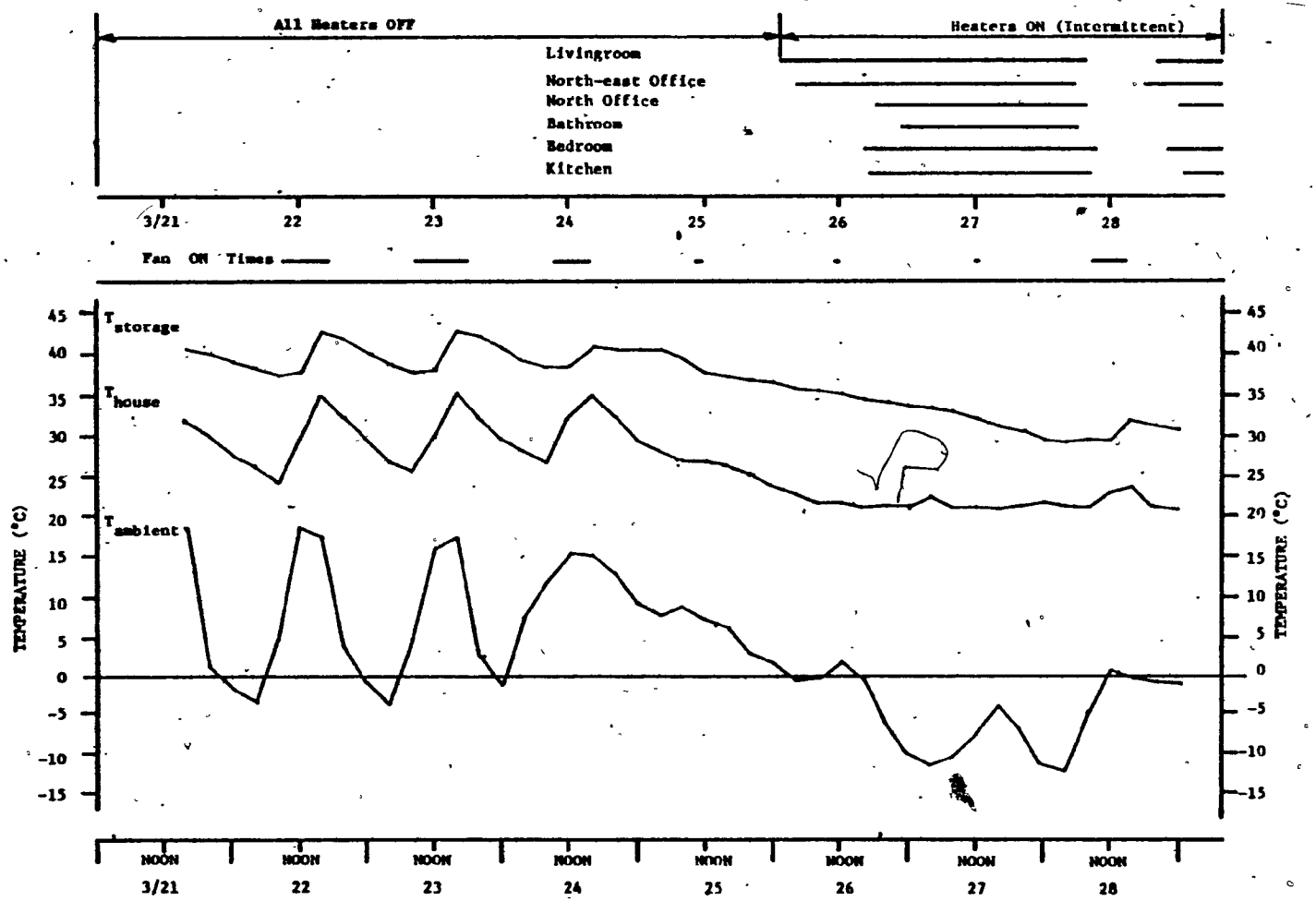

FIG. 19 - TEMPERATURE DATA, FAN AND HEATER EVENTS, FOR THE WEEK OF MARCH 21st

On March 22nd, 84 kwh of heat were collected. The 24 hour average storage temperature was 39°C. The storage loss to the ground was then:

$$Q_{s,g} = \frac{14.4 \text{ w}}{^\circ\text{C}} \quad (39 - 6) \ (^\circ\text{C}) \ (24 \text{ hr}) = 11 \text{ kwh}$$

The average temperature of the cold side of the storage was 38°C. Therefore, the storage loss to the unheated basement was :

$$Q_{s,b} = \frac{7.0 \text{ w}}{^\circ\text{C}} \quad (38 - 9) \ (^\circ\text{C}) \ (24 \text{ hr}) = 5 \text{ kwh}$$

The net heat stored over the 24 hour period is proportional to the increase in the storage temperature. There was a gain in stored heat of 21 kwh. Since 84 kwh were collected, the amount of energy consumed was 84 - 21 = 63 kwh. The losses to the ground and the unheated basement were 11 and 5 kwh, respectively. Therefore, the energy transferred to the house from storage was :

$$Q_{s,h} = Q_{s,\text{loss}} - Q_{s,g} - Q_{s,b}$$

$$Q_{s,h} = 63 - 11 - 5 = 47 \text{ kwh}$$

The total heat supplied to the house is the sum of the heat from storage, the internal gain, and the passive solar gain.

The passive solar gain has been determined for the afternoon of March 23rd as follows. The solar radiation incident on the west facing windows is plotted in Fig. 20. The hourly values are approximate and were determined in the following manner. Comparing the actual solar radiation measured on the vertical collector with the theoretical "sky only" values indicates that the augmentation of the daily integrated incident energy is about 4%. The hourly values in Fig. 20 were determined by multiplying the "sky only" radiation incident on a surface normal to the sun by the cosine of the angle of incidence with the west wall, and adding 4% for the augmentation. The total radiation incident on the west wall, calculated using simple trapezoids adjusted for the curvature, was 2.7 kwh/m^2 for the afternoon of March 23rd. Assuming 75% of this energy is transmitted through the double glazed west window area of 3.5m^2, the west window passive solar gain is approximately (.75)(2.7)(3.5) = 7 kwh. The east windows provide an equal amount in the morning. The "Total Daily Solar Radiation Measured on the Vertical Solarimeter" (c.f. Table 7) on March 23rd was 217 kwh. The passive heat gain through the south facing windows at the top of the collector is approximately 2 kwh. The total passive gain for the day is then 16 kwh. Therefore, the passive heat gain is approximately (16)/(217) = 7% of the total heat energy incident on the collector.

Returning to March 22nd, the total energy incident on the collector was 223 kwh. The passive solar gain was then (.07)(223) = 16 kwh. The internal heat gains of the house are assumed constant at 5 kwh.

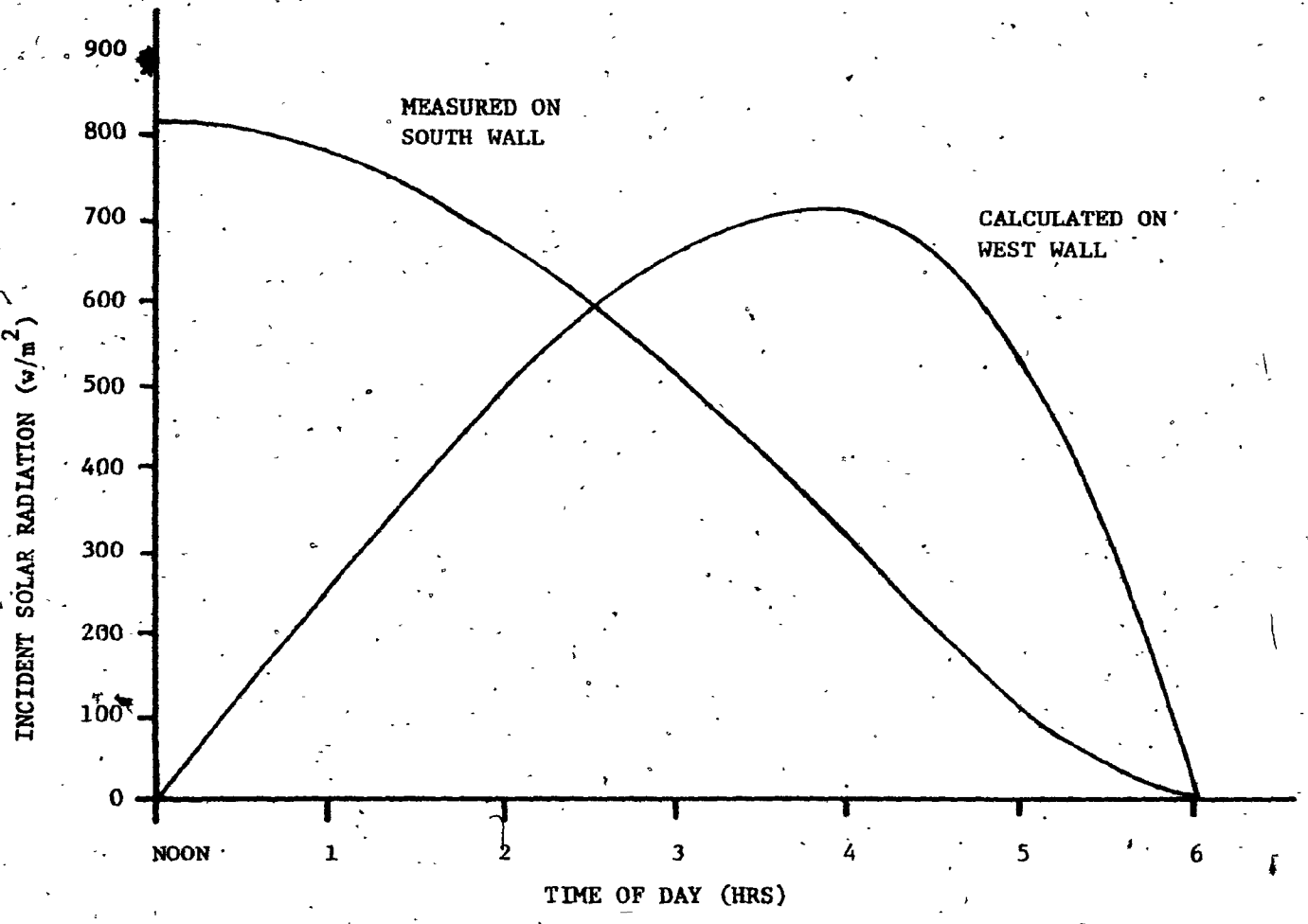

FIG. 20 – SOLAR RADIATION ON WEST AND SOUTH FACING VERTICAL SURFACES ON THE AFTERNOON OF MARCH 23rd

Therefore, the total heat input to the house on March 22nd can be determined as : $Q_{s,h}$ + (internal gains) + (passive solar gain) = 47 + 5 + 16 = 68 kwh.

The overall heat transfer coefficient can now be determined as :

$$UA_{overall} = \frac{68 \text{ kwh}}{(29 - 6)\ (^{\circ}C)\ (24 \text{ hr})} = 123 \text{ w/}^{\circ}C$$

Similarly, the total heat supplied to the house on March 23rd was 74 kwh, and the overall heat transfer coefficient is :

$$UA_{overall} = \frac{74 \text{ kwh}}{(30 - 6)\ (^{\circ}C)\ (24 \text{ hr})} = 128 \text{ w/}^{\circ}C$$

The pertinent data used in the heat balance for March 22 and 23 is given in Table 14.

TABLE 14

HEAT BALANCE DATA FOR MARCH 22 AND 23

DATE	MARCH 22	MARCH 23
Total Daily Solar Radiation Measured on the Vertical Solarimeter (KWH) (c.f. Table 7)	223	217
Daily Average Outside Temperature (°C)	6	6
Daily Average Indoor Temperature (°C)	29	30
Daily Average Storage Temperature (°C)	39	40
Storage to Ground Heat Loss (KWH)	11	12
Storage to Basement Heat Loss (KWH)	5	5
Calculated Heat Collected (KWH) (c.f. Table 6)	84	71
Storage Net Heat Gain (KWH)	21	0
Storage Heat Transferred to House (KWH)	47	54
Internal Heat Gains (KWH)	5	5
Passive Solar Gain (KWH) (7% of Total Daily Solar Radiation Measured on the Vertical Solarimeter)	16	15
Total Heat Supplied to House (KWH)	68	74

3.4.3 Case 3 : Combined Effects

The data collected on February 9th provides the information necessary to verify the analyses of the two base cases, i.e. no solar input and no auxiliary heat input. Due to the failure of the differential thermostat, as described in section 3.1, this was the only day on which complete and reliable data was available for the heat balance between February 8th and March 21st.

The morning was partly cloudy and the afternoon was clear. The total daily radiation measured on the vertical solarimeter was 247 kwh. Fifty-six percent of this amount was incident in the afternoon, and 44% in the morning. The wind was relatively constant from the north-west throughout the day, averaging 19 km/hr.

The data pertinent to the heat balance for February 9th is given in Table 15.

The passive solar gain was determined by the same procedure as for March 23rd. The augmentation due to reflection was 27%. The calculated passive gain was 15 kwh, or 6% of the "Total Daily Solar Radiation Measured on the Vertical Solarimeter". This agrees well with the value of 7% determined for March 23rd.

Using the data in Table 15, the overall heat transfer coefficient for February 9th, is :

$$UA_{overall} = \frac{153 \text{ kwh}}{(21 - (-17))\ (^{\circ}C)\ (24 \text{ hr})} = 167 \text{ w/}^{\circ}C$$

TABLE 15.

HEAT BALANCE DATA FOR FEBRUARY 9

DATE	FEBRUARY 9
Total Daily Solar Radiation Measured on the Vertical Solarimeter (KWH) (c.f. Table 7)	247
Daily Average Outside Temperature (°C)	-17
Daily Average Indoor Temperature (°C)	21
Daily Average Storage Temperature (°C)	31
Storage to Ground Heat Loss (KWH)	9
Storage to Basement Heat Loss (KWH)	3
Calculated Heat Collected (KWH) (c.f. Table 6)	74
Storage Net Heat Gain (KWH)	26
Storage Heat Transferred to House (KWH)	36
Internal Heat Gains (KWH)	5
Passive Solar Gain (KWH) (6% of Total Daily Solar Radiation Measured on the Vertical Solarimeter)	15
Electric Baseboard Heater Input (KWH)	97
Total Heat Supplied to House (KWH)	153

Two additional days are considered during which energy was added to meet the load on the house from heat stored in the thermal mass of the house. Kerr estimated the heat capacity of the house to be 2.5 kwh/°C (4.75 MBTU/°F) for the structural components. A reasonable estimate, including all furnishings, would be 3.5 kwh/°C. Due to the high level of solar heating and the warm ambient temperatures, the house became overheated between March 21st and 24th (c.f. Fig. 19). Although no solar heat was collected on March 25th, there was sufficient heat in storage and in the mass of the house to meet the load without any contribution from the baseboard heaters. The net heat transferred to the house from storage, $Q_{s,h}$, was calculated to be 31 kwh; the internal heat gain was 5 kwh, and the passive solar gain was 4 kwh, taken as 6½% of the incident radiation on the vertical collector. Because the house temperature had remained high for several days, it is assumed that the thermal mass of the walls and furnishings was at the inside air temperature. Figure 19 shows that the temperature of the house dropped by 5°C during the day of March 25th. This represents a transfer of heat from the thermal mass to the house air of approximately (3.5)(5) = 18 kwh; therefore, the total heat gain of the house to meet the load was 31 + 5 + 4 + 18 = 58 kwh. The average ambient temperature was 6.5°C and the average indoor temperature was 26°C. Therefore, the overall heat transfer coefficient was :

$$UA_{overall} = \frac{58 \text{ kwh}}{(26 - 6.5)\ (°C)\ (24 \text{ hr})} = 124 \text{ w/°C}$$

A similar situation occurred on March 26th. The energy gain due to heat lost from the mass of the house was 4 kwh. The storage contributed 24 kwh. The internal heat gain and the passive solar heat gain were each 5 kwh. The baseboard heaters added 36 kwh. Therefore, $Q_{h,in} = 4 + 24 + 10 + 36 = 74$ kwh, and :

$$UA_{overall} = \frac{74 \text{ kwh}}{(22.2 - (-1.8))\ (°C)\ (24 \text{ hr})} = 128 \text{ w/°C}$$

March 30th was similar to the days of Case 1, plus an additional amount of passive solar gain. The overall heat transfer coefficient was determined to be 118 w/°C.

3.4.4 Heat Balance Analysis

A heat balance was performed for 17 days. The overall heat transfer coefficient, degree days, and wind speed and direction are given in Table 16 for each day. The detailed analyses of the energy balance for the eight days of February 9 through March 31 were presented in sections 3.4.1 through 3.4.3. The overall heat transfer coefficients for the nine days of December 26 through February 8 were calculated using the same procedures as in the base case analyses. The pertinent temperature data is given in Table 17. Figure 21 is a plot of the daily overall heat transfer coefficient as a function of wind speed. Figure 22 is a plot of the daily overall heat transfer coefficient as a function of degree days. The lines drawn through the data are the least squares best fit straight lines obtained using the D.B.R. Curvfit program in the Grapple system for various groups of points, chosen for the following reasons.

TABLE 16

HEAT BALANCE SUMMARY

DATE	OVERALL HEAT TRANSFER COEFFICIENT (w/°C)	DEGREE DAYS (°C)	WIND SPEED AND DIRECTION (km/hr)
Dec. 26	144	26.9	12 W
Dec. 29	140	33.3	4.9 NW
Jan. 2	145	26.7	13.4 W
Jan. 21	163	28.2	17 E
Jan. 22	152	29.1	20.4 W
Jan. 26	144	20.0	16.4 N
Jan. 27	137	21.0	10.4 N
Jan. 29	155	24.4	19 NW
Feb. 8	154	33.0	10.5 N
Feb. 9	167	38.0	19 NW
Mar. 22	123	23.0	6 W
Mar. 23	127	24.0	7 ESE
Mar. 25	124	19.5	10 WNW
Mar. 26	128	23.8	19 W
Mar. 29	137	19.1	12 Variable
Mar. 30	118	19.0	9 ESE
Mar. 31	123	15.2	8 W

TABLE 17

TEMPERATURE DATA FOR DEC. 26 - FEB. 8 HEAT BALANCES

DATE	T_{inside} (°C)	$T_{ambient}$ (°C)	$T_{storage}$ (°C)	$\Delta T_{storage}$ (°C)
Dec. 26	21	-5.9	21	-
Dec. 29	21	-12.2	26.1	+6.1
Jan. 2	21	-5.7	21	-
Jan. 21	22	-6.1	23.8	-2.2
Jan. 22	22	-7.1	22	-
Jan. 26	22	2	22	-
Jan. 27	22	1	20	-
Jan. 29	22	-2.4	19	-
Feb. 8	21	-12	32.8	-4.4

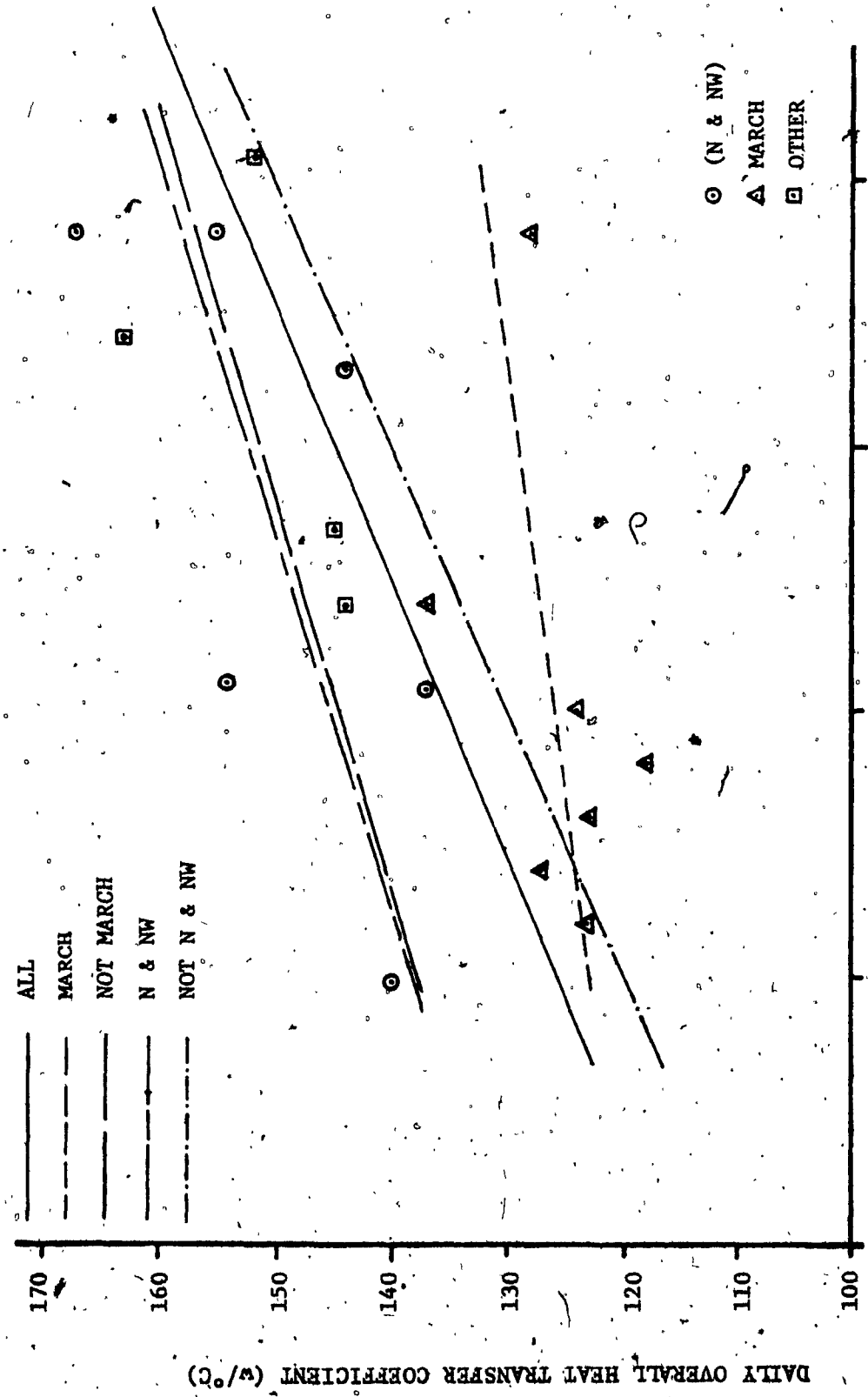

FIG. 21 - DAILY OVERALL HEAT TRANSFER COEFFICIENT AS A FUNCTION OF WIND SPEED

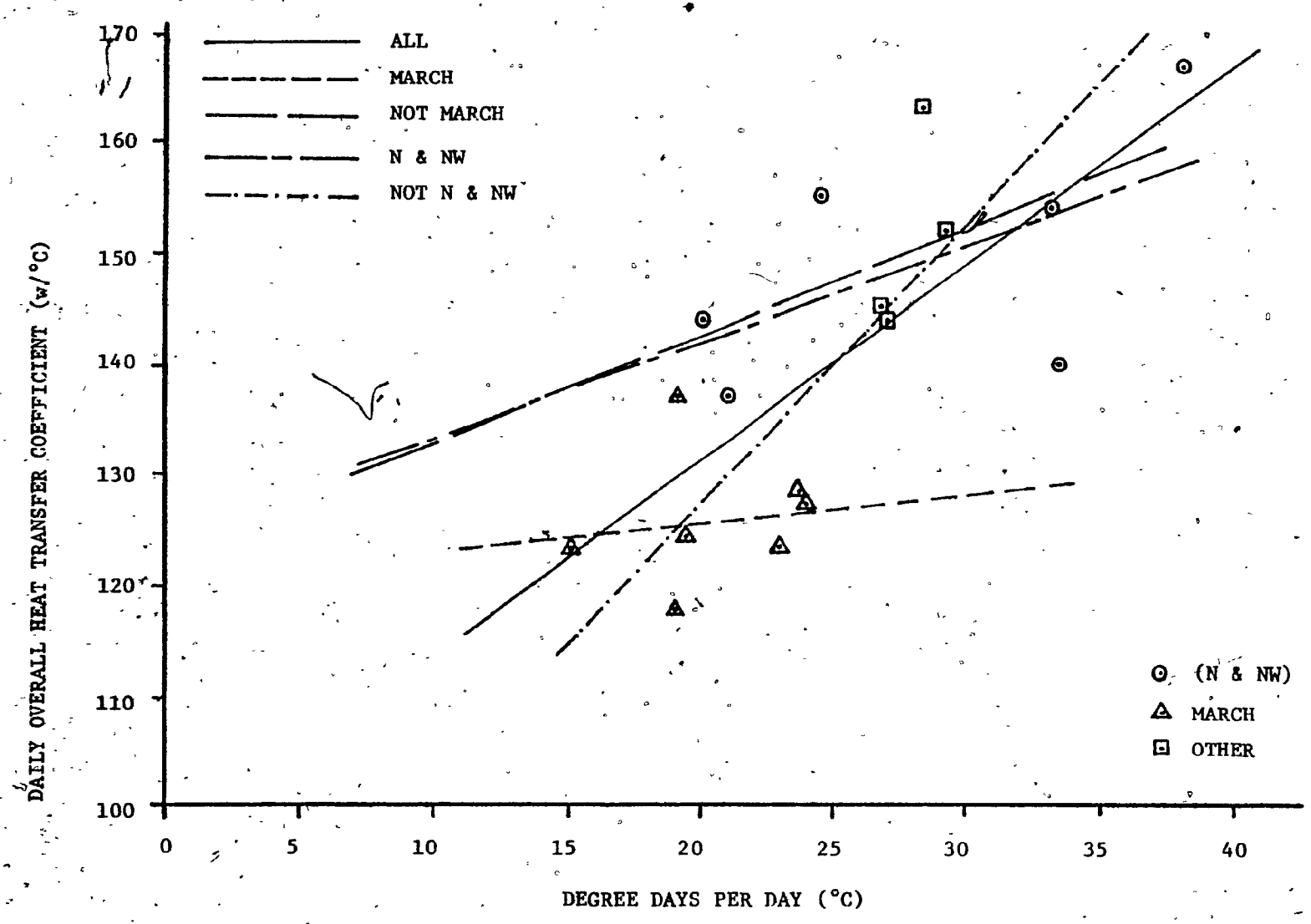

FIG. 22 - DAILY OVERALL HEAT TRANSFER COEFFICIENT AS A FUNCTION OF DEGREE DAYS

The four month average wind speed was 13 km/hr. From Fig. 21, the corresponding overall heat transfer coefficient is 141 w/°C. The corresponding value from Fig. 22 is 153 w/°C, based on a four month average of 31 degree days (°C) per day. The average value is (141+153)/2 = 147 w/°C with a relative agreement of 8.2%.

Examination of the degree-day and wind data shows that a distinction can be made between the first three months and March. The average degree-day value for December, January and February is 1016 degree-days/month, with a maximum difference of -2.4% from the mean, in December. The March value is 23% below the three month mean. The average wind speed for the first three months is 14 km/hr from a north-westerly direction, while in March the average wind was 11 km/hr from a south-easterly direction.

Table 18 is a summary of the overall heat transfer coefficient data plotted in Figs. 21 and 22 according to the degree day and wind direction distinctions made above. There is a good relative agreement between the degree day and wind direction analyses for each of the four cases examined, ranging from 1.6 to 4.6% of the mean. The mean values for the "Days other than March" (152.5) and the "Wind from N and NW" (151.5) agree to less than 1%. This suggests that the data days selected from the months of December, January and February represent the average values for these months well. The relative agreement between the mean values of the "March days only" (127) and the "Wind not from N and NW" (139.5) is 9.4%. Thus, a major portion of the 8.2% difference of the seasonal average heat transfer coefficient can be

TABLE 18

OVERALL HEAT TRANSFER COEFFICIENT SUMMARY

	FROM FIG. 21 (W/°C)	FROM FIG. 22 (W/°C)	MEAN (W/°C)	% DIFFERENCE FROM MEAN
All 17 days	141	153	147	8.2
March days only	126	128	127	1.6
Days other than March	149	156	152.5	4.6
Wind from N and NW	149	154	151.5	3.3
Wind not from N and NW	138	141	139.5	2.2

due to a poor selection of the March data. (This is evident from Table 16 which shows only two of the seven days selected are consistent with the monthly average wind direction, and these are below the average wind speed). However, the repair of the differential thermostat was not made until March 21st (section 3.1) and data before this date is unreliable for an accurate heat balance. Although these days of March are not representative of the monthly average, they provided unique data (i.e. the electric baseboard heaters were off for five consecutive days) for the base case analyses (sections 3.4.1 and 3.4.2).

Figure 23 shows the influence of wind speed and direction, and temperature on the overall heat transfer coefficient. It is a plot of selected groups of data from Fig. 21 without the days of January 21, and March 23, 29 and 30.

Lines 1 and 2 are least squares fits for points with winds only from the north and north-west. The two sets of data were chosen for degree days below room temperature of about 35°C and 22°C. The lines are approximately parallel and their slope indicates that an increase in wind speed of 10 km/hr results in an increase in the loss coefficient of about 20 w/°C, for a given temperature difference across the building envelope. A portion of this increase is due to the greater pressure difference across the envelope which increases the infiltration of outside air. For a given wind speed, a decrease of ambient temperature also increases the infiltration loss coefficient by enlarging the cracks in the walls. Although there is only one small window in the north wall, the spruce timbers and oakum caulking used in the wall construction are susceptible to considerable contraction at low outside temperatures. This results in a large air flow path for infiltration.

The change in infiltration loss due to an increase in wind speed is not as great in the case of a west wind (curves 3 & 4). The loss coefficient increases by about 8 w/°C for an increase in wind speed of 10 km/hr, for a given temperature. Part of the reason for this is that the west wall is already quite leaky due to the large window and door areas. There was no outer door on the vestibule and the inner door was not weatherstripped well.

Normalizing the loss coefficient for all wind speeds does not result in a corresponding normalized loss for degree days. While part of this discrepancy is due to increased crack widths in the walls with

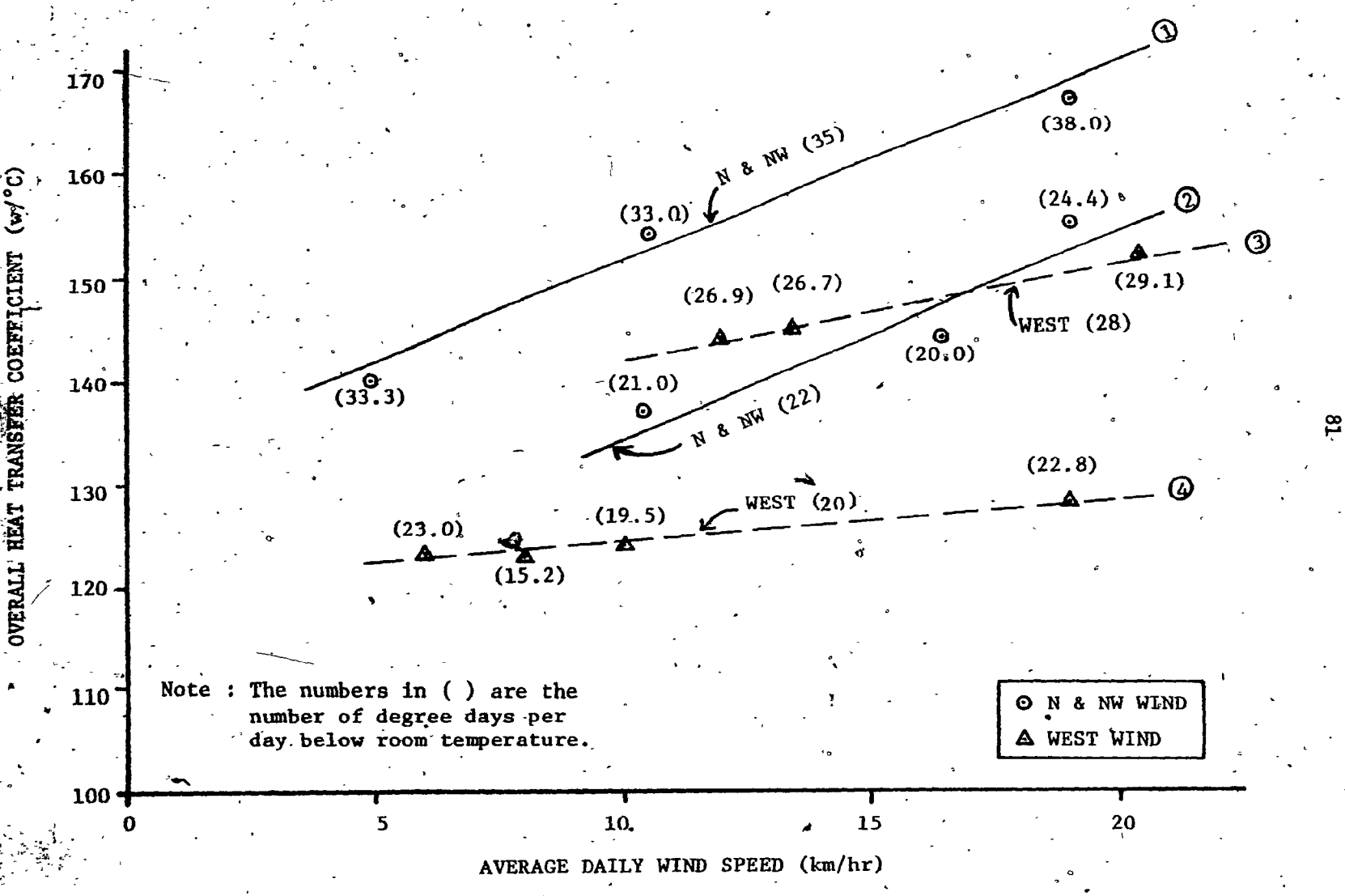

FIG. 23 - OVERALL HEAT TRANSFER COEFFICIENT AS A FUNCTION OF WIND SPEED, FOR A GIVEN WIND DIRECTION AND AT A GIVEN TEMPERATURE DIFFERENCE

lower outside temperatures, there are other factors which contribute to the higher losses with an increase in the number of degree days. Night-time radiation from the house to a clear sky will increase with temperature difference, independent of wind speed. There is insufficient data to quantify this loss. It is difficult to know if the roof was covered in snow or if the sky was clear on a particular night, based on the available data. The higher temperature in the peak of the roof will result in higher transmission losses which are less affected by the wind due to shielding by the collector. There was a 10 cm diameter vent in the bathroom which provided a thermosiphon stack to induce infiltration partly independent of wind.

3.5 OVERALL SYSTEM PERFORMANCE AND ECONOMICS

There are several ways to measure the performance of a solar heating system. The ultimate criterion used to evaluate the feasibility of using solar energy to meet the heating needs of a building is economic viability. The life cycle cost of the installed solar system should be offset by the cost of the conventional energy resources saved in the future. The "Solar Fraction" is a term commonly used to express the percentage of conventional energy which is replaced by solar energy. In a standard residential application, the solar fraction can be determined simply as :

$$SF = \frac{\text{Heating Load} - \text{Conventional Fuel Input}}{\text{Heating Load}}$$

The heat contributions due to occupancy (i.e. appliances, lighting, people, etc.) are assumed to be the same whether or not solar heating is used, and can be a significant portion of the total heat input. They are not included in the heating load. The heating load is the sum of the solar and conventional fuel inputs.

During the winter of the present study, the house at La Macaza was unoccupied. The heat which would normally have been supplied due to occupancy was supplied by the electric baseboard heaters. Thus, using the above equation to determine the solar fraction without modification would result in an unfair assessment of the solar system under normal operating conditions (i.e. with occupancy).

Now, the total seasonal heating load can be expressed as the sum of the active solar heat collected, the electric baseboard heater input, the passive solar heat gain through the windows, and the internal heat gains. The total solar heat collected (c.f. Table 6) during the four months was 4022 kwh. The storage losses were calculated to be 913 kwh, based on an average storage temperature of 22°C. Therefore, the net heat collected was : 4022 - 913 = 3109 kwh. The four month total electric baseboard heater input was measured as 10248 kwh (Table 9). The passive solar gain is approximately 6% (see section 3.4.2) of the total solar radiation incident on the collector (Table 8), or (.06)(13554) = 813 kwh. The internal gain was taken as 5 kwh per day for the data acquisition system and occasional lighting. Therefore, the total seasonal heating load can be determined from the sum of the heat inputs as : 3109 + 10248 + 813 + 5(121) = 14775 kwh per season.

The overall heat transfer coefficient for the house can now be determined using the total degree-days from Table 10 as : 14775 kwh/ 3828 degree-days = 3.86 kwh/degree-day, or 160 w/°C. This agrees within 9% to the mean value of 147 w/°C determined in the heat balance analysis (section 3.4.4 and Table 18). The relative agreement with the degree-day analysis in Fig. 22 is wfthin 5% of the value of 153 w/°C.

In order to determine the fraction of the heating load which would be supplied by the solar heater in an actual situation (i.e. if the house had been occupied) an assumption must be made about the internal heat gains due to occupancy. In order to compare with Kerr's study, his figures for internal gains were used.

Based on actual current measurements, Kerr reports that 3600 kwh of heat were generated within the house due to occupany by two adults during the three months of October through December, 1976. A value of 4800 kwh will be used here for the four month period of December through March. The heating load is then 14775 - 4800 = 9975 kwh, and the electric baseboard heater input required for heating is (10248 + 605) - 4800 = 6053 kwh. Therefore, the solar fraction is :

$$(9975 - 6053)/(9975) = 40\%$$

The solar fraction of 40% was determined by extrapolating Kerr's data for the internal heat generated when the house was occupied by two adults for three months in the winter of 1976. However, the solar

fraction can be quite sensitive to the amount of heat generated due to occupancy. Sonderegger [22] has reported the results of a study of energy consumption patterns in over 200 residences through two winters in the New Jersey climate. He found that 46% of the total energy consumed was related to occupancy, and that 71% of this amount was dependent on individual behaviour patterns.

Since the house at La Macaza was unoccupied during these measurements, the total energy input gives a good indication of the minimum heating requirement of the house. Figure 24 is a plot of the expected solar fraction for various internal gains.

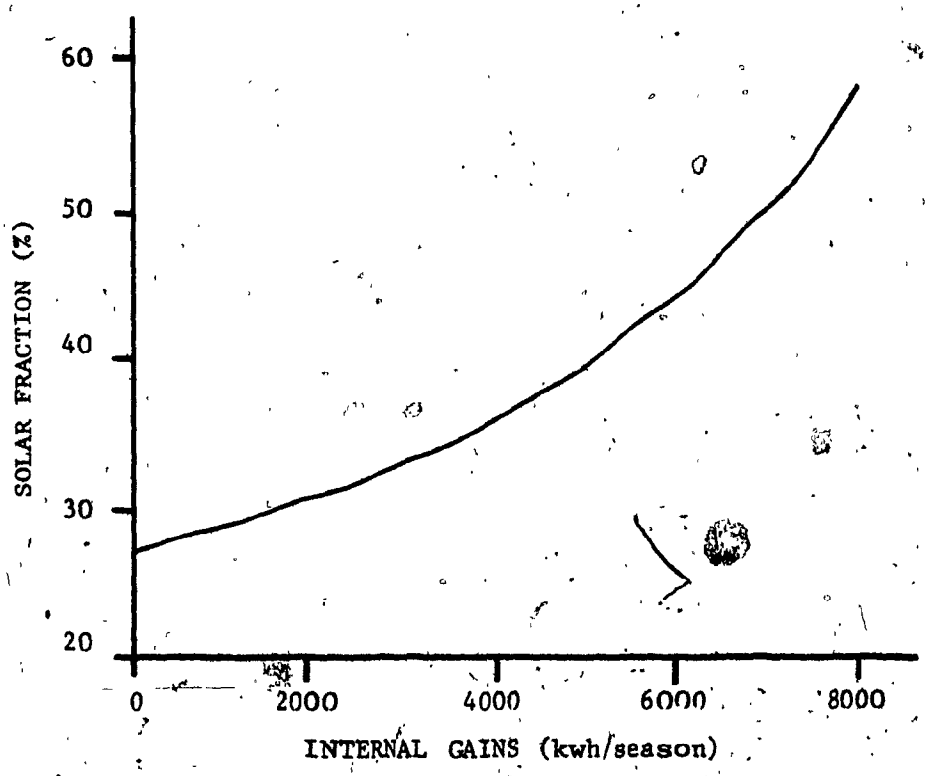

FIG. 24 - SOLAR FRACTION AS A FUNCTION OF INTERNAL GAINS DUE TO OCCUPANCY

The seasonal heating load with normal occupancy has been calculated above as 9975 kwh. At the current (1980) Hydro-Québec domestic rate of $0.027 per kwh, the cost of heating with electricity alone would be (0.027)(9975) = $270, for the four months of this study. Using the solar fraction of 40%, the saving with partial solar heating is (.40)(270) = $108.

The zero wind intercept of the heat transfer coefficient line (Fig. 21) is 116 w/°C. The heat loss on an average winter day (31 degree days per day, and 13 km/hr wind) is about 150 w/°C for a north or west wind, in Fig. 23. Therefore, the increase in the heat transfer coefficient due to wind from the north or the west for the average winter day is estimated as 150 - 116 = 34 w/°C. The increased loss approximates the effect of air infiltration due to wind. A rough figure for the total seasonal heat loss due to wind infiltration would then be :

$$\frac{34 \text{ w}}{^\circ\text{C}} \cdot \frac{31^\circ\text{C day}}{\text{day}} \cdot 121 \text{ days} \cdot \frac{24 \text{ hrs}}{\text{day}} = 3060 \text{ kwh}$$

The major portion of this loss is through the north wall and the west door entrance. It is reasonable that the installation of an air barrier on the north, east and west walls and proper sealing of the west door could reduce this loss by about two-thirds. The heating load would then become 9975 - 2040 = 7935 kwh. This reduction in the heating load would reduce electricity consumption from 6053 to 4013 kwh, a saving of $55 for the four months of the study. It is reasonable that the cost of these improvements to the house could be paid

for in one or two seasons by the electricity savings. Beyond that time, the annual savings could help offset the cost of the solar system. The solar fraction with the reduced heating load is :

$$\frac{7935 - 4013}{7935} = 50\%$$

CHAPTER 4

DISCUSSION OF RESULTS AND CONCLUSIONS

The Snow Reflector

The "rule of thumb" optimum tilt angle of a solar collector for winter heating is generally taken as the latitude plus 15 degrees. A collector tilted at 60° will always receive more "sky only" incident radiation than a vertical one at La Macaza, 46° 24' north latitude (Fig. 14). However, when reflections from a snow covered foreground are included, the total daily radiation on a vertical collector will be greater on a clear day during most of the heating season (Fig. 14). The augmentation of incident energy due to the extra light reflected and scattered from the snow was in the order of 35% above the theoretical clear day "sky only" value for the vertical solarimeter (Table 2). The measured total daily radiation was greater on the vertical than on the 60° tilted surface by as much as 16% on clear days during a 60 day period after winter solstice (Fig. 15). The same enhancement would occur for 60 days before solstice when snow is present.

There was not a significant difference between the incident radiation on either surface on cloudy days. An experiment conducted on the vertical solarimeter under hazy sky conditions indicated that approximately 30% of the incident light was due to snow reflections.

It has been shown that a vertical collector with ground snow reflection has a seasonal advantage for winter heating over a roof

mounted 60° tilted collector. Savings in capital cost are achieved when the collector is built integrally with a south facing wall, because it is easier to build there than on the roof, no special supports or anchors are required, and no special waterproofing techniques are needed around the collector or its anchors. In addition, the air handling system can be much simpler, shorter and cheaper with a wall collector.

Instrumentation and Controls

The details of the monitoring were described in Section 3.1. The simplicity of the data acquisition system resulted in reliable data collection, even though the house was unattended for several weeks at a time. The data proved adequate for many of the studies undertaken. The lack of on-site wind measurements restricted the accuracy of some of the detailed analyses. However, the Ste-Agathe data was adequate for forming general conclusions regarding wind effects on the house. (Kerr has shown that on days with steady winds, the direction and velocity of the wind is nearly identical at the two sites). A detailed energy balance across the collector was not done. More temperature and air flow measurements would be desirable in future studies.

The Collector

The instantaneous collector efficiency was calculated at half hour intervals near noon for nine days. The results indicate that the collector efficiency was uniformly high, regardless of variations in

the ambient temperature and the incident solar radiation. During the five months of January through May, the efficiency was consistently within the range of 40 to 50%. The two curves (A & B) plotted in Fig. 18, for the present study, indicate that system parameters, such as the storage temperatures, can have a considerable effect on the calculation of instantaneous collector efficiency. When testing an installed collector, selection of data should include consideration of the storage temperature history, particularly within one or two days prior to the test. A detailed discussion of the efficiency calculations was presented in Section 3.3.5.

The direction of the air flow in the collector was reversed in order to increase the instantaneous efficiency. By reversing the flow from that of Kerr's investigation, the collector inlet temperature was reduced. Kerr's inlet temperature was at the average storage temperature because he had a nearly isothermal storage. With the stratified storage of this study, the coldest storage temperature was the temperature of the inlet air to the collector. Reducing the inlet temperature increases the efficiency by reducing the collector losses. In addition, the inlet air is now closest to the glazing rather than the hotter outlet air, further reducing the glazing losses. Figure 18 shows that Kerr's instantaneous efficiency was approximately equal to the results obtained in this study. The reasons why the measurements do not support the theory are not clear, because there were several differences between the experiments. Kerr calculated an average monthly efficiency of 34% for the four months of December through

March, by dividing the total heat collected by the total incident radiation on the collector. He did not use the days on which there was less than 40 kwh incident radiation. Subtracting these days, in the present study, the value of I_D in Table 8 becomes 12634 kwh, and the monthly efficiency is 4022/12634 = 32%.

Based on this comparison of results, there does not appear to be an improvement in the performance of the collector. However, reducing the inlet temperatures should produce a positive effect. Also, the leak plugging that was done in the duct (section 3.3.5) indicates that the mass flow rate Kerr used in his collector calculations may have been higher than the actual flow rate. An additional source of error in the comparison is that the collector inlet and outlet temperature sensors were not in the same location during both studies.

The Storage

Due to the air flow being reversed from that of Kerr's investigation, and because the thermal blanket was installed over the south two-thirds of the rocks, the storage became stratified. By the end of a sunny day, the temperature of the north end of storage was typically 5 to 8°C warmer than the south end. This produced two favourable effects for night time heat distribution. First, the horizontal temperature gradient in the storage induced convective flow to the living quarters through the insulated floor joist ducting. The return air to storage was through the fan duct to the cold end of the storage. Secondly, the higher temperature at the north end of storage accentuated

a natural convection flow directly to the north wall baseboard registers in the bedrooms. This flow was partly induced by putting extra insulation on the south 3/4 of the bedroom floor above storage. When the storage was charging the north 1/4 of the bedroom floor heated up more quickly than the south 3/4, causing a convection loop within the bedrooms. This flow within the bedrooms induced a flow of warm air from the north end of storage with a return flow of cooler air to the south end through baseboard registers at the interior walls. The heat loss from the storage was calculated to be 913 kwh. This is about 23% of the total heat collected of 4022 kwh. This loss could be reduced by improving the storage insulation.

The Energy Balance

An energy balance on the entire system (i.e. the house, the collector, and the storage) was presented in Section 3.4. The overall heat transfer coefficient of the house was determined for 17 days both as a function of wind speed and direction (Fig. 21) and of degree-days (Fig. 22). The results agreed to less than 9% with the seasonal value of 160 w/°C calculated in Section 3.5.

This value of 160 w/°C is about 40% higher than Kerr's simulation model prediction. About 20% of Kerr's value was attributed to infiltration due to wind and half of this was through the west entrance. A major source of infiltration heat loss in this study was the entrance door on the west side of the house. The door on the outside of the vestibule during Kerr's study had been removed prior to this

investigation and was never replaced. The inner door was poorly sealed and it is possible that infiltration through this door was two or three times Kerr's predicted value.

The effects of wind speed and direction on the overall heat transfer coefficient were presented in Fig. 23. The results of the analysis indicated that the infiltration heat loss due to a north wind is greater than for a west wind, at a given ambient temperature. A decrease in the ambient temperature causes contraction of the north wall log construction, which further increases the loss coefficient by increasing the air flow path for infiltration.

Another source of the disagreement between Kerr's prediction and the calculated values of this study is the existence of thermal bridging at the roof rafters. Rigid insulation was placed between the rafters, but they were in direct contact with the roof deck. Loose fitting insulation would result in heat flow paths along the rafter edges with a thermal resistance equivalent to that of the plywood decking and metal roofing. Severe condensation which occurred on the ceiling of the sloped portion of the roof is evidence of the poor thermal resistance of that area. Kerr predicted 25% of the total heat loss of the house was through the roof. Because of the thermal bridging, cracks between the insulation and rafters, and the higher temperatures at the peak of the roof, it is reasonable that Kerr predicted roof loss factor could be doubled. This would result in the roof losses being about 35 to 40% of the total house losses. This would increase Kerr's predicted overall heat loss value by about 10%.

There is insufficient measured data to make a conclusive comparison between Kerr's simulation and the performance of the house calculated in this study. However, it is likely that the infiltration and thermal bridging effects are the major sources of discrepancy between the values reported in the two studies. The heating load can be reduced by improving the insulation near the rafters, by installing an air barrier and improving the weatherstripping. These measures can be cost effective, with payback in one or two years. The solar fraction can increase to more than 50% with these improvements.

REFERENCES

1. McCloskey, B., "Appropriate Building and Energy Systems for Quebec Indian Communities," Final Report by Shelter Systems Group, McGill University, 1976.

2. Hamilton, B., M.Sc. Thesis, McGill School of Architecture, 1977. (Draft copy).

3. Kerr, R.G., "A Study of a Solar Heated House in Quebec," M.Eng. Thesis, Centre for Building Studies, Concordia University, Montreal, Canada, March 1978.

4. Kerr, R.G. and Shapiro, M.M., "The Performance of a Site Built, Air Heating Vertical Collector with Snow Reflector in Quebec," Renewable Alternatives, Proceedings of Annual SESCI Conference, London, Ontario, Paper 3-1-10, 1978.

5. Hamilton, B. and McConnell, R., "Experimental Evaluation of a Solar House Heating System in Quebec," Sharing the Sun, Proceedings of the Joint ISES and SESCI Annual Conference, Winnipeg, Vol, 3, p. 120, 1976.

6. Kerr, R.G., Turaga, M., Shapiro, M.M. and McConnell, R.D., "A Performance Evaluation of a Solar House in Quebec," Proceedings of the Annual Meeting of the American Section of ISES, Orlando, Florida, Vol. 1, Sect. 13, p. 13-1, 1977.

7. McDaniels, D.K., Lowndes, D.H., Mathew, H., Reynolds, J. and Gray, R., "Enhanced Solar Energy Collection Using Reflector-Solar Thermal Collector Combinations," Solar Energy, Vol. 17, p. 277, 1975.

8. Grassie, S.L. and Sheridan, N.R., "The Use of Planar Reflectors for Increasing the Energy Yield of Flat-Plate Collectors," Solar Energy, Vol. 19, p. 663, 1977.

9. Grimmer, D.P., Zinn, K.G., Herr, K.C. and Wood, B.E., " Augmented Solar Energy Collection Using Different Types of Planar Reflective Surfaces; Theoretical Calculations and Experimental Results," Solar Energy, Vol. 21, p. 497, 1978.

10. Bäer, K.W., "The Solar Spectrum at Typical Clear Weather Days," Solar Energy, Vol. 19, p. 525, 1977.

11. ASHRAE Handbook of Fundamentals, Chapter 26, 1977.

12. Dave, J.V., "Validity of the Isotropic-Distribution Approximation in Solar Energy Estimations," Solar Energy, Vol. 19, p. 331, 1977.

13. Seitel, S.C., "Collector Performance Enhancement with Flat Reflectors," Solar Energy, Vol. 17, p. 291, 1975.

14. Liu, B.Y.H. and Jordan, R.C., "The Long-Term Average Performance of Flat-Plate Solar-Energy Collectors," Solar Energy, Vol. 7, No. 2, p. 53, 1963.

15. Hunn, B.D. and Calafell, D.O., "Determination of Average Ground Reflectivity for Solar Collectors," Solar Energy, Vol. 19, p. 87, 1977.

16. Kalitin, N.N., "The Measurement of the Albedo of a Snow Cover," Monthly Weather Review, U.S. Weather Bureau, Vol. 58, p. 59, 1930.

17. Hague, R.J. and Werren, G.L., "The Influence of a Snowpack on the Amount of Solar Radiation Received by a Vertical, South-Facing Wall," Climatological Bulletin of the Department of Geology, McGill University, No. 20, p. 8, 1976.

18. Farber, E.A. and Morrison, C.A., "Clear-Day Design Values," ASHRAE GRP 170, Applications of Solar Energy for Heating and Cooling of Buildings, p. IV-1, 1977.

19. Threlkeld, J.L. and Jordan, R.C., "Direct Solar Radiation Available on Clear Days," ASHAE Transactions, Vol. 64, p. 45, 1958.

20. Yager, A.J., Dow, J.O. and Feng, C.C., "Shading Design for Parallel Rows of Solar Collectors," Department of Civil, Environmental and Architectural Engineering, University of Colorado at Boulder, 1978 (Unpublished paper).

21. ASHRAE Standard 93-77, "Methods of Testing to Determine the Thermal Performance of Solar Collectors," ANSI B 198.1-1977.

22. Sonderegger. R.C., "Movers and Stayers : The Resident's Contribution to Variation across Houses in Energy Consumption for Space Heating," Energy and Buildings, Vol. 1, p. 313, 1978.

23. Lindgren, B.W. and McElrath, G.W., Introduction to Probability and Statistics, Macmillan, New York, 1959.

BIBLIOGRAPHY

1. Duffie, J.A. and Beckman, W.A. Solar Energy Thermal Processes, New York: John Wiley & Sons, 1974.

2. Kreider, J.F. and Kreith, F. Solar Heating and Cooling, Washington, D.C.: Hemisphere Publishing Corporation, McGraw-Hill Book Company, 1975.

3. Kreith, F. and Kreider, J.F. Principles of Solar Engineering, Washington, D.C.: Hemisphere Publishing Corporation, McGraw-Hill Book Company, 1978.

4. Krenz, J.H. Energy Conversion and Utilization, Boston: Allyn and Bacon, 1976.

5. Threlkeld, J.L. Thermal Environmental Engineering, Englewood Cliffs: Prentice Hall, 1970.

APPENDIX A

SOLAR RADIATION DATA

NOTES FOR FIGURES A.1 - A.13

1. These are copies of the actual data tapes used to determine the "Clear Day Measured Total Radiation" values in Table 2.

2. Where only one curve appears in a figure, it is for the vertical solarimeter. Where two curves are shown in a figure, the top one is for the vertical and the bottom one is for the 60° tilted solarimeter.

3. On the days which had some cloud cover, a smooth radiation curve was assumed from sunrise to sunset in order to compare the percent difference in total radiation for both surfaces as if the day had been completely clear.

4. A different scale factor was used for the vertical and 60° solarimeter records. Intercalibration was done by placing the two solarimeters side by side on the vertical collector and matching the scales for all intensities.

5. In each case, the data curves were redrawn and the daily total intensities were determined by summing simple trapezoids. Typical examples are given in Figs. A.14 and A.15.

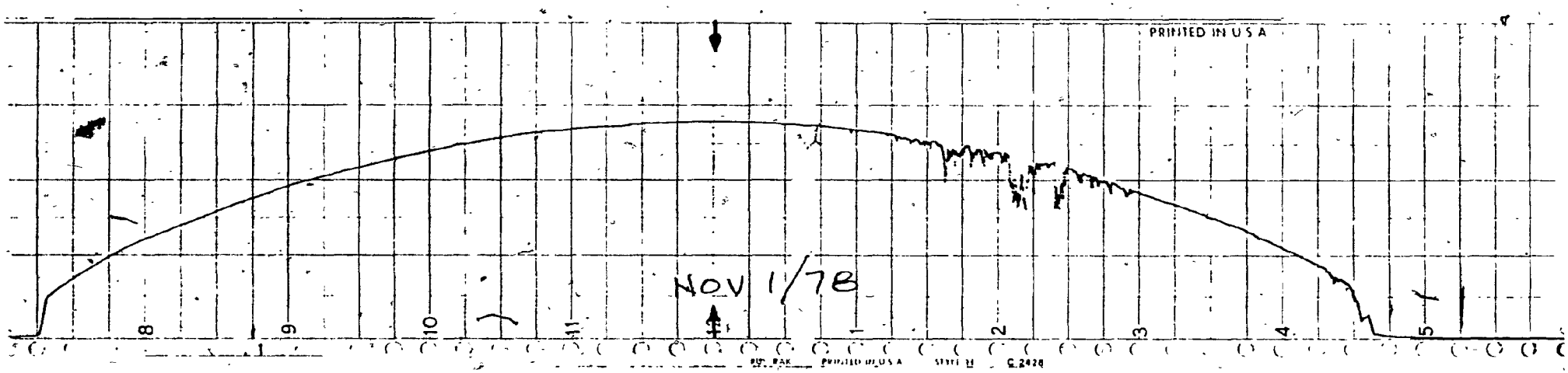

FIGURE A.1

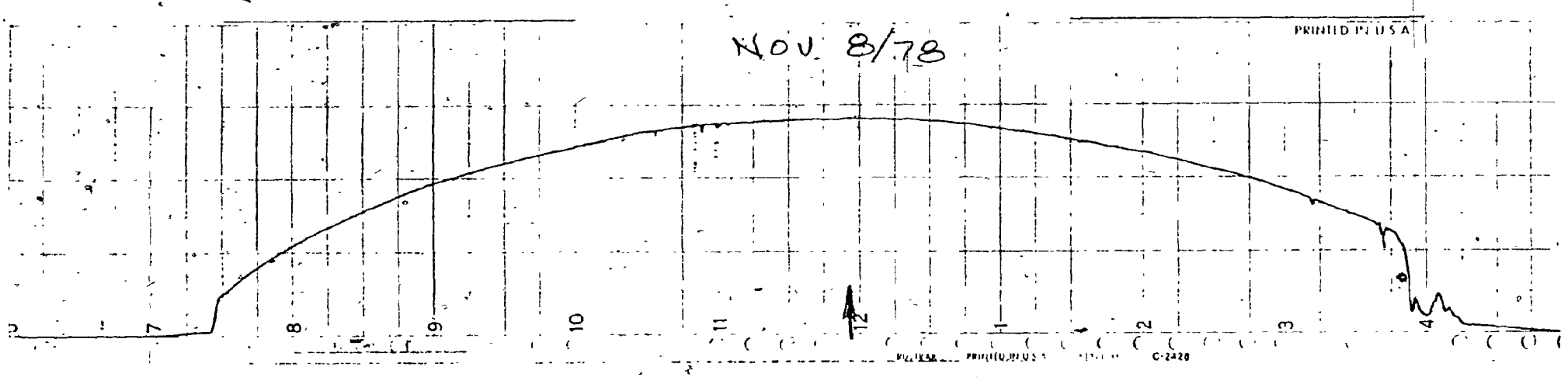

FIGURE A.2

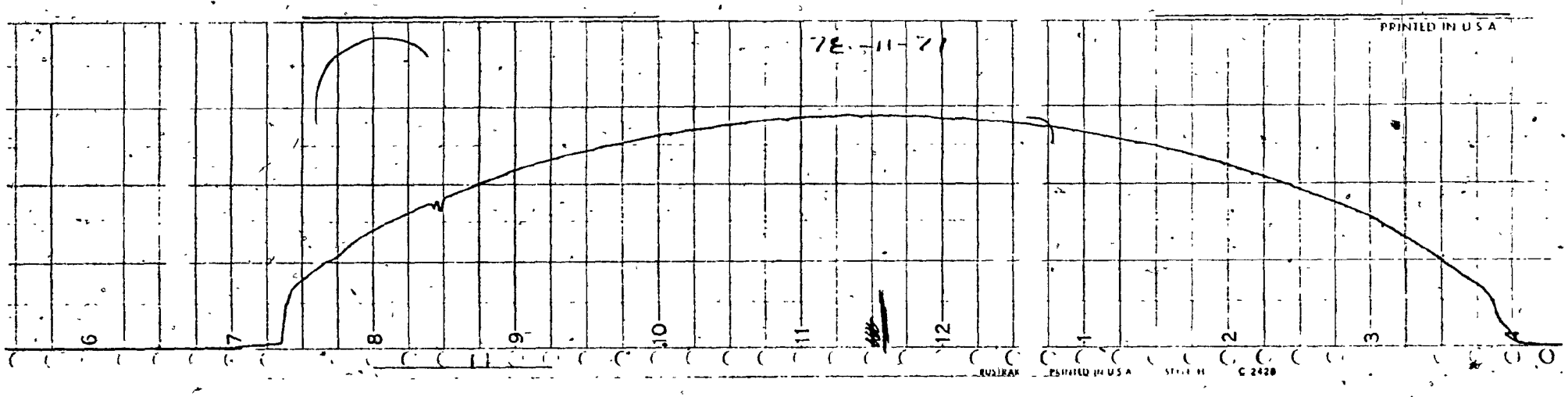
PRINTED IN U.S.A.
12-11-71
6
7
8
9
10
11
12
1
2
3
4
5
PRINTED IN U.S.A.
C 2420

FIGURE A.3

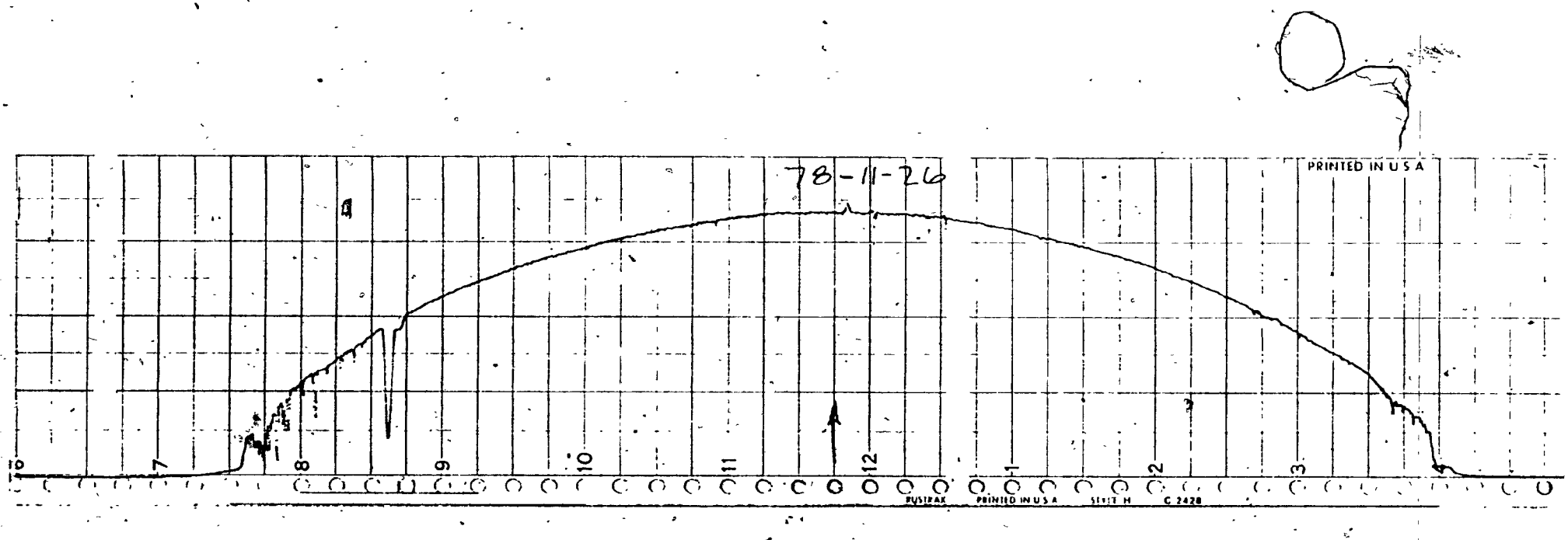
78-11-26
PRINTED IN U S A
7
8
9
10
11
12
1
2
3
PUSTRAK
PRINTED IN U S A
SERIES H
C 2428

FIGURE A.4

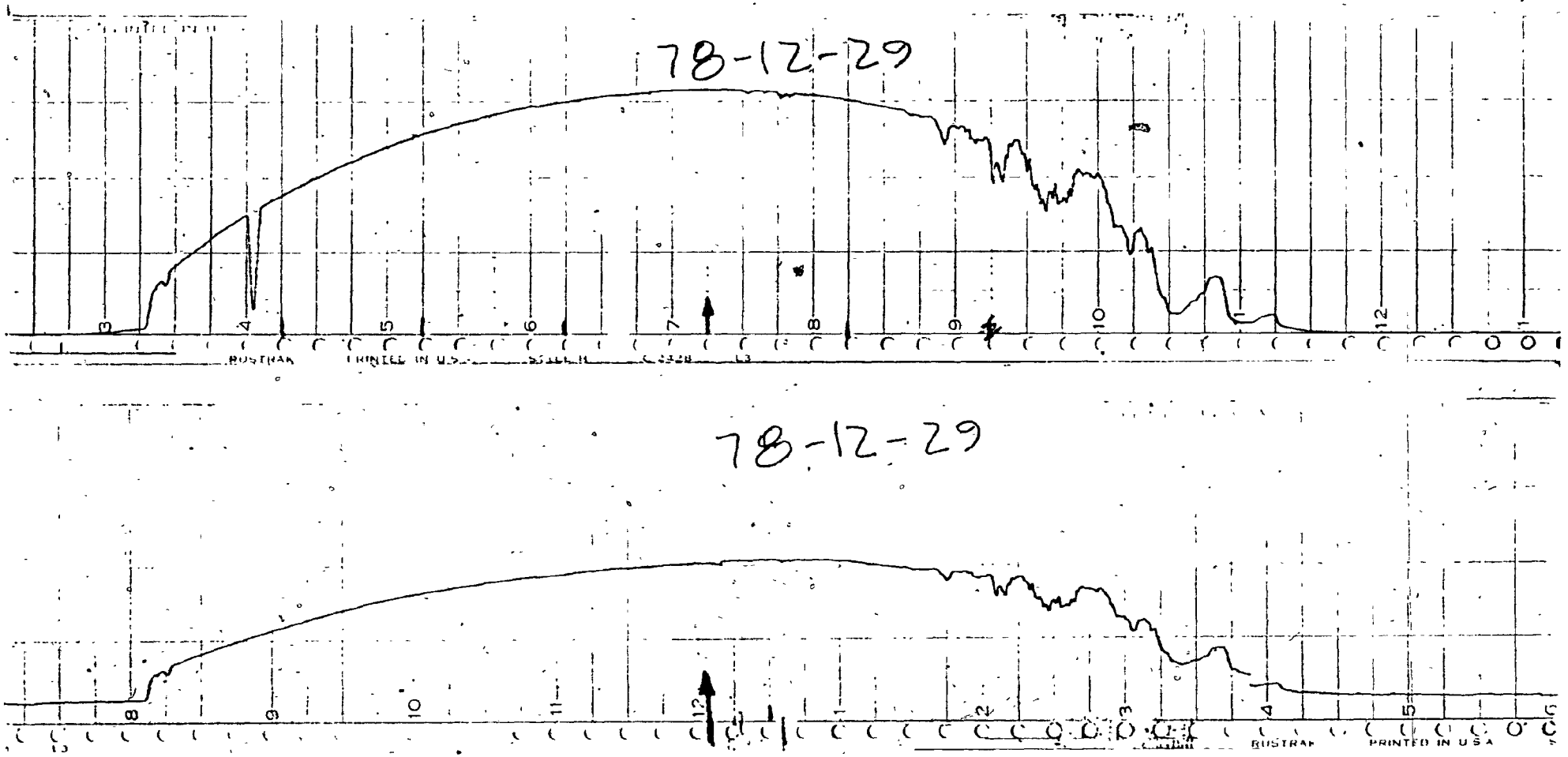

FIGURE A.5

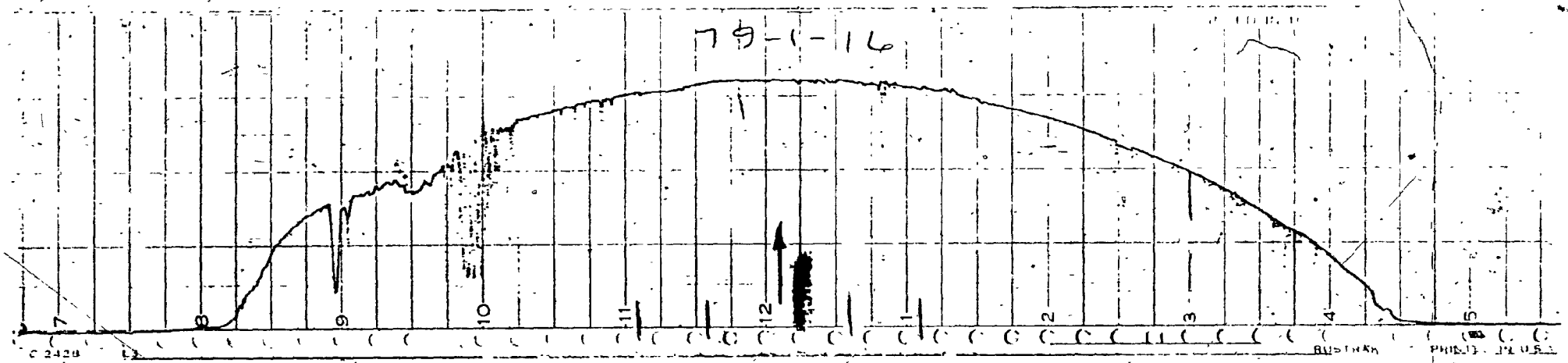

FIGURE A.6

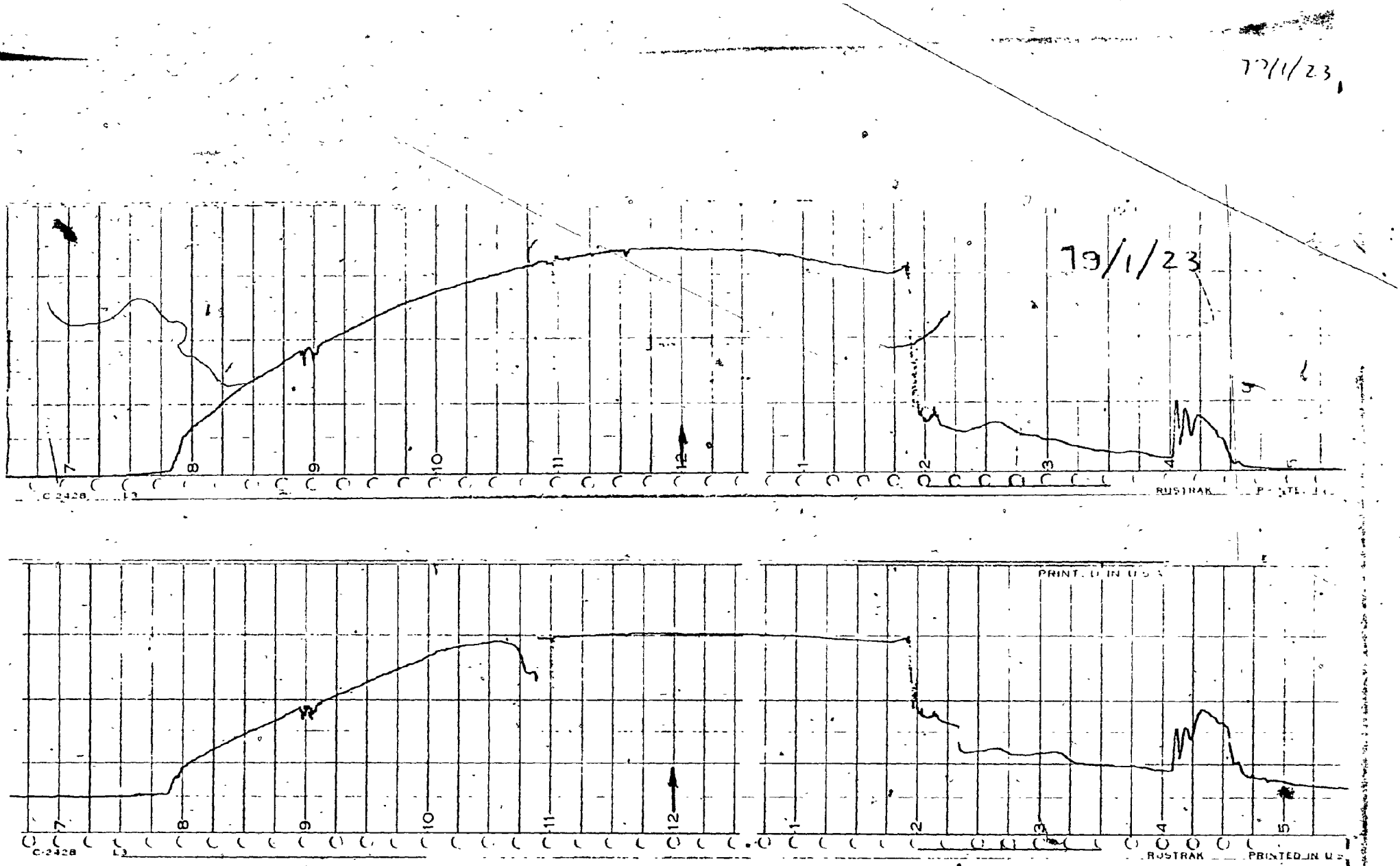

FIGURE A.7

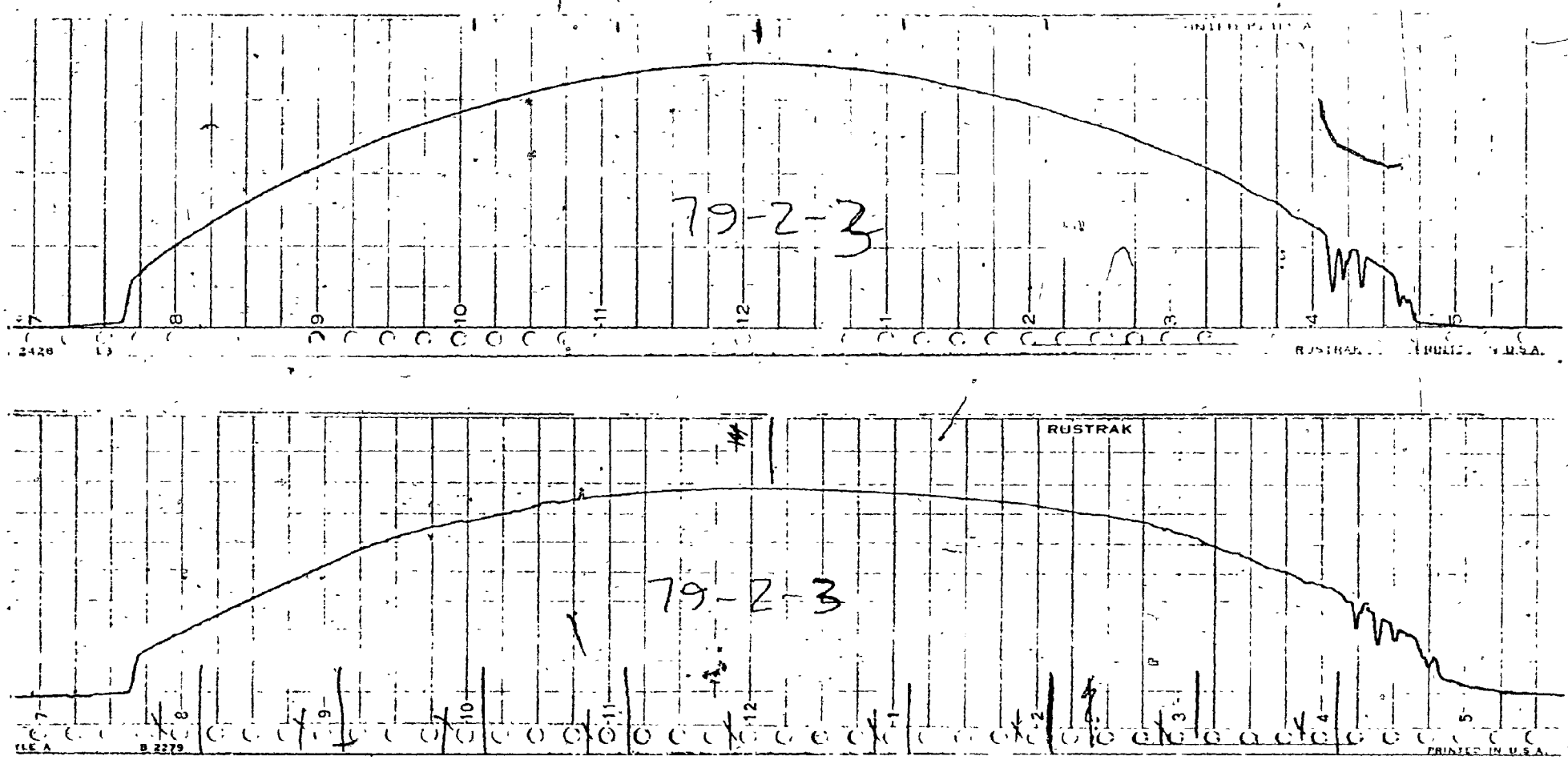

FIGURE A.8

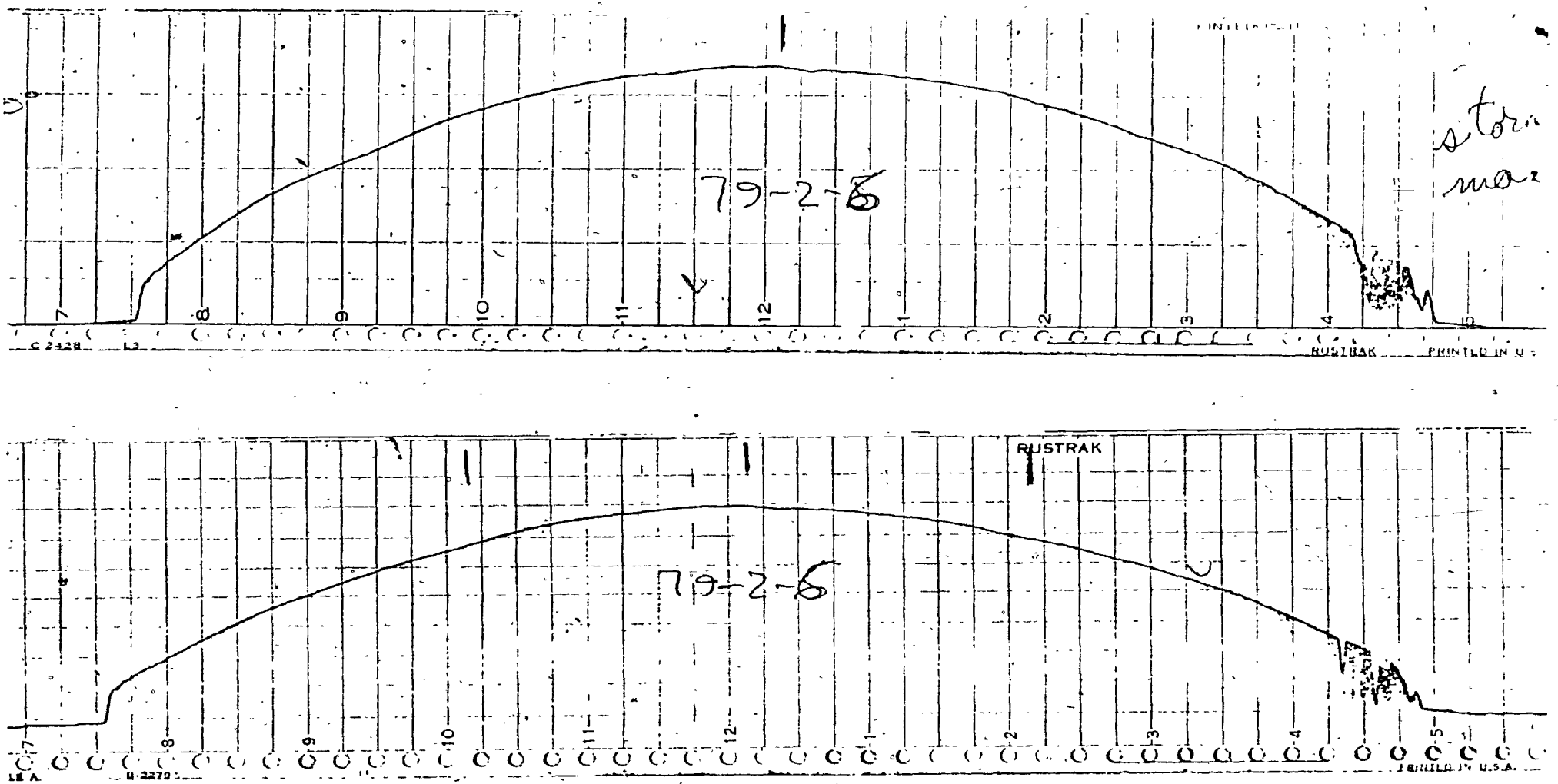

FIGURE A.9

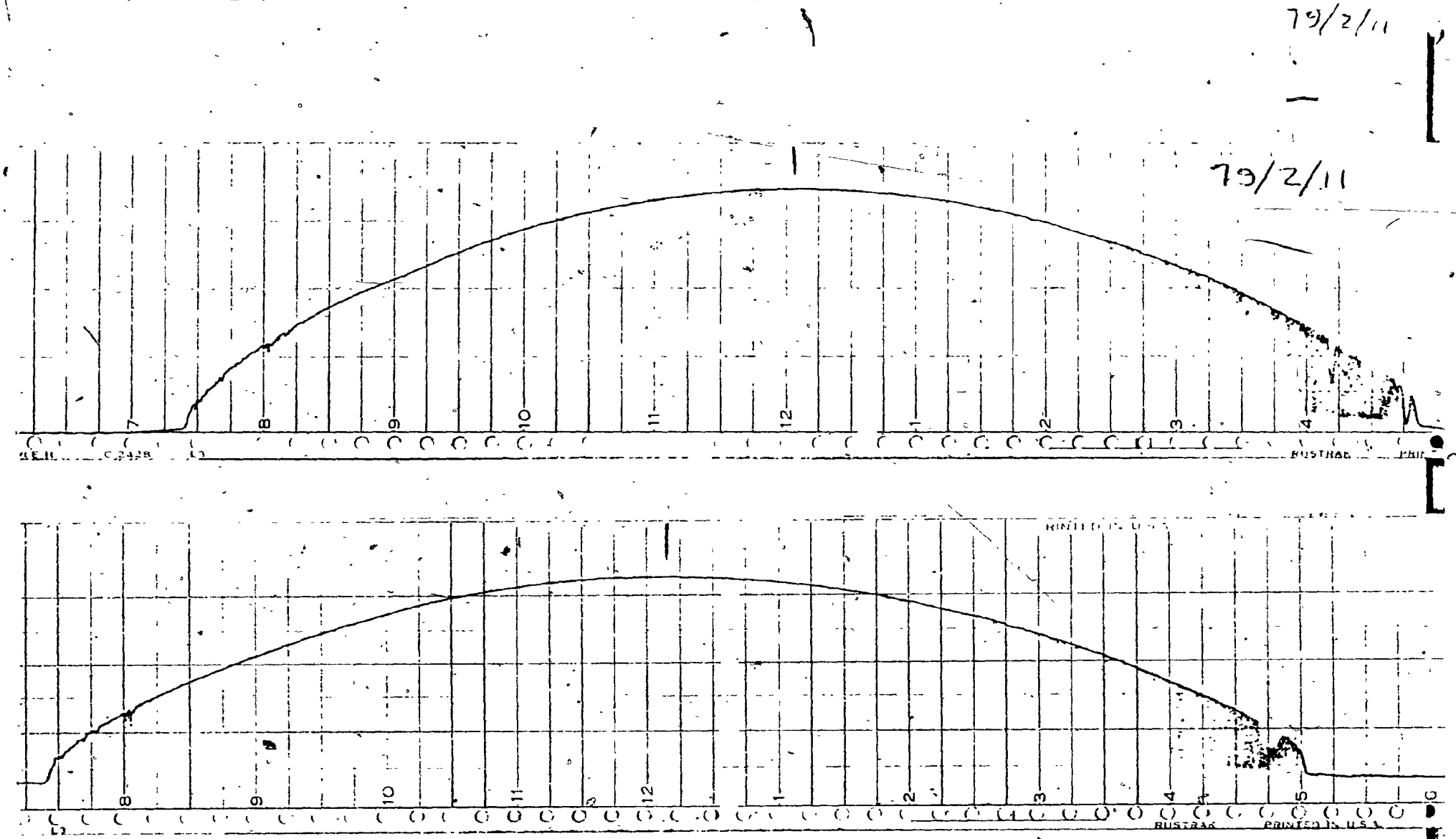

FIGURE A.10

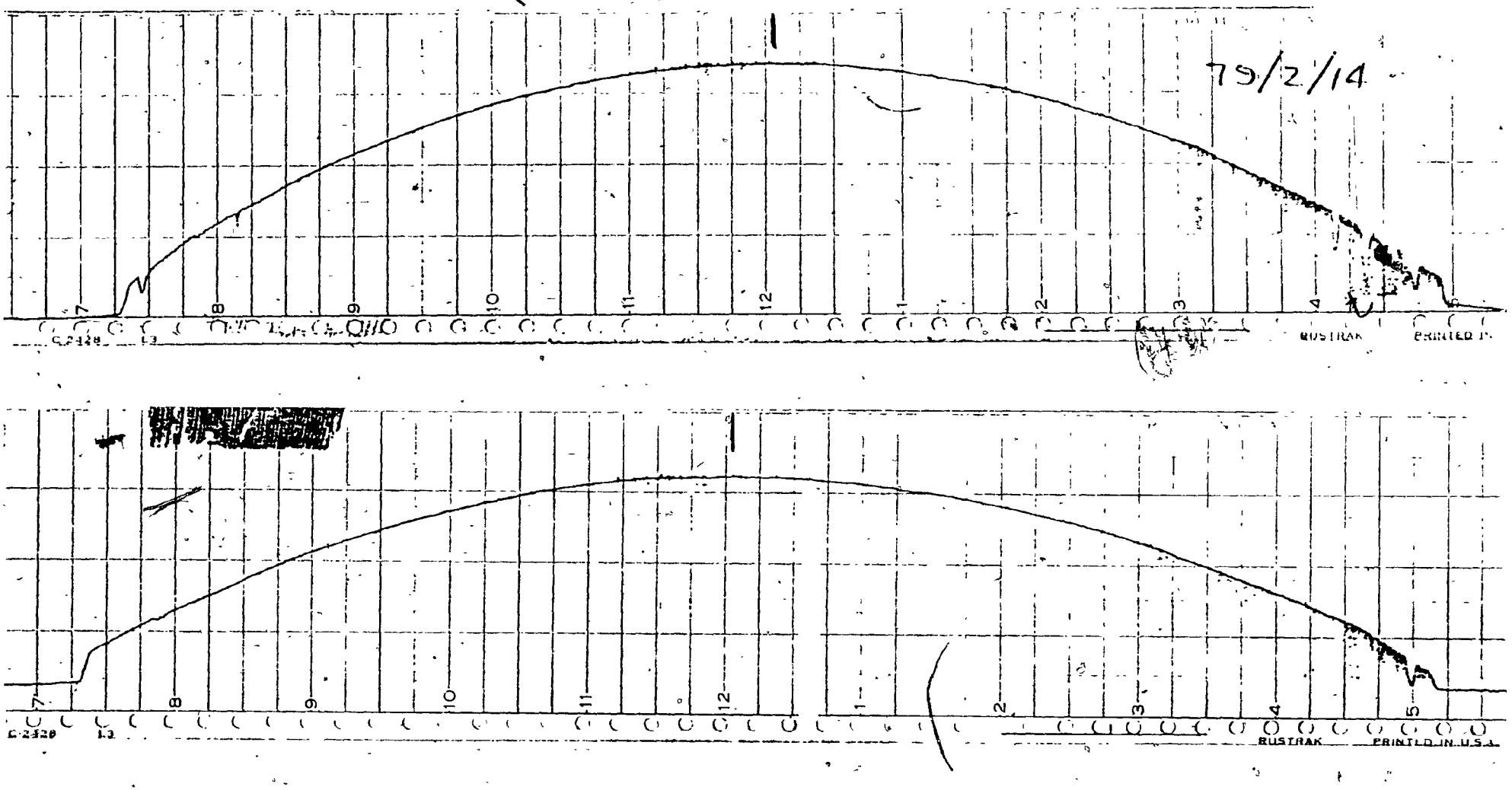

FIGURE A.11

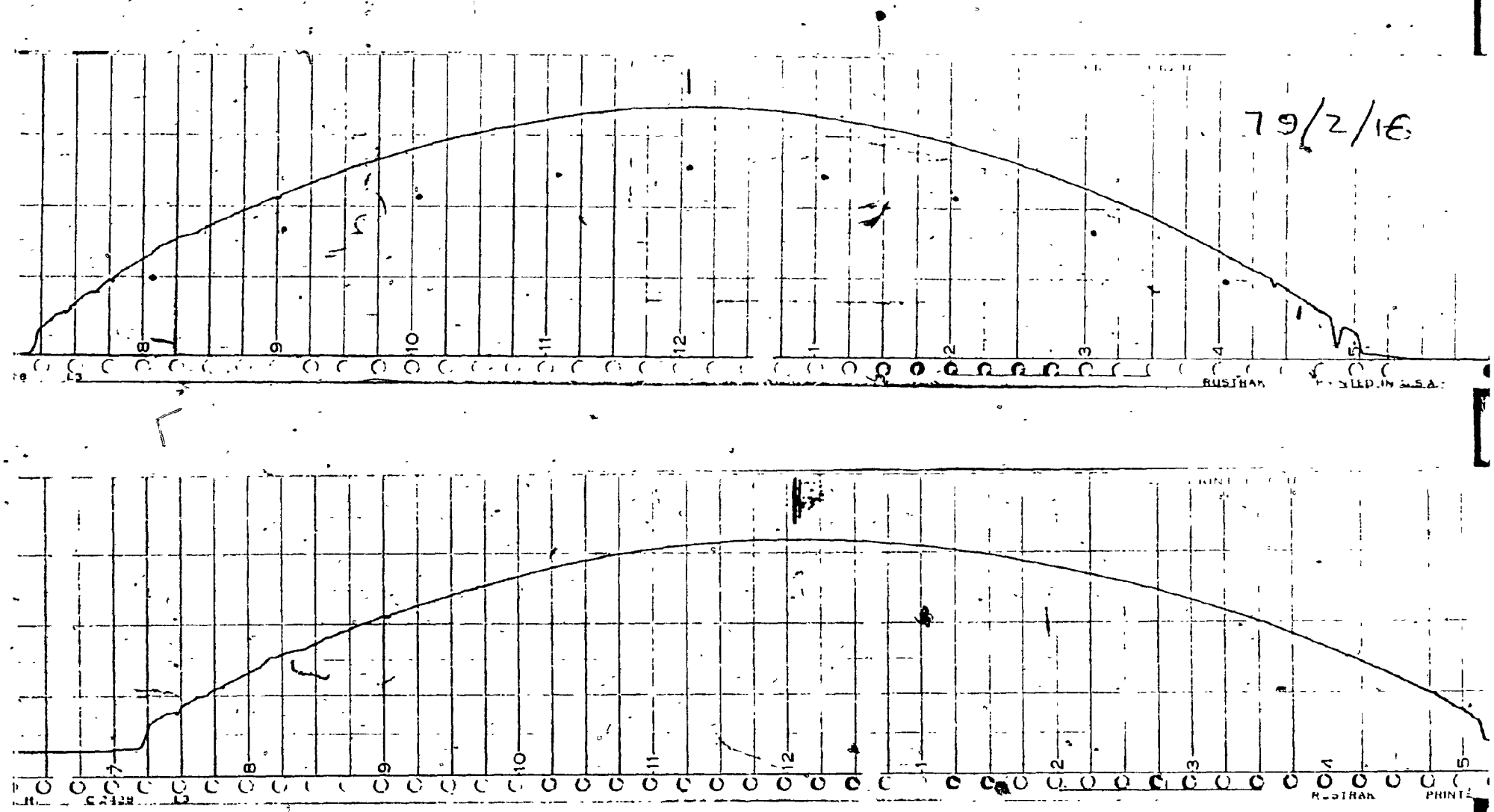

FIGURE A.12

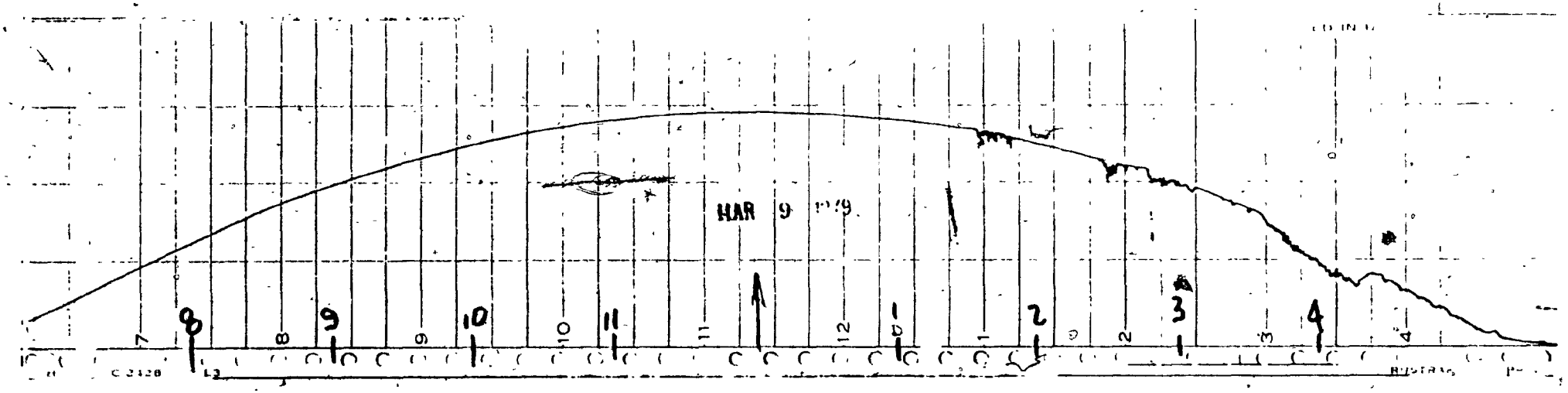

FIGURE A.13

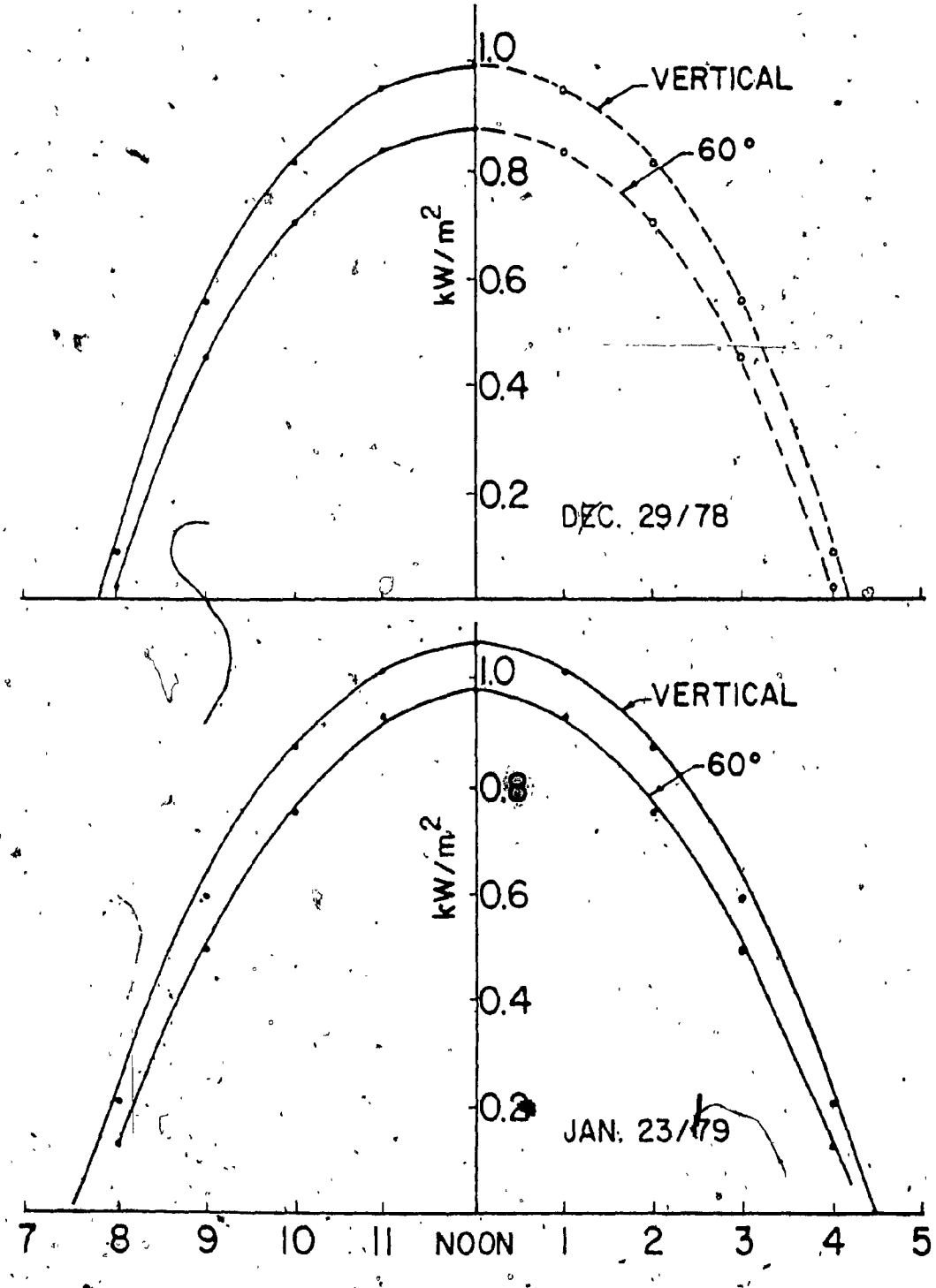

FIG. A.14 - TYPICAL SCALED SOLARIMETER DATA.

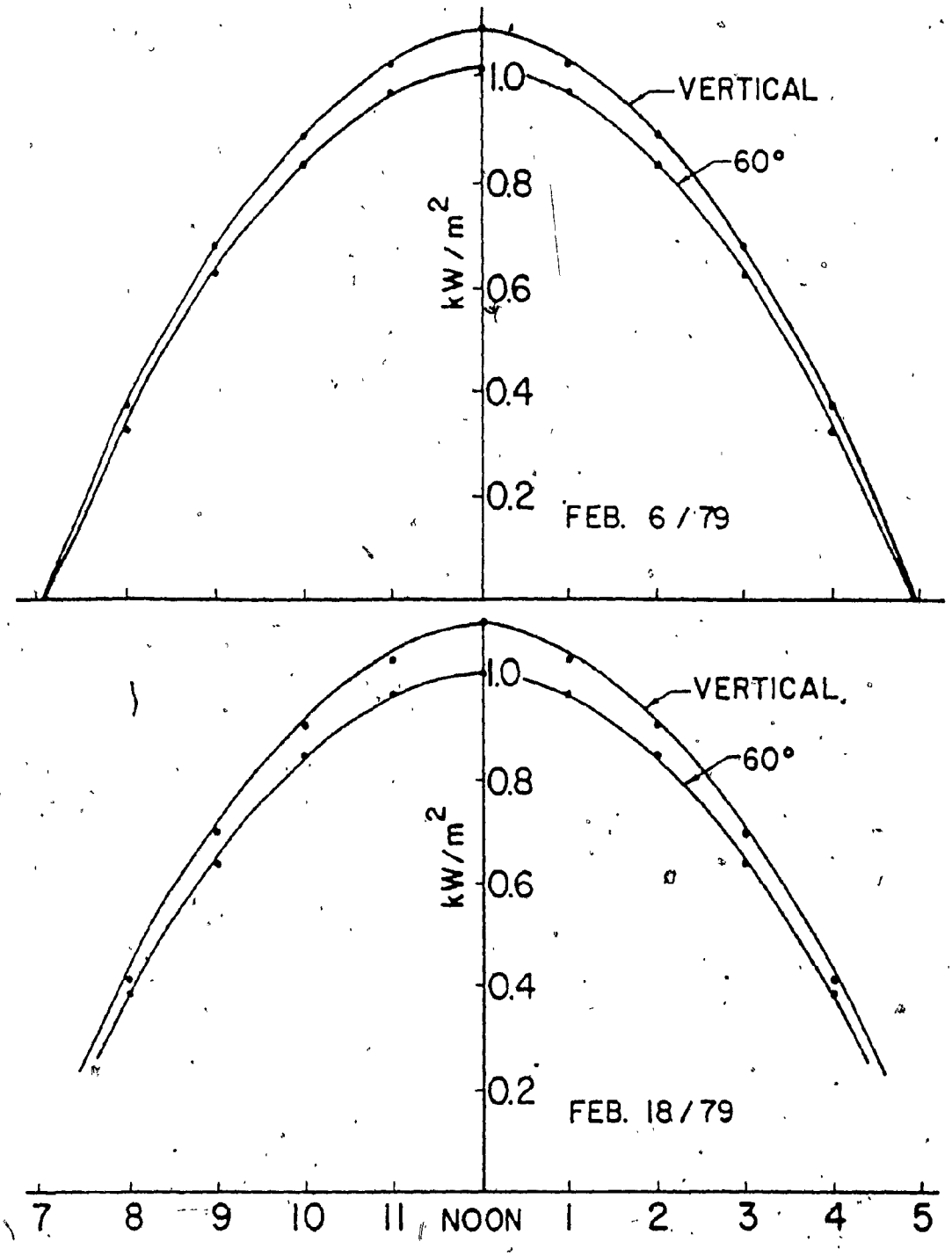

FIG. A.15 - TYPICAL SCALED SOLARIMETER DATA.

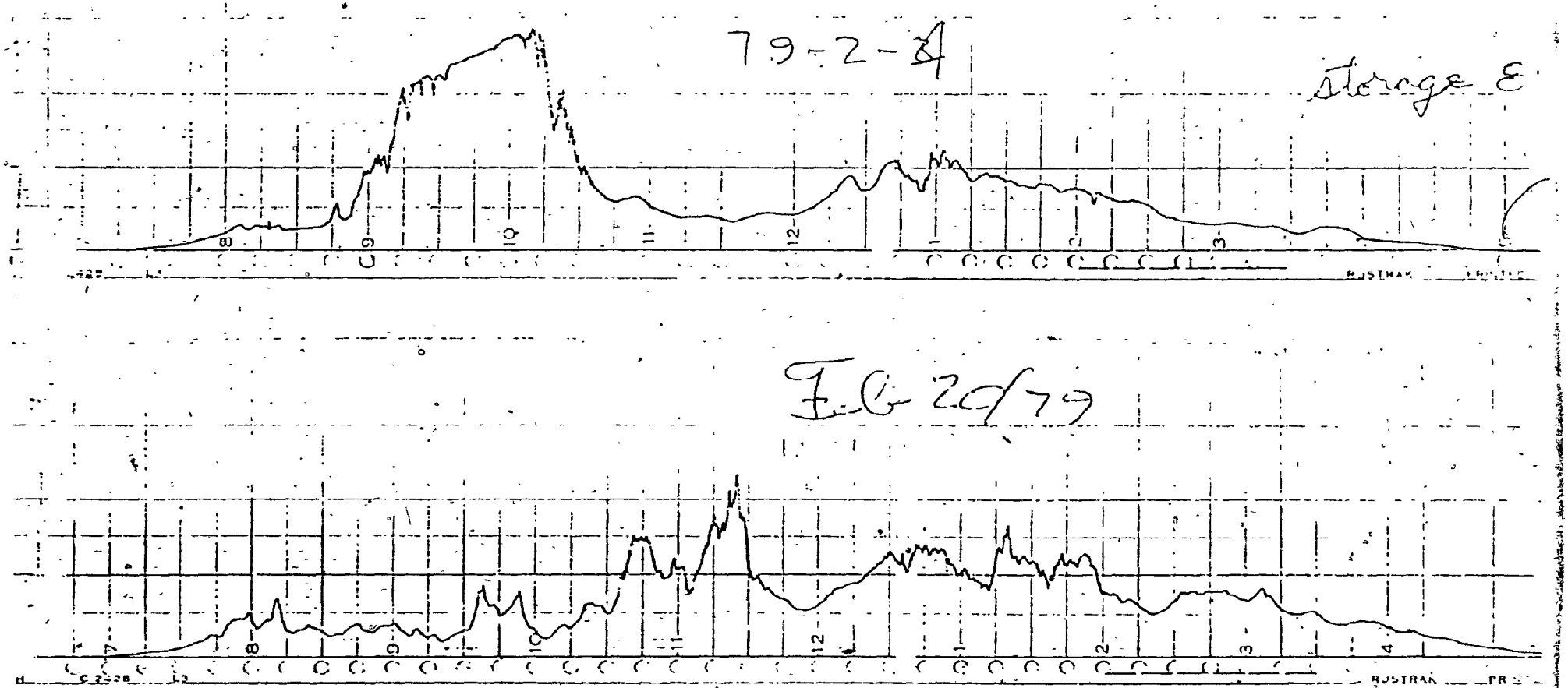

FIG. A.16 - TYPICAL HAZY CLOUDY DAYS.

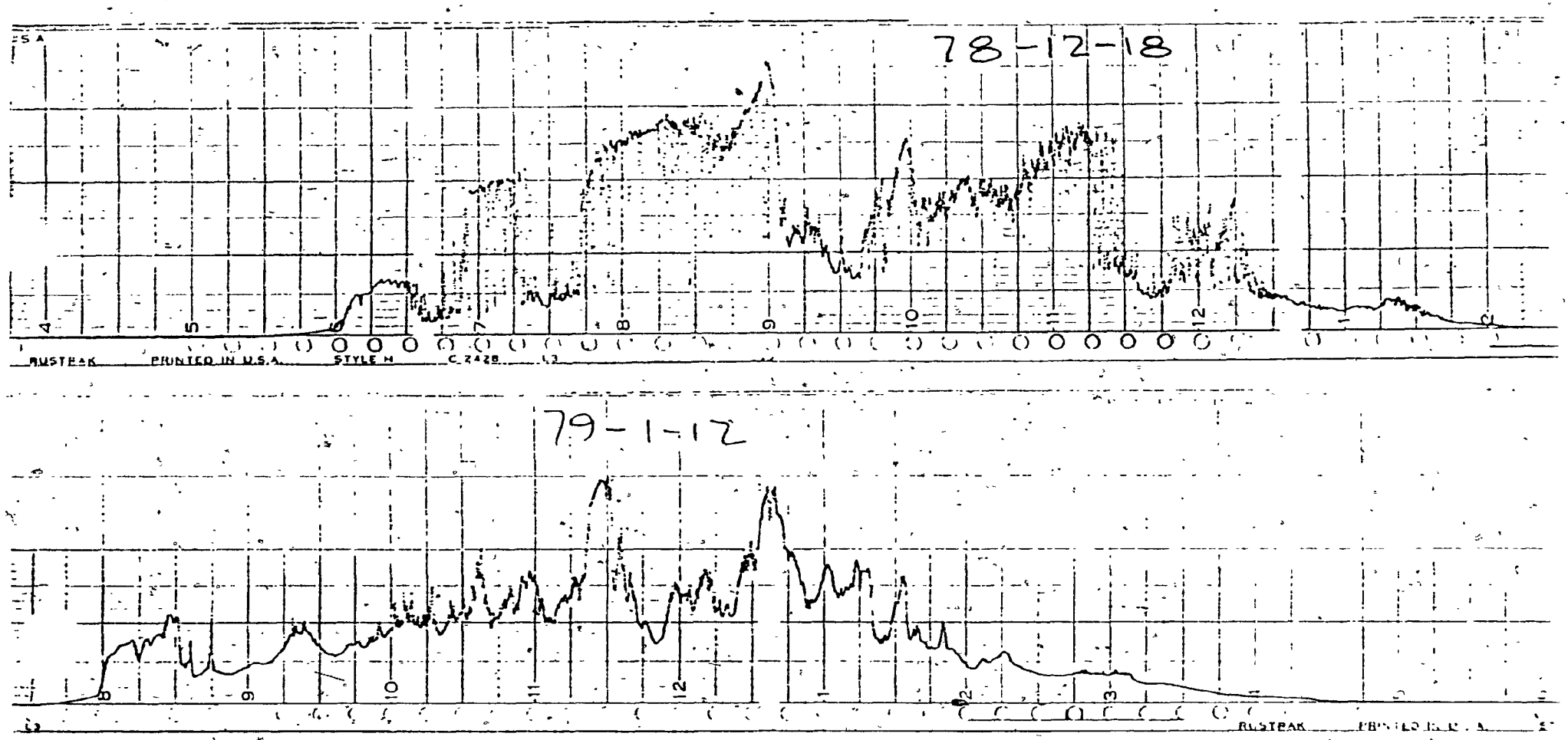

FIG. A.17 – TYPICAL SCATTERED CLOUDY DAYS.

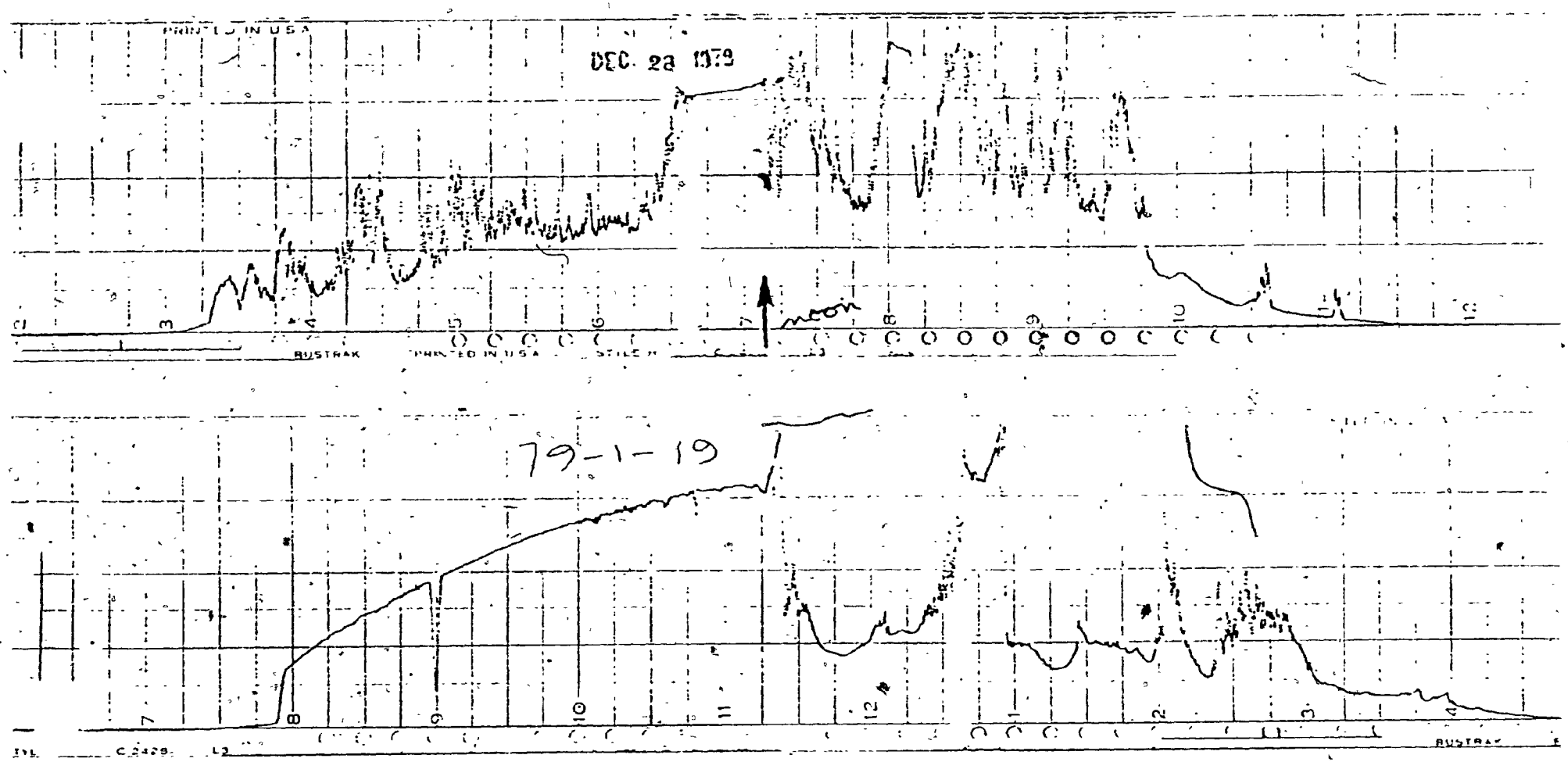

FIG. A.18 - TYPICAL SCATTERED CLOUDY DAYS WHEN THE INCIDENT RADIATION INCREASED DUE TO REFLECTION FROM LUMINOUS WHITE CLOUDS.

APPENDIX B

PROBABLE ERRORS

The probable errors in data collection and their impact on the major calculated results are as follows :

The manufacturer's stated tolerance for the thermistors was $\mp$0.1°C in the range of temperatures measured. The nine thermistors used were intercalibrated before the experiment. They agreed to within 0.25°C over the range of 0°C to 60°C. The absolute accuracy was checked with a Kaye Instruments Ice Point apparatus. Again, the thermistors were within 0.25°C at the ice point. The accuracy of the recorder was $\mp$0.5°C, with the major part of this error due to paper shifts. However, where temperature differences were used in the calculations, most of this error was eliminated because all the nine temperatures were recorded on the same chart. (The locations of the thermistors were given in Section 3.1).

The planimeter integrations of solar radiation, heater events, and temperature differences were performed within a tolerance of $\mp$2% of the mean value determined by at least 3 repetitions. With sensor and recorder errors, the integrated solarimeter data were accurate to $\mp$2%.

The average percentage difference of the velocity head measurements, given in Fig. 17, taken at the 15 pairs of symmetrical locations about the vertical centerline, is 30%. This is indicative of the error in the measurements due to turbulence because of the shortness of the duct section at which the test was done. (Most accurate results would be obtained at a section about 6 duct diameters downstream of any bends; however, the only suitable section of duct available for

the velocity measurements was just one and one half duct diameters long. This section was close both to the fan and the storage air exit openings, where turbulence was created). The flow in the collector was less than the value measured at the fan due to leaks at the dampers. Assuming the flow in the collector to be 5% less than that measured at the fan and completely random velocity variations arising from the turbulence, the deviation of the flow in the collector is roughly -20% to +10% of the flow rate measured near the fan. Based on hourly calculations using the measured temperature data on two typical clear days, the root-sum-square deviation [23] of the total daily heat collected, Q_u, ranges from -8% to +4%. Using the same method on a seasonal basis, the probable error in the total heat collected is from -1.1% to +0.6%.

The calculation of the instantaneous collector efficiency, $\eta_c = Q_u/A_c I_c$, is directly affected by the error in the mass flow rate of -20% to +10% and the error in the solar radiation measurement of $\pm$4%. Therefore, the maximum probable error in η_c is -24% to +14%. The error in the factor $(T_{in} - T_{amb})/I_c$ is $\pm$4% and is neglected relative to the error in η_c. Using the root-sum-square method above, the probable error of η_c for the best fit line in Fig. 16 through the instantaneous efficiency data points ranges from -3.6% to +2.1%.